Elsevier Editorial System(tm) for Journal of CO2 Utilization
Manuscript Draft

Manuscript Number: JCOU-D-14-00006R2

Title: Bench-scale study of electrochemically assisted catalytic CO2 hydrogenation to hydrocarbon fuels on Pt, Ni and Pd films deposited on YSZ

Article Type: Full Length Article

Keywords: Bench scale; CO2 hydrogenation; Pt/YSZ; Ni/YSZ; Pd/YSZ

Corresponding Author: Dr. Esperanza Ruiz Martínez, Ph.D.

Corresponding Author's Institution: CIEMAT

First Author: Esperanza Ruiz Martínez, Ph.D.

Order of Authors: Esperanza Ruiz Martínez, Ph.D.; Domingo Cillero Carrera; Pedro Juan Martínez Román; Ángel Morales Sabio; Gema San Vicente Domingo; Gonzalo de Diego Velasco; José María Sánchez Hervás

Abstract: Electrochemically assisted CO2 hydrogenation to fuels was studied at bench scale over different tubular (Pt, Ni or Pd)/YSZ electrochemical catalysts, under atmospheric pressure, at temperatures between 225 and 400 ºC and using high gas flow rates, gas compositions representative of CO2 capture exiting streams and changing H2/CO2 ratios (to simulate a discontinuous renewable H2 flow), as an approach towards its potential practical application.
Pt catalyst film was deposited from a precursor paste, while Ni and Pd films were deposited by a more easily scalable "electroless" technique. Both procedures resulted in relatively big metal particles which probably determined the comparatively high selectivity to methanol (up to 8 % at 400 ºC and H2/CO2=2), hydrocarbons (almost 100 % to C2H6 and C3H6) and dimethyl ether (up to 96 % at 300º C and H2/CO2=3) obtained for Pt, Ni and Pd, respectively, and the unusual small selectivity to CH4 and CO observed for Ni and Pd.
CO2 hydrogenation can be electrochemically enhanced for both positive and negative potentials by up to 3.2, 2.4 and 1.3 times for Pt, Ni and Pd, respectively, depending on the utilized operating conditions. Selectivity to the different fuels of industrial interest can be modulated by modifying applied potential.

Suggested Reviewers: Alexandros Katsaounis
alex.katsaounis@chemeng.upatras.gr

Evangelos Papaioannou
evangelos.papaioannou@ncl.ac.uk

Ángel Caravaca
a.caravaca@qub.ac.uk

Opposed Reviewers:

Response to Reviewers:

"Reviewer 2, comment 1":
1. The author mentioned XPS measurement many times in the manuscript, for example in the section of "2.2 Catalyst characterization"(p7.), in the section of "3.1 Catalyst characterisation studies"(p.12,p.14), in the section of "3.2.2 Electrochemically assisted CO2 hydrogenation tests on Ni"(p.30), in the section of "4. Conclusions"(p.37). The author should show the figures for XPS spectra of the samples and the C1s spectra.
"Response to Reviewer 2 comment No. 1:"
The figures for XPS spectra of the samples (Figs. 7a, 7b, 8a, 8b, 9a and 9b) and the C 1s spectra (Figs. 16a and 16b) have been included in the revised version of the paper.

"Reviewer 2, comment 2":
2. In p.28, "As can be observed in Fig. 10b, for H2/CO2 ratios of 4, the hydrogenation of CO2 over Pt/YSZ/Au, at 400 ºC and 90 l h-1, gives rise also to the formation of CO (2), CH3OH (16), C2H6 (7) and C3H6 (8), and it is, as well, affected by the applied potential, with selectivities to C2H6, C3H6, CO and CH3OH up to 4.8 %, 73.3 %, 72.5 % and 0.9 %, respectively."
In p.28, "and for H2/CO2 ratios equal to two (of about 2 %), which is that required for stoichiometric synthesis of methanol by hydrogenation of the CO(20) resulting from CO2 dissociative adsorption, and, therefore, thermodynamically favours the formation of CH3OH as the expenses of other CO2 hydrogenation products."
In P.29, "As commented above, nickel is reported to favour the C-C bond rupture and, therefore, CO2(18) and CO (14) dissociation to surface carbon."
What is the meaning of CO (2), CH3OH (16), C2H6 (7), C3H6 (8), CO(20), CO2(18) and CO (14), respectively?
"Response to Reviewer 2 comment No. 2:"
The number between brackets refers to the corresponding reaction/equation number. Therefore, CO(2) refers to equation (2), i.e., CO formation by RWGS reaction, CH3OH (16), C2H6 (7) and C3H6 (8) refer to CH3OH, C2H6 and C3H6 formation by CO2 hydrogenation reaction, respectively. CO (20) refers to equation 20, i.e., CH3OH formation by hydrogenation of adsorbed CO resulting from CO2 dissociation. CO2 (20) and CO(14) refer to equations 20 and 14, i.e. CO2 and CO dissociation to surface carbon, respectively.

Madrid, September 3, 2014

Dear Sir.

I am sending you a revised version of the manuscript entitled: " Bench-scale study of electrochemically assisted catalytic CO2 hydrogenation to hydrocarbon fuels on Pt, Ni and Pd films deposited on YSZ ", which include the answers to the different suggestions and comments raised by the reviewers.

The paper deals with the electrochemically assisted CO_2 catalytic hydrogenation to renewable fuels in model gases of postcombustion CO_2 capture plants over (Pt, Ni or Pd)/YSZ electrochemical catalyst systems at bench scale. Firstly, the Pt catalyst film was deposited from a precursor paste, while Ni and Pd films were prepared by electroless. The different electrochemical catalysts were characterised, both as prepared and after reduction and testing, by SEM, XRD and XPS techniques, in order to correlate changes in catalyst morphology, cristallinity and surface chemical composition with the electrochemically assisted catalytic performance. Subsequently, we evaluate the influence of catalyst type and operating conditions (temperature, applied potential and H_2/CO_2 ratio) on the reaction extent and magnitude of the electrochemical promotion of the catalysts for CO_2 hydrogenation and on the selectivity for the different hydrocarbons or oxygenates fuels of more industrial interest.

The relevance of the paper comes from the fact that we report original experimental data on electrochemically assisted CO_2 hydrogenation to valuable fuels under realistic postcombustion CO_2 capture exhaust conditions and under H_2/CO_2 ratios representative of a potential discontinuous flow of renewable H_2, obtained at a representative scale and over different tubular electrochemical catalyst systems. Therefore, this study addresses some scale-up aspects, such as operation at high flow rates and atmospheric pressure, under realistic gas compositions and using catalyst-electrode configurations easily adaptable to the existing catalytic devices (conventional flow reactors), and, in the case of Ni, based on a cheap, widespread and non-precious catalyst, and prepared by a commercial ready procedure, which may have an impact on the potential practical application of the process for CO_2 recycling, contributing not only to controlling the global “Green-house Effect”, but also to the availability of fuel sources for the future.

Yours sincerely,

Dr. Esperanza Ruiz Martínez
Scientific researcher

Reviewer 2

Comment:
1. 1. The author mentioned XPS measurement many times in the manuscript, for example in the section of "2.2 Catalyst characterization"(p7.), in the section of "3.1 Catalyst characterisation studies"(p.12,p.14), in the section of "3.2.2 Electrochemically assisted CO2 hydrogenation tests on Ni"(p.30), in the section of "4. Conclusions"(p.37). The author should show the figures for XPS spectra of the samples and the C1s spectra..
Answer:
The figures for XPS spectra of the samples (Figs. 7a, 7b, 8a, 8b, 9a and 9b) and the C 1s spectra (Figs. 16a and 16b) have been included in the revised version of the paper.

Comment:
2. . In p.28, "As can be observed in Fig. 10b, for H2/CO2 ratios of 4, the hydrogenation of CO2 over Pt/YSZ/Au, at 400 ºC and 90 l h-1, gives rise also to the formation of CO (2), CH3OH (16), C2H6 (7) and C3H6 (8), and it is, as well, affected by the applied potential, with selectivities to C2H6, C3H6, CO and CH3OH up to 4.8 %, 73.3 %, 72.5 % and 0.9 %, respectively."
In p.28, "and for H2/CO2 ratios equal to two (of about 2 %), which is that required for stoichiometric synthesis of methanol by hydrogenation of the CO(20) resulting from CO2 dissociative adsorption, and, therefore, thermodynamically favours the formation of CH3OH as the expenses of other CO2 hydrogenation products."
In P.29, "As commented above, nickel is reported to favour the C-C bond rupture and, therefore, CO2(18) and CO (14) dissociation to surface carbon."
What is the meaning of CO (2), CH3OH (16), C2H6 (7), C3H6 (8), CO(20), CO2(18) and CO (14), respectively?
Answer:
The number between brackets refers to the corresponding reaction/equation number. Therefore, CO(2) refers to equation (2), i.e., CO formation by RWGS reaction, CH3OH (16), C2H6 (7) and C3H6 (8) refer to CH3OH, C2H6 and C3H6 formation by CO2 hydrogenation reaction, respectively. CO (20) refers to equation 20, i.e., CH3OH formation by hydrogenation of adsorbed CO resulting from CO2 dissociation. CO2 (20) and CO(14) refer to equations 20 and 14, i.e. CO2 and CO dissociation to surface carbon, respectively.

Bench-scale study of electrochemically assisted catalytic CO_2 hydrogenation to hydrocarbon fuels on Pt, Ni and Pd films deposited on YSZ

Esperanza Ruiz [*], Domingo Cillero, Pedro J. Martínez, Ángel Morales, Gema San Vicente, Gonzalo de Diego, José María Sánchez

Centro de Investigaciones Energéticas, Medioambientales y Tecnológicas (CIEMAT), Av. Complutense, 40, 28040 Madrid, Spain

*Corresponding author: Tel.:+34-91-346-0887; fax.:+34-91-346-6269.

E-mail address: esperanza.ruiz@ciemat.es

Abstract

Electrochemically assisted CO_2 hydrogenation to fuels was studied at bench scale over different tubular (Pt, Ni or Pd)/YSZ electrochemical catalysts, under atmospheric pressure, at temperatures between 225 and 400 ºC and using high gas flow rates, gas compositions representative of CO_2 capture exiting streams and changing H_2/CO_2 ratios (to simulate a discontinuous renewable H_2 flow), as an approach towards its potential practical application.

Pt catalyst film was deposited from a precursor paste, while Ni and Pd films were deposited by a more easily scalable "electroless" technique. Both procedures resulted in relatively big metal particles which probably determined the comparatively high selectivity to methanol (up to 8 % at 400 ºC and H_2/CO_2=2), hydrocarbons (almost 100 % to C_2H_6 and C_3H_6) and dimethyl ether (up to 96 % at 300º C and H_2/CO_2=3) obtained for Pt, Ni and Pd, respectively, and the unusual small selectivity to CH_4 and CO observed for Ni and Pd.

CO_2 hydrogenation can be electrochemically enhanced for both positive and negative potentials by up to 3.2, 2.4 and 1.3 times for Pt, Ni and Pd, respectively, depending on the utilized operating conditions. Selectivity to the different fuels of industrial interest can be modulated by modifying applied potential.

Keywords: Bench scale; CO_2 hydrogenation; Pt/YSZ; Ni/YSZ; Pd/YSZ.

1. Introduction

Due to the increase in CO_2 atmospheric levels and the diminishing fossil fuel resources arising from wide spread production of energy by fossil fuels combustion, valorisation of CO_2 emissions to clean fuels is viewed as a complementary strategy to capture and storage for an effective quantitative reduction of the CO_2 emissions, allowing their recycling and, therefore, a more sustainable use of the energy resources. Chemical recycling of carbon dioxide from combustion power plants, as an energy carrier, can be accomplished via its capture and subsequent hydrogenation to renewable, useful and environmentally neutral fuels (methane, methanol, dimethyl ether, etc.), provided that any available renewable energy source (wind, solar or hydraulic) is used for both production of necessary hydrogen (by water electrolysis) and chemical conversion of CO_2. Moreover, it has been foreseen that increasing amounts of cheap CO_2 will be available from carbon sequestration in the near future. In this way, carbon dioxide can be chemically converted from a harmful greenhouse gas causing global warning into a valuable, renewable, environmentally neutral and inexhaustible fuel source for the future [1–4].

Two main reactions can occur on co-feeding CO_2 and H_2 over a hydrogenation catalyst:

$$x\,CO_2 + (2x - z + y)\,H_2 \rightarrow C_xH_yO_z + (2x - z)\,H_2O \quad (1)$$

$$CO_2 + H_2 \rightarrow CO + H_2O \qquad \Delta G^o = 19.9\ kJ\ mol^{-1} \quad (2)$$

The former is the synthesis reaction resulting in the formation of hydrocarbons and/or oxygenates (alcohols or ethers). The latter is the reverse water gas shift (RWGS) reaction.

Most studies on the catalytic hydrogenation of CO_2 have been accomplished over metal catalyst supported on metal oxides at high pressures, to increase the thermodynamic equilibrium conversion of the hydrogenation reaction, and using fixed-bed reactor configurations [3, 5, 6]. These catalysts are susceptible of electrochemical promotion which

may allow operation of the catalyst under milder conditions [7].

Electrochemical promotion of catalysis (EPOC), by coupling electrochemistry to catalysis, has been considered as an alternative approach to classical chemical promotion of catalyst by electrochemically supplying and controlling the concentration of a promoter on an active metal catalyst surface. The application of small currents or potentials between a metal catalyst which is in contact with a solid electrolyte, which acts as a source of promoter species, and a counter electrode results in the migration of promoting species to or from the catalyst surface, allowing increasing the catalytic activity for the CO_2 hydrogenation reaction and modifying the selectivity to the desired products, as well as to simultaneously monitor and control the reaction during the process [4, 8]. However, there are few previous studies of electrochemically promoted catalytic CO_2 hydrogenation. It has been studied over Cu on $SrZr_{0.9}Y_{0.1}O_{3-\alpha}$ (a proton conductor) [7], Pt on YSZ (an O^{2-} conductor) [5, 9], Pd on YSZ or Na-βAl_2O_3 (a Na^+ conductor) [10], Rh on YSZ [5, 11], Cu on TiO_2-YSZ [5], Ru on YSZ [12] and Ni or Ru impregnated carbon nanofibers on YSZ [13]. In addition, most of these studies have been carried out using catalyst configurations, reaction conditions and gas compositions that are not representative of real postcombustion CO_2 capture exit streams. Therefore, aspects regarding the practical application of the technology have not been addressed in detail [14–16]. We have recently reported [17] a bench-scale study of electropromoted CO_2 hydrogenation to valuable hydrocarbon and oxygenated fuels over Pt on K-βAl_2O_3 (a K^+ conductor), at high gas flow rates, under atmospheric pressure and at relatively low temperature, using gas compositions representative of CO_2 capture exit streams and catalyst-electrode tubular configurations easily adaptable to the existing catalytic devices (conventional flow reactors) and prepared by easily scalable procedures. In the present work, we extend the study to other electrochemical catalyst systems, more specifically to Pt, Ni and Pd on YSZ (an O^{2-} conductor). Therefore, the aim of this work is to ascertain whether these

tubular electrochemical catalyst systems (Pt/YSZ/Au, Ni/YSZ/Au and Pd/YSZ/Au) can be electrochemically promoted for the CO_2 hydrogenation to renewable fuels under atmospheric pressure, at relatively low temperatures, high gas flow rates and under realistic postcombustion CO_2 capture exiting gas compositions, as an approach towards the practical application of EPOC for CO_2 valorisation. Moreover, in this study, we evaluate the influence of catalyst type and operating conditions (temperature, applied potential and H_2/CO_2 ratio) on the magnitude of the electrochemical promotion of the catalysts for CO_2 hydrogenation and on the selectivity for the different hydrocarbons or oxygenates fuels of more industrial interest.

2. Experimental

2.1 Electrochemical catalysts

The electrochemical catalysts evaluated in the present work consisted of a metal (Pt, Ni or Pd) film (catalyst-working electrode) deposited in the outer side of a 26-mm-i.d., 100-mm-long, 1-2-mm-thick YSZ (8 % mol Y_2O_3-stabilized ZrO_2) tube. A gold counter electrode was deposited on the inner side of the solid electrolyte tube to allow polarizations. Both Pt and Au electrodes were prepared by decomposition of precursor metal pastes, whereas, Ni and Pd films were prepared by "electroless".

Au was chosen as the auxiliary electrode material because it is reported [5, 12] to be inert for the CO_2 hydrogenation reaction.

The Au counter electrode was prepared by painting the inner side of the YSZ tube with a gold paste (HERAEUS-C5729). As well, the Pt catalyst-working electrode was deposited also by painting the outer side of the YSZ tube with a Pt paste (HERAEUS-CL-11-5349). In both

cases, the deposited paste was dried at 150 ºC during 10 min, heated to 850 ºC at a controlled rate and, finally, annealed at 850 ºC during 10 min.

Ni and Pd layers have been also coated on the outer surface of the YSZ tube by electroless deposition technique after deposition of the Au counter electrode on the inner side of the tube. Electroless deposition is the process of depositing a metallic coating from a solution without the application of external electrical power, so it is therefore applicable to non-conducting substrates, as is the case. Substrates need to be activated with a catalyst, usually palladium, to start deposition. Most metals, including Ni, are electrocalatytic so, once deposition starts, it keeps on going increasing layer thickness. An electroless solution typically consists of: a source of metal ions; a reducing agent or reductant; a complexant for the metal ions, to keep these dissolved ions in solution and to minimize homogenous reaction between the metal ions and the reducing agent and most likely a pH adjustment buffer.

Substrates were firstly cleaned with absolute ethanol in an ultrasonic bath, rinsed with absolute ethanol and dried in an oven at 90 ºC.

Prior to nickel and palladium deposition, substrates need to be catalysed with palladium to allow electroless deposition to start. A very thin palladium layer was deposited by dip-coating using a diluted dip-coating palladium solution and burned in the oven at 400 ºC, during 15 minutes. This solution was composed of 2-(2-aminoethylamino)ethanol, ethanol, palladium chloride and chlorhydric acid, according to European patent EP1321539 [18].

Palladium coating has been deposited using a precursor solution composed of palladium chloride stabilized with 2-(2-aminoethylamino)ethanol and sodium hipophosphyte as reducing agent, during 5 minutes at 50 ºC. Nickel coating has been deposited using a conventional solution with sodium hipophosphyte as reducing agent and nickel stabilized with tartrate ion, during 15 minutes at 70 ºC. After layer deposition, all substrates were rinsed with distilled water and dried in an oven at 90 ºC.

2.2 Catalyst characterisation

A small fragment of each electrochemical catalyst was characterized, both as prepared and after reduction and testing, by Scanning Electron Microscopy (SEM), X-Ray Diffraction (XRD) and X-ray Photoelectron Spectroscopy (XPS) techniques.

The morphology of the catalyst films was investigated via SEM using a HITACHI S-2500 instrument of 25 kV of accelerating voltage and 35 Å of resolution.

XRD patterns of the catalyst-working electrode films were recorded on a PHILIPS "Xpert-MPD" instrument using a Cu Kα X-ray source (45 kV and 40 mA), a 2θ range of 15-75º, a step size of 2θ=0.03º and a step time of 2 s.

The surface chemical composition of the catalyst electrode films was examined by XPS using a Perkin-Elmer PHI 5400 System equipped with a Mg Kα (hν = 1253.6 eV) excitation source running at 15 kV and 20 mA and having a beam diameter of 1 mm. Base pressure in the analysis chamber was maintained at about 10^{-9} Torr. The pass energy was set at 89.5 eV for general spectra (0-1100 eV) and at 35.75 eV for high resolution spectra. The energy scale was referenced to the carbon 1s signal at 285.0 eV.

2.3 Experimental set-up

Electrochemically assisted CO_2 hydrogenation over Pt, Pd and Ni based catalyst films was studied in a bench-scale plant, described in detail elsewhere [17], which is able to treat up to 20 m^3 h^{-1} (at 273 K and 1 atm) of gas with temperatures ranging between 250 and 450 ºC, at about atmospheric pressure.

The different gas constituents of a post-combustion CO_2 capture exit stream and hydrogen can be provided by mass flow controllers from bottled gases. Steam can be supplied by vaporising water fed into a boiler by a metering pump. The mixed wet gas is then preheated and directed to a fixed-bed down-flow quartz reactor, with 35 mm of diameter and 900 mm of length, heated by a three-zone electrical furnace. Polarization across the cell was measured and controlled via a potentiostat-galvanostat.

Gaseous products from the reactor were delivered through a heated transfer line to the gas analysis system in order to avoid condensation of any volatile products. Gas composition was simultaneously determined using a gas microchromatograph and an NDIR CO_2/CO on line analyser [17], allowing the analysis of: H_2, N_2, CO, CH_4, CO_2, C_2H_2, C_2H_4, C_2H_6, C_3H_6, C_3H_8, methanol, dimethyl ether and ethanol.

2.4 Operating conditions and procedure

The electrochemical catalysts were properly situated in the reactor in order to lessen by-pass phenomena and to enhance catalyst-reactive gas contact. The electrical connections in the reactor were made from gold wires (HERAEUS), which is reported to be catalytically inert in the process [5]; therefore, all the potential-induced changes in catalytic activity and selectivity can be exclusively attributed to the metal film.

The metallic films were reduced in a stream of H_2 at 400 ºC during 1 h [17], before performing the electropromoted CO_2 hydrogenation experiments.

In some cases (Pt), the temperature value was selected from previous cyclic voltammetry studies of the catalyst (not shown) which revealed that the promotional effect was maximum for 400 ºC and because methane production is reported to be produced only at high operation temperatures over this catalyst [5].

Open circuit potential (0 V) was maintained during 30 min prior to each test to define a reproducible reference state. Electrochemically assisted hydrogenation tests were performed, over different tubular (Pt, Ni or Pd)/YSZ electrochemical catalysts, under H_2/CO_2 binary mixtures, at different applied potentials (between -2 and 2 V), H_2/CO_2 ratios (from 1 to 4) and temperatures (225 – 400 ºC) and using a total gas flow rate of 90 l h^{-1}, in order to determine the effect of the utilized catalyst and operating conditions on CO_2 conversion, efficiency of electrochemical promotion and selectivity to the different fuel products.

CO_2 hydrogenation tests were performed under H_2 and CO_2 binary mixtures, although a small amount of N_2 (about 0.5 %) was added to the reaction gas mix as an internal standard. Accordingly [17], CO_2 conversion (X_{CO_2}) and "CO_2 free selectivity" is defined as (3) and (4), respectively:

$$X_{CO_2} = \left(1 - \frac{[CO_2]_o \times [N_2]_i}{[CO_2]_i \times [N_2]_o}\right) \times 100 \quad (3)$$

$$Si = \frac{n_i \times M_i}{\sum_{i=1}^{i=n} n_i \times M_i} \times 100 \quad (4)$$

Where $[CO_2]_i$ and $[CO_2]_o$ are the corresponding CO_2 molar quantities at the inlet and outlet of the reactor. As well, $[N_2]_i$ and $[N_2]_o$ are N_2 molar quantities at the inlet and outlet of the reactor, respectively. Additionally, S_i is the selectivity to product i, n_i is the number of carbon atoms of product i and M_i is moles of product i, respectively.

The effect of polarization on catalyst performance for the CO_2 hydrogenation reaction was gauged only in terms of CO_2 rate enhancement ratio (5) [17], because, according to literature [5, 12, 13], in the case of CO_2 hydrogenation on metal catalysts deposited on YSZ (an O^{2-} ion conductor), O_2 is not a reactant and, therefore, any positive potential-induced catalytic rate change is due to electrochemical promotion independently of the value of the Faradaic

efficiency. The same can be reasoned in the case of negative potential, because even if CO_2 is decomposed via O^{2-} removal from the catalyst surface, this does not lead to H_2O formation.

CO_2 rate enhancement ratio is defined as (5):

$$\rho CO_2 = \frac{rCO_2^p}{rCO_2^{up}} \quad (5)$$

Where rCO_2^p and rCO_2^{up} are the CO_2 catalytic rates with (under application of a given potential V) and without (unpromoted reference state, under open circuit conditions 0 V) electrochemical promotion, respectively.

3. Results and Discussion

3.1 Catalyst characterisation studies

As reported in literature [6, 19–24], the utilised preparation technique determines also porous structure, surface morphology and particle size of the metal thin film and therefore the electrochemically assisted catalytic behaviour of the system. SEM micrographs of Pt, Ni and Pd catalyst-working electrode films, both as prepared (a) and after reduction and testing (b), are shown in Figs. 1 to 3, respectively. In all cases, the obtained metal film seems to resemble a typical foam structure [25], suggesting that they are porous (allowing reactants and products diffusion), and continuous, as verified by electrical conductivity measurements. Therefore, the utilised preparation methods led to catalyst films with suitable morphology and electrical properties for electropromoted experiments [20].

As can be obtained from Figs. 1a to 3a, the particle diameter of as deposited Pt, Ni and Pd catalyst films was about 500 nm (typically obtained for conventional Pt-painted films [8]), 300 nm and 150 nm, respectively. The catalyst film metal dispersion has been also estimated

from the obtained particle diameter and resulted to be of about 0.4 % [26], 0.28 % [13] and 0.75 % [27], for Pt, Ni and Pd, respectively.

XRD patterns of the Pt, Ni and Pd catalyst-working electrode films, both as prepared and after reduction and testing, are also depicted in Figs. 4 to 6, respectively. XPS spectra of the fresh (as deposited) and used (after reduction and testing) Pt, Ni and Pd catalyst films are, as well, shown in Figs. 7 to 9, correspondingly.

XRD spectra of the fresh (as prepared) and used (after exposure to reaction conditions) samples of Pt film are compared in Fig. 4. The peaks at 2θ=39.8º, 46.2º, 67.5º, 81.3º and 85.7º were identified as the typical diffraction peaks of Pt metal (JCPDS card no. 04-0802); whereas the rest of peaks were assigned to the YSZ solid electrolyte (JCPDS card no. 98-009-0891). No peaks of platinum oxide, or other phases, were detected for the samples both as prepared and after reduction and testing,

As can be deduced by SEM and XRD analysis (Figs. 1 and 4), it seems that exposure of the Pt catalyst film to hydrogen and reducing testing gas environment resulted in sintering and agglomeration of Pt particles, giving rise to an increase in crystallinity, as resembled by the fact that typical XRD peaks of metallic Pt exhibited higher intensity in the used sample.

The XPS analysis of both the fresh (as deposited) and used (after reduction and testing) samples seems to indicate that Pt is mainly present as metal as suggested by the appearance of peaks at binding energies of about 70.5 and 70.7 eV [28], respectively, in the Pt $4f_{7/2}$ spectra.

XRD spectra of the fresh (as prepared) and used (after exposure to reaction conditions) samples of Ni film are compared in Fig. 5. The following peaks correspond to the Ni phases:

- Metallic nickel. Peaks at 2θ=44.4º, 51.8º and 76.3º, 2θ=39.2º, 42.6º and 45.3º and 2θ=41.7º which matched well with the reference JCPDS cards no. 98-026-0169, 89-7129 and 45-1027, respectively

- Nickel oxides. Peaks observed at 2θ of 36.3º, 43.6º and 75.2º can be identified, respectively, for NiO_2 (JCPDS card no. 89-8397), Ni_2O_3 (JCPDS card no. 14-0481) and NiO (JCPDS card no. 04-0835) phases.
- Nickel hydroxides. Peaks at 2θ equal to 46.6º and 52.7º could be indicative of the presence of α-$Ni(OH)_2$ (JCPDS card no. 38-0715) and γ-$Ni(OH)_2$ (JCPDS card no. 84-1459) phases, respectively.

The rest of the peaks may be ascribed to the YSZ solid electrolyte (JCPDS card no. 98-009-0891). Apart from a weak diffraction corresponding to the main peak (at 2θ=44.4º) of face centred cubic (fcc) Ni phase (JCPDS card no. 98-026-0169), reflections of the rest of Ni phases (oxides and hydroxides) were undetectable in the XRD pattern of the fresh sample. This seems to indicate that the as-deposited film is almost XRD-amorphous or nanocrystalline.

It can be observed in Figs. 2 and 5 that the used sample showed higher particle size (SEM) and higher crystallinity (XRD), as resembled by the fact that additional reference XRD peaks of metallic Ni, Ni oxides and hydroxides appeared and the main metallic Ni XRD peak at 2θ=44.4º exhibits higher intensity in the used sample. The XPS analysis of the fresh (as prepared) sample revealed the presence of several superficial compounds that could not be identified by XRD, resulting in Ni being present as 23.5 % metal, 12.4 % oxide (NiO) and 64.1 % hydroxide/oxohydroxide as shown by the appearance of peaks at binding energies of about 852.53, 854.47 and 856.16 eV [29, 30], respectively, in the Ni $2p_{3/2}$ spectra. The appearance of two peaks at 531.64 and 533.5 eV in the O1s spectra seems to confirm the presence of OH groups (94.5 %) and NiO (5.5 %) [29] in the fresh sample.

The XPS spectra of the used sample revealed also the coexistence of Ni, NiO and Ni hydroxides/oxohydroxides as resembled by the appearance of peaks at binding energies of about 851.3, 853.21 and 856.13 eV, respectively, in the Ni $2p_{3/2}$ spectra. However, the

percentage of metallic Ni and NiO increases (to 36.9 % and 39.1 %, respectively) and of Ni hydroxides/oxohydroxides decreases (to 24.1 %) in used samples. The O1s spectra showed also that oxygen could be present as OH groups (85.7 %) and NiO (14.3 %) as indicated by the appearance of peaks at binding energies of about 532 and 530 eV [29], respectively. These results suggest that the Ni film could be partially reduced under reaction gas environment to Ni and oxidized/re-oxidized to NiO in the presence of surface O^{2-} ions.

XRD spectra of the fresh (as prepared) and used (after exposure to reaction conditions) samples of Pd film are compared in Fig. 6. The following peaks correspond to the Pd phases:

- Metallic palladium consistent with a face centred cubic (fcc) structure where reflections appear at 40.1º, 46.6º, 68.1º corresponding, respectively to the (111), (200) and (220) planes of Pdº (JCPDS card no. 05-0681).
- Palladium oxide consistent with a tetragonal structure where a reflection appears at 33.9º corresponding to the (101) plane of PdO (JCPDS card no. 41-1107).

The rest of the peaks may be ascribed to the YSZ solid electrolyte (JCPDS card no. 98-009-0891). There was no clear sign of the PdO_2 phase in the XRD patterns of both fresh and used samples.

The fresh sample (as prepared) of Pd film showed reflections of both metallic palladium and palladium oxide (PdO), whereas the used sample exhibited only higher characteristic peaks of the metallic phase.

It seems that exposure of the Pd catalyst film to hydrogen and reducing testing gas environment resulted in an almost complete reduction of Pd oxide to metallic Pd and in sintering of metallic Pd particles, giving rise to an increase in Pd particle size (Fig. 3), as resembled by the fact that reference XRD peak of PdO almost disappeared and metallic Pd XRD peaks turned sharper in the used sample. It suggests that the cristallinity of Pd film significantly increases upon reduction and testing.

The XPS analysis of the fresh (as prepared) sample results in Pd being present as 78 % PdO and 22 % PdO_2, as resembled by the appearance of peaks at binding energies of about 336.7 and 338.17 eV [31, 32], respectively, in the Pd $3d_{5/2}$ spectrum. For the used sample, the Pd $3d_{5/2}$ band was observed at 335.14 eV [31, 32], indicating that most of the Pd was reduced to the Pd^o state, in accordance with XRD results.

3.2 Electrochemically assisted CO_2 hydrogenation tests

3.2.1 Electrochemically assisted CO_2 hydrogenation tests on Pt

The steady state effect of polarization on the behaviour of Pt/YSZ/Au was investigated through potentiostatic experiments performed at different H_2/CO_2 ratios (1, 2, 3 and 4) at 400 ºC and 90 l h^{-1}. The behaviour of the catalyst under low H_2/CO_2 ratios, which correspond to a lack of H_2 in relation to the stoichiometry of the synthesis (1) and, more specifically, methanation (6) reactions, was analysed in order to consider the less favourable, although more realistic, conditions associated with a discontinuous flow of H_2 [2].

$$CO_2 + 4\,H_2 \rightarrow CH_4 + 2\,H_2O \qquad \Delta G^o = -130.7\ \text{kJ mol}^{-1} \quad (6)$$

Fig. 10a depicts the response of CO_2 conversion and CO_2 rate enhancement ratio to different applied catalyst potentials (between -2 and 2 V). As well, Fig. 10b shows the effect of applied potential on the selectivity to CO, C_2H_6 and C_3H_6, respectively. The experiments were carried out at 400 ºC and 90 l h^{-1} and using a H_2/CO_2 ratio of 1.

As can be observed in Fig. 10b, for H_2/CO_2 ratios of 1, the hydrogenation of CO_2 over Pt, at 400 ºC and 90 l h^{-1}, gives rise to CO (2), C_2H_6 (7) and C_3H_6 (8) formation and is affected

significantly by the applied potential, with selectivities to CO, C_2H_6 and C_3H_6 up to 64.4 %, 44.8 % and 2.9 %, respectively.

$$2\,CO_2 + 7\,H_2 \rightarrow C_2H_6 + 4\,H_2O \qquad \Delta G^o = -192.7\ kJ\ mol^{-1} \quad (7)$$

$$3\,CO_2 + 9\,H_2 \rightarrow C_3H_6 + 6\,H_2O \qquad \Delta G^o = -177\ kJ\ mol^{-1} \quad (8)$$

The CO_2 hydrogenation can be electrochemically assisted for both positive and negative potentials, but CO_2 rate enhancement ratios are rather low (up to about 2), whereas CO_2 conversion attained a maximum value of 4.5 %.

The catalyst shows an "inverted volcano" electrochemical behaviour (Fig. 10a), i.e., CO_2 rate enhancement ratio exhibits a minimum at certain potential. This behaviour can be attributed to the increase of hydrogen (electron donor) and CO_2 (electron acceptor) adsorption strength and surface coverage upon positive and negative polarization, respectively, as expected from the rules of electrochemical promotion [5, 12]. The difference in the rate enhancement observed for negative and positive potential application can be attributed to the difference in the chemisorption propensity of CO_2 and hydrogen on Pt. CO_2 is less easily adsorbed on Pt compared to H_2, thus enhancement of its chemisorption via negative polarization is expected to have a more significant impact on the rate [10].

However, selectivity to hydrocarbons (C_2H_6 and C_3H_6) diminished with potential decrease within the negative range (Fig. 10b), i.e., an electrophobic electrochemical behaviour is observed, while selectivity to CO increases with decreasing catalyst potential (Fig. 10b), showing an electrophilic electrochemical behaviour [8, 33].

As can be deduced from Fig. 10b, CO and C_3H_6 are formed dominantly for all range of potentials, showing opposite trends against applied potential, whereas C_2H_6 production is strongly promoted at positive potentials, being a competition for the formation of the different hydrogenation products over the catalyst surface.

In fact, as shown in Fig. 10b, with increasing catalyst potential by approximately 1.5 V (from 0.5 to 2 V), the selectivity to C_2H_6 increases by up to 6 times. As can be also observed in Fig. 10b, with decreasing catalyst potential by about 1 V (from -0.5 to -1.5), CO selectivity increases and C_3H_6 selectivity decreases by up to about 1.2 times.

RWGS reaction (2) is thermodynamically favoured under the utilised stoichiometric H_2/CO_2 ratio of 1 [2, 34] in front of hydrocarbon formation reactions.

Chemisorption of reactive molecules on a catalyst surface is the previous step to any catalytic process. Chemisorption of an adsorbate on a metal gives rise to a real chemical bond, thus implying electron donation from adsorbate to metal or from metal to adsorbate. In the first case, the adsorbate is called electron donor (electropositive), whereas in the second, is called electron acceptor (electronegative). There is a certain scale of electronegativity or electron acceptor capacity, in which oxygen is one of the strongest electron acceptors. The concept of electropositive or electronegative is also valid for the promoter ions in charge of the phenomenon, being these cations (electropositive promoters) and anions (electronegative promoters), respectively [8].

The origin of the electrochemical activation relies on the modification of adsorption phenomena. In the electrochemical promotion, promoter species are ions which electrochemically migrate in a controlled manner from the support (solid electrolyte) to the metal. The migration of these ions are accompanied by that of the corresponding charge compensation ion, forming neutral surface dipoles which are distributed along the metallic surface giving rise to the «effective double layer». Formation of the effective double layer gives rise to a change in the work function of the metal catalyst (Φ), modifying its bond capacity which each reactives, and therefore its catalytic behaviour [8, 33].

On the one hand, the increment in catalyst work function of the metal catalyst by addition of an electronegative promoter (O^{2-} for YSZ), via application of positive potentials, favoured

the adsorption of electron donor species (H_2), because the electrode becomes positively charged (due to a defect of electrons), favouring the transfer of electrons from electron donor molecules, like H_2, to the Pt catalyst and thus the adsorption of the latter on the Pt catalyst surface, whereas at the same time hindered the adsorption of electron acceptor species (CO_2 in this case), giving rise to an increase in H_2 (electron donor) coverage and to a decrease in the coverage of CO_2 (electron acceptor). The opposite occurs for application of negative potentials which results in the removal of O^{2-} promoter species from the Pt catalyst electrode to the solid electrolyte, giving rise to a decrease of the catalyst work function, i.e., the electrode becomes negatively charged (due to an excess of electrons), which favours the transfer of electrons from the Pt catalyst to electron acceptor molecules, like CO_2, and, thus, the adsorption of the latter on Pt catalyst surface, whereas at the same time hindered the adsorption of electron donor species (H_2 in this case), giving rise to an increase in CO_2 (electron acceptor) coverage and to a decrease in the coverage of H_2 (electron donor) [8–10, 12, 33].

In this way, depending on the relative electronegativity of the different adsorbates involved in the reaction and on which of them is in excess over the catalyst surface, the application of polarization will have a positive or negative effect on the overall kinetics of the process [8, 33]. Namely, the electrochemical promotion allows modifying the adsorption of the different reactive molecules over the catalyst-electrode surface. Thus, there is a given value of potential or promoter coverage which optimizes catalyst activity and selectivity to the desired product, which depends on temperature and gas composition.

Therefore, the observed electropromoted catalytic behaviour can be rationalized considering the effect of varying applied potential on the chemisorptive bond strength of reactants and intermediate surface species [8, 33] and in accordance with the mechanisms proposed for the CO_2 hydrogenation reaction [5, 7, 9–13, 35–41]. CO_2 does not chemisorb on

clean Pt surfaces, only physisorbs weakly and molecularly at low temperature and desorbs without undergoing detectable dissociation at high temperature [42–44].

The pumping of O^{2-} species away from the catalyst surface to the solid electrolyte YSZ, enhances CO_2 adsorption and activation (9), resulting in the formation of a highly distorted CO_2 molecule (CO_2^{*-}) interacting strongly with the surface [45], which indicate that CO_2 is always adsorbed as an electron acceptor [8].

$$CO_2 + e \rightarrow CO_2^{*-} \text{ (ads.)} \qquad \Delta G^o = 183.3\,\text{kJ mol}^{-1} \quad (9)$$

The application of positive potentials give rise to a migration of oxygen ions to the catalyst surface, favouring H_2 (electron donor) dissociative adsorption (10) on Pt surface and resulting in an increase of the surface coverage of hydrogen and in a decrease in CO_2 coverage, being CO_2 (electron acceptor) adsorption the reaction limiting step.

$$H_2 \rightarrow 2\,H^{*+} \text{ (ads.)} + 2\,e \qquad \Delta G^o = 38.9\,\text{kJ mol}^{-1} \quad (10)$$

At high O_2^- coverage or positive potentials, CO_2 dissociative adsorption on Pt is considered to be enhanced by the presence of coadsorbed hydrogen (11) [10, 11, 35, 39, 46]. CO adsorbed species resulting from CO_2 dissociation may desorb in the gas phase (12) or can be gradually hydrogenated resulting finally in hydrocarbon (mainly C_2H_6 and C_3H_6) formation, expressed as (13) [23, 36, 37, 39, 47]. CO dissociation (14) is restricted on the big Pt particles of this low dispersed electrocatalyst [10, 19], as seems to be confirmed by the fact that CH_4, which can be potentially formed by hydrogenation of surface carbon species resulting from CO dissociation [5, 9, 11, 13, 41], was not detected in the reactor effluent.

$$CO_2^{*-} \text{ (ads.)} + e + 2\,H^+ \rightarrow CO^* \text{ (ads.)} + H_2O \qquad \Delta G^o = 19.9\,\text{kJ mol}^{-1} \quad (11)$$

$$CO^* \text{ (ads.)} \rightarrow CO \qquad (12)$$

$$x\,CO^* \text{ (ads.)} + (2x + y)\,H \text{ (ads.)} \rightarrow C_xH_y + x\,H_2O \qquad (13)$$

$$CO^* \text{ (ads.)} \rightarrow C^* \text{ (ads.) } (CH_4 \text{ precursors}) + O \qquad \Delta G^o = 137.2\,\text{kJ mol}^{-1} \quad (14)$$

Even though that the electropromoted experiments were carried out at a H_2/CO_2 ratio of 1, which is lower than the stoichiometrically required for C_2H_6 and C_3H_6 formation (about 3), at high positive potentials (hydrogen adsorption region), hydrogen coverage is supposed to be higher than that of CO adsorbed species resulting from CO_2 dissociation [12], and, thus, they can be gradually hydrogenated to hydrocarbons. CO adsorption may be also retarded at high positive potentials (CO is a weaker electron donor than hydrogen) and it tends to desorb (12) and, thus, RWGS may become the predominant reaction under these conditions.

Upon application of negative polarization, a migration of oxygen ions from the catalyst surface to the solid electrolyte is produced, decreasing oxygen surface coverage [8]. As a result, the adsorption of electron acceptor species, as CO_2 (9), is favoured [33] due to its higher electronegativity [48], increasing their surface coverage at the expense of electron donors (hydrogen) and giving rise to a progressive increase in surface CO formation by dissociative adsorption of CO_2, whereas H_2 (electron donor) dissociative adsorption on Pt is hindered and therefore hydrogen evolution is favoured [5, 12]. As a result, CO selectivity increases and selectivity to C_3H_6 and C_2H_6 decreases on decreasing catalyst potential [12].

In fact, under application of negative potentials, a strengthening of the Pt-(CO_2)* bond strength is achieved [12], since O^{2-} species are pumped away from the catalyst surface to the solid electrolyte (YSZ), enhancing CO_2 adsorption and activation (9), whereas H_2 dissociative adsorption (10) on Pt surface is hindered. Negative polarization also strengths Pt-C bond and weakens C-O bond enhancing CO_2 dissociation to CO (15), resulting in an enhancement of CO formation [9, 10, 12]. Moreover, CO dissociative adsorption is less favoured at negative potentials (CO has a lower electron acceptor capacity than CO_2) [8, 10, 33, 49] and it tends to desorb (12). Both phenomena result in an increase in the selectivity to CO.

$$CO_2^{*-}\ (\text{ads.}) + e \rightarrow CO^{*}\ (\text{ads.}) + O^{2-} \qquad \Delta G^{o} = 257.2\ \text{kJ mol}^{-1} \quad (15)$$

On the contrary, selectivity to C_2H_6 and C_3H_6 decreases for negative potentials, because H_2 adsorption is retarded and therefore tends to be evolved from the catalyst surface [5, 12]. In addition, as commented above, the utilised H_2/CO_2 ratio is lower than that stoichiometrically required for hydrocarbon formation (about 3) and therefore, at negative potentials (hydrogen evolution region), H_2 coverage is lower than the coverage of species resulting from CO_2 dissociation and they cannot be completely hydrogenated to hydrocarbons [2, 11, 12].

Fig. 11a shows the steady state effect of the applied potential on CO_2 conversion and CO_2 rate enhancement ratio (Fig. 11a) and on the selectivity to CO, C_2H_6, C_3H_6, CH_4 and CH_3OH (Fig. 11b), respectively, at 400 ºC and 90 l h^{-1} and using a H_2/CO_2 ratio of 2.

As can be observed in Fig. 11b, for H_2/CO_2 ratios of 2, the hydrogenation of CO_2 over Pt/YSZ/Au, at 400 ºC and 90 l h^{-1}, gives rise to the formation of CH_4 (6) and CH_3OH (16) in addition to CO (12), C_2H_6 and C_3H_6 (13), being a competition for the formation of the different hydrogenation products over the catalyst surface, and it is, as well, perceptibly influenced by the applied potential, with selectivities to CH_4, C_2H_6, C_3H_6, CO and CH_3OH up to 3 %, 1.3 %, 42.7 %, 59.1 % and 8.1 %, respectively.

$$CO_2 + 3H_2 \rightarrow CH_3OH + H_2O \qquad \Delta G^o = -9.1 kJ\,mol^{-1} \quad (16)$$

Also in this case, CO and C_3H_6 are produced dominantly for all range of potentials, but showing similar trends against potential variation for potentials above -0.5 V and opposite tendency for lower potential values, where the formation of the rest of the products is almost negligible.

CO_2 rate enhancement ratio values are rather low (around the unity), but CO_2 conversion is fairly high (up to 24.5 %). The catalyst showed also an “inverted volcano type” electrochemical behaviour, i.e., CO_2 rate enhancement ratio exhibits a minimum at a certain potential (under open circuit conditions approx.) (Fig. 11a) [8, 33]. By comparison of Figs. 10 and 11, it can be deduced that, at a given applied potential, CO_2 conversion and CO_2 rate

enhancement ratio obtained for a H_2/CO_2 ratio of 2 are shifted to higher and lower values, respectively, relative to those obtained using a H_2/CO_2 ratio of 1. Therefore, there is an increase in CO_2 conversions and a decrease in promotion levels on increasing H_2/CO_2 ratio from 1 to 2. The increase in CO_2 conversions is thought to be due to the fact that a H_2/CO_2 ratio of 2 corresponds to that stoichiometrically required for total carbon dioxide reduction (17), being it thermodynamically favoured and contributing in a greater extent to CO_2 conversion under this H_2/CO_2 ratio [2, 34].

$$CO_2 + 2\,H_2 \rightarrow C + 2\,H_2O \qquad \Delta G^o = -79.9\ kJ\ mol^{-1} \quad (17)$$

As commented above, CH_4 (6) was also detected to be produced at positive potentials under these conditions, supposedly resulting from the formation via CO_2 reduction (18) [2, 13, 41], which is thermodynamically favoured under these conditions [34], and subsequent hydrogenation (19) of reactive surface carbon species.

$$CO_2^{*-}(ads.) + 4\,e \rightarrow C^*(ads.)\,(CH_4\ precursors) + 2\,O^{2-} \qquad \Delta G^o = 394.4\ kJ\ mol^{-1} \quad (18)$$

$$C^*(ads.) + 4H(ads.) \rightarrow CH_4 \qquad \Delta G^o = -50.7\ kJ\ mol^{-1} \quad (19)$$

Selectivity to CH_4 sharply decreases upon application of negative polarization (Fig. 11b), showing an electrophobic electrochemical behaviour. In fact, as Fig. 11b shows, the selectivity to methane increases by up to 30 times on increasing applied potential by approximately 1 V (from 0 to 1 V). CH_4 selectivity drops to almost zero for negative potentials because H_2 adsorption is retarded and H_2/CO_2 ratio is lower than that required by stoichiometry for CH_4 formation (about 4) [2], and, therefore, coverage of carbon species resulting from CO_2 reduction [13, 41] are expected to be higher than H_2 coverage [12]. As a result, H_2 tends to be evolved from the catalyst surface while carbon species may accumulate on the catalyst surface [2].

As commented above, the variation of CO_2 rate enhancement ratio vs. potential resembles an “inverted volcano type” behaviour. However, the differences are not significant between

results obtained at different potentials and CO_2 rate enhancement ratio is always around 1. As commented before, the electrochemical promotion of catalysis is due to electrochemically controlled migration of promoting ions between the solid electrolyte support and the metal catalyst surface, through the catalyst-gas-electrolyte three-phase boundary (tpb). Therefore, the low promotion levels observed under these experimental conditions could be indicative of partial blocking of the tpb [12] by carbonaceous species formed via the electrochemical reduction of CO_2 (17) taking place at the tpb which is thermodynamically favoured under this H_2/CO_2 ratio [34], hindering the migration of oxygen promoter ions through the "tpb" [12].

CH_3OH was also detected to be formed under these conditions. The equilibrium conversion of CO_2 to methanol increases with the increase of pressure and decreases strongly as the temperature increases [47, 50]. In addition, methanol is reported to be transformed into hydrocarbons at temperatures about 400 ºC [50], where RWGS and methanation reactions are also favoured [5]. However, CH_3OH formation seems to be thermodynamically favoured for the utilised H_2/CO_2 ratio of 2, because this value corresponds to the stoichiometric ratio required for CH_3OH formation by hydrogenation of the CO (20) resulting from CO_2 dissociative adsorption (equations 11 or 15).

$$CO^{*}\,(ads.) + 4\,H\,(ads.) \rightarrow CH_3OH \qquad \Delta G^{o} = -29.1\,kJ\,mol^{-1} \quad (20)$$

As can be observed in Fig. 11b, the optimum applied potential for CH_3OH formation is about 0.5 V, which corresponds with an enhancement in their selectivity of up to about 800 times, increasing or decreasing applied potential from this value resulted in a decrease in CH_3OH selectivity. CO selectivity and selectivity to C_3H_6 exhibit a concomitant minimum at this potential, which correspond with a decrease in CO and C_3H_6 formation of up to approximately 4.4 % and 20.5 %.

As commented above, around open circuit conditions (0 V), at low negative or positive potentials, selectivity to CH_3OH exhibited a maximum, showing a "volcano type"

electrochemical behaviour. In fact, formation of CH_3OH is reported to be enhanced over almost free Pt surfaces (low surface coverage of both CO_2 and H_2). CO_2 does not adsorb on clean Pt surfaces [42–44] and, at the same time, Pt is very catalytic for hydrogen evolution, therefore, a strong competition between CO_2 and H_2 adsorption could be expected within this potential range, being surface coverage of both reactants very similar, and, thus, according to this mechanism, it is expected that the formation of CH_3OH will be limited by the dissociative adsorption of both H_2 and CO_2 [36, 37]. As a consequence, for a H_2/CO_2 ratio of 2, hydrocarbon and CO formation competitive reactions are hindered and, as a result, selectivity to C_3H_6 and CO exhibited a minimum at the same potential value, resembling an "inverted volcano type" electrochemical behaviour. Negative potential application gives rise to an enhancement of CO_2 dissociative adsorption on Pt surface, via formation of adsorbed CO species, and to a decrease in H_2 dissociative adsorption. As a result, selectivity to C_3H_6 and CO increases on decreasing applied potential within negative values due to the enhanced adsorbed CO species formation and CO evolution, as a result of the improved CO_2 dissociation via O^{2-} abstraction, because, in spite of hydrogen evolution (which may limit the CO_2 hydrogenation) is also favoured on decreasing applied potential, under a stoichiometric H_2/CO_2 ratio of 2, hydrogen coverage is still enough [12] for CO adsorbed species to be hydrogenated to C_3H_6, given that CH_3OH formation is inhibited (sharply decrease to almost zero) for negative potentials [36]. As a consequence, C_3H_6 formation and RWGS competitive reactions are increasingly promoted, resulting in an increase in CO and C_3H_6 selectivity, showing opposite trends, with the decrease in potential.

Selectivity to C_2H_6 is almost negligible reaching a maximum of 1.3 % under open circuit conditions (0 V), resembling also a "volcano type" electrochemical behaviour.

The steady state response of CO_2 conversion and CO_2 rate enhancement ratio to different applied catalyst potentials (between -2 and 2 V) is displayed in Fig. 12a. Fig. 12b shows the

effect of applied potential on the selectivity to CO, CH_3OH, C_2H_6, and C_3H_6, respectively, at 400 ºC and 90 l h^{-1} and using a H_2/CO_2 ratio of 3.

As can be observed in Fig. 12b, for H_2/CO_2 ratios of 3, the hydrogenation of CO_2 over Pt/YSZ/Au, at 400 ºC and 90 l h^{-1}, gives rise to the formation of CO (2), CH_3OH (16), C_2H_6 (7) and C_3H_6 (8), and it is, as well, considerably influenced by the applied potential, with selectivities to C_2H_6, C_3H_6, CO and CH_3OH up to 53 %, 32.7 %, 55 % and 2.8 %, respectively.

In this case, the electrochemical behaviour is very similar to that observed for a H_2/CO_2 ratio of 2.

The main products resulting from CO_2 hydrogenation are CO, C_2H_6 and C_3H_6. The selectivity to C_2H_6 and C_3H_6 follows opposite and similar trends, respectively, vs. applied potential with respect to that of CO selectivity. CO_2 rate enhancement ratio values are also low (up to about 2.3) with CO_2 conversions up to 9 %. The catalyst showed also an "inverted volcano type" electrochemical behaviour, showing also a minimum in CO_2 rate enhancement ratio at around 0 V (open circuit conditions) (Fig. 12a) [8, 33]. As can be observed in Fig. 12b, up to - 0.5 V, selectivity to CH_3OH and C_2H_6 showed also a maximum at 0 V, whereas CO and C_3H_6 selectivities exhibit a concomitant minimum at the same potential value. However, for potential values below -0.5 V, selectivities to CH_3OH, C_3H_6 and C_2H_6 increase on decreasing applied potential, while CO selectivity diminishes on lowering applied potential.

A H_2/CO_2 ratio of 3 is about the stoichiometric ratio required for C_2H_6, C_3H_6 and CH_3OH formation by CO_2 hydrogenation via reactions (7), (8) and (16), respectively, and thus they are thermodynamically favoured under these conditions. As can be observed in Fig. 12b, in this case, for potential values above -0.5 V, the optimum applied potential for CH_3OH and C_2H_6 formation is about 0 V, which corresponds with an enhancement in their selectivity of

up to about 4 and 11 times, respectively. CO selectivity and selectivity to C_3H_6 exhibit a concomitant minimum at this potential, which correspond with a decrease in CO and C_3H_6 formation of up to approximately 64 % and 46 %, correspondingly. As commented above, formation of CH_3OH and C_2H_6 are enhanced around open circuit conditions (0 V), as a consequence, C_3H_6 and CO formation competitive reactions are retarded.

A subsequent decrease in potential below -0.5 V, gives rise to an increase in CH_3OH, C_3H_6 and C_2H_6 selectivity and a concomitant decrease in selectivity to CO, as a result of the improved CO_2 dissociative adsorption, via O^{2-} abstraction, because, in spite of hydrogen evolution (which may limit the CO_2 hydrogenation) is also favoured on decreasing applied potential, under a stoichiometric H_2/CO_2 ratio of 3, hydrogen coverage is higher enough for CO adsorbed species to be further hydrogenated to hydrocarbons and CH_3OH, given that CH_3OH is reported to block active sites for RWGS reaction, forming surface intermediates which favours the hydrocarbon synthesis reaction [5]. Moreover, as more water is formed from CO_2 hydrogenation reactions, the amount of CO could decrease also trough the WGS (water gas shift) (21) reaction [51], resulting in a concomitant decrease in CO yield.

$$CO + H_2O \rightarrow CO_2 + H_2 \qquad \Delta G^o = -19.9\ kJ\ mol^{-1} \quad (21)$$

The steady state response of CO_2 conversion and CO_2 rate enhancement ratio to different applied catalyst potentials (between -2 and 2 V), at 400 ºC and 90 l h^{-1} and using a H_2/CO_2 ratio of 4, is displayed in Fig. 13a. Fig. 13b shows the effect of applied potential on the selectivity to CO, CH_3OH, C_2H_6, and C_3H_6, respectively, under the same conditions.

As can be observed in Fig. 13b, for H_2/CO_2 ratios of 4, the hydrogenation of CO_2 over Pt/YSZ/Au, at 400 ºC and 90 l h^{-1}, gives rise also to the formation of CO (2), CH_3OH (16), C_2H_6 (7) and C_3H_6 (8), and it is, as well, affected by the applied potential, with selectivities to C_2H_6, C_3H_6, CO and CH_3OH up to 4.8 %, 73.3 %, 72.5 % and 0.9 %, respectively.

The obtained results are very similar to those found for a H_2/CO_2 ratio of 3.

The main products resulting from CO_2 hydrogenation are again CO, and C_3H_6. The selectivity to C_2H_6 and C_3H_6 follows the same trend vs. applied potential, and opposite tendency in relation to that of CO selectivity. CO_2 rate enhancement ratio values are again rather low (up to about 3.2) with CO_2 conversions up to 10 %. The catalyst resembled, as well, an "inverted volcano type" electrochemical behaviour, showing also a minimum in CO_2 rate enhancement ratio at about 0.5 V (Fig. 13a) [8, 33]. However, contrary to that observed for a H_2/CO_2 ratio of 3, for potential values above – 0.5 V (Fig. 13b), selectivity to C_3H_6 shows a "volcano type" electrochemical behaviour reaching a maximum at 0 V, whereas selectivity to CH_3OH is almost negligible. However, for potential values below -0.5 V, the variation of C_3H_6, C_2H_6 and CO selectivities vs. applied potential is the same than that observed for a H_2/CO_2 ratio of 3. The above commented change in the electrochemical behaviour of the catalyst in terms of C_3H_6 selectivity on increasing H_2/CO_2 ratio from 3 ("inverted volcano type" behaviour) to 4 ("volcano type" behaviour) could be because for H_2/CO_2 ratios of 4 (higher than the required stoichiometric ratio), hydrogen coverage is always higher than that of adsorbed CO resulting from CO_2 dissociation [12] and, thus, it can be gradually hydrogenated to the different products. Therefore, the competition between the different hydrogenation reactions is less pronounced as a result of the increased H_2 availability.

In this case the maximum in C_3H_6 and C_2H_6 formation corresponds with an enhancement in their selectivity of up to about 3 and 2 times, respectively, whereas the concomitant minimum in CO formation corresponds with a decrease in its selectivity of up to approximately 69 %.

For better understanding of the influence of H_2/CO_2 ratio on catalyst behaviour and selectivity to the different products, the potentiostatic variation of CO_2 conversion, CO_2 rate enhancement ratio and selectivity to CO, C_3H_6, C_2H_6, and CH_3OH is plotted for different

H_2/CO_2 ratios in Figs. 14a to 14f, respectively. Results indicate that, in general, for highly positive and negative potentials, CO_2 conversion increases with the increment in H_2/CO_2 ratio from about 4 % for H_2/CO_2=1 to 10 % and 9 % for H_2/CO_2 ratios of 4and 3, respectively, supposedly as a result of the increased hydrogen availability with respect to the stoichiometrically required for the synthesis of the different hydrogenated products. Except in the case of H_2/CO_2 ratio of two where the CO_2 conversion vs. potential curve is shifted to the highest values of conversion (around 24.5 %), being ascribed, as commented above, to the additional contribution of total CO_2 reduction reaction (18) to CO_2 consumption. On the contrary, as can be deduced from Fig. 14b, CO_2 rate enhancement ratios, i.e., promotion levels, decrease on increasing H_2/CO_2 ratio, from about 1.9 for H_2/CO_2=1 to around 1.7 for H_2/CO_2=4, being minimum for a H_2/CO_2 ratio of 2 (around 1.3), which is thought to be due to, as indicated before, hindering of O^{2-} ions migration by partial blocking of the tpb [12] via deposition of carbonaceous species resulting from the electrochemical reduction of CO_2 (18).

As can be also deduced from Fig. 14c, at highly positive and very negative potentials, selectivity to CO decreases and increases, from about 57 % to 39.5 % and from 55 % to 76 %, respectively, on increasing H_2/CO_2 ratio, clearly showing a minimum at about open circuit conditions at H_2/CO_2 ratios of 3 (of about 27 %) and 4 (of around 23 %), while selectivity to C_3H_6 (Fig. 14d) and/or C_2H_6 (Fig. 14e) showed, in general, an opposite trend vs. H_2/CO_2 ratio in relation to that of CO selectivity and a maximum of 73.3 % and 53 % at H_2/CO_2 ratios of 4 and 3, respectively, around open circuit conditions, depending on the balance between the different competitive CO_2 hydrogenation reactions involved and on the excess of surface hydrogen with respect to that theoretically required by stoichiometry for the hydrocarbon synthesis.

CH_3OH selectivity (Fig. 14f) exhibits a maximum (of about 8 %) around open circuit conditions, because the surface reaction could be restricted by the coverage of both CO_2 and

H_2 adsorbed on the Pt surface [36, 37], and for H_2/CO_2 ratios equal to two (of about 2 %), which is that required for stoichiometric synthesis of methanol by hydrogenation of the CO (20) resulting from CO_2 dissociative adsorption, and, therefore, thermodynamically favours the formation of CH_3OH as the expenses of other CO_2 hydrogenation products.

3.2.2 Electrochemically assisted CO_2 hydrogenation tests on Ni

Fig. 15 shows the steady-state effect of temperature on the conversion of CO_2 under open-circuit state (0 V, unpromoted conditions) and upon cathodic (-2 V) and anodic (+2 V) polarization conditions, at temperatures from 225 to 400 ºC and using 90 l h^{-1} of total gas flow rate and a H_2/CO_2 ratio of 4. The main products obtained (not shown) were hydrocarbons (mainly C_2H_6 and C_3H_6), although an almost negligible amount of CH_4 and CO was observed to be formed under certain polarization conditions at high temperatures.

As can be observed in Fig 15, CO_2 conversion monotonically decreases as temperature increases for whatever value of applied potential. This fact is in disagreement with the results obtained by other authors over carbon nanofiber supported Ni catalyst electrodes deposited on YSZ [13], but in this case the main products of CO_2 hydrogenation were CH_4 and CO.

The mechanism of CO_2 hydrogenation over Ni/YSZ [13] has been proposed to be the same as commented above for Pt/YSZ. Positive potential application, i.e., O^{2-} supplying from solid electrolyte to the catalyst surface favours H_2 (electron donor) dissociative adsorption (10) on Ni. CO_2 dissociative adsorption on Ni has been also considered to be enhanced by the presence of coadsorbed hydrogen (11) [52]. On the contrary, under negative polarization, O^{2-} species are pumped away from the catalyst surface to the solid electrolyte YSZ, enhancing CO_2 dissociative adsorption to CO (15). No CO was detected in the reactor effluent. It seems that the formed CO would be then irreversibly (owing rapid removal of surface O by

hydrogenation) dissociated into surface carbon species [6, 40, 53]. The adsorbed carbon species could accumulate on the surface or could be hydrogenated, resulting in the formation of adsorbed CH species [6, 40, 53]. Addition of hydrogen to these species would then lead to methane, whereas combination reaction of two or more adsorbed CH units would result in hydrocarbon formation (mainly C_2H_6 and C_3H_6) [53]. In agreement with literature, Ni is less active and selective toward CH_4 (chain lengthening occurs) synthesis from CO than in the Sabatier reaction (CO_2+H_2) [52]. In addition, it has been reported [54] that supported Ni enhanced the formation of higher molecular weight hydrocarbons compared to unsupported Ni. This modification in catalytic behaviour was attributed to changes in the adsorbed state of CO on Ni surfaces resulting from metal-support interactions or variations in nickel crystallite size [52]. As commented above, nickel is reported to favour the C-C bond rupture and, therefore, CO_2 (18) and CO (14) dissociation to surface carbon [55–58]. In addition, carbon deposition on Ni/YSZ has been reported [59] to originate from the dissociation of hydrocarbons and CO. The adsorbed carbon could accumulate, blocking pores and reactive sites, resulting in an excess of carbon on the catalyst surface and in a decrease in catalytic activity and, then, in catalyst deactivation [2, 59, 60]. Therefore, the obtained CO_2 conversion will be determined by the balance of carbon species formation and accumulation on the catalyst surface and their removal by gasification agents [56, 59]. Moreover, it has been reported that deactivation by carbon deposition on the catalyst surface may be favoured on the relatively large Ni particles (low dispersion and worse catalytic behaviour) obtained by the utilised “electroless” technique, because large Ni particles are reported to promote encapsulation of Ni particles with carbon plates, resulting in Ni poisoning due to the growing carbon layer on the catalyst surface [2, 57, 58, 60], reducing also access to gasification agents and therefore the reversibility of the carbon deposit [59]. In addition, larger Ni particles are reported to induce lower interaction with the oxygen ion conducting support (YSZ in this case), resulting in low oxygen mobility and

therefore hindering gasification of carbonaceous deposits with spillover of oxygen species to the catalyst surface [61, 62].

XPS results seem to confirm these assumptions. As commented above, the tested samples were characterised by XPS to obtain information about the nature and amount of the carbonaceous compounds formed. The carbon content in used samples increases regarding that initially present, which is usually found in fresh samples, due to contamination or from the catalyst preparation procedure. As determined by XPS, the C/Ni ratio in used samples (around 38) about doubled that of fresh samples (about 20). Three different types of carbon species were identified in the C 1s spectra of both fresh (Fig. 16a) and used (Fig. 16b) Ni samples. The main peak at binding energies around 284.6 eV could be attributed to graphitic-like carbon (C–C or C–H) [63, 64]. It was found that, in the used sample, the main peak increases and the difference spectrum (284.7 eV for fresh sample and 284.8 for used sample) may indicate the formation of graphite intercalation compounds [65]. Two additional shoulder peaks appear, together with the main peak, in the C 1s spectrum of the fresh/used sample, at binding energies at about 286.5/286.9 and 288.3 eV which may be assigned as ether groups (C–O) and carboxylic groups (C=O), respectively. The contribution of graphitic carbon (C–C or C–H) increases (from 87.3% to 93.5%), whereas those of ether (C–O) and carboxylic (C=O) groups decreases (from 7.4 % to 4.8 % and from 5.3 % to 1.7 %, respectively) in the used sample, suggesting that carbon deposition might preferentially create graphitic-like carbon structures.

Therefore, the decrease on CO_2 conversion on increasing temperature observed in Fig. 15 is thought to be due to Ni poisoning by carbon deposition, given that the amount of surface carbon adsorbed on the catalyst surface is expected to increase with time and temperature [2]. Moreover, the surface carbon formed is more strongly bound at increasing temperatures, as well, the maximum rate of surface carbon removal also increase with temperature [66]. The increase of carbon deposits around or near the metal particle is reported [67] to inhibit CO_2 dissociation and,

therefore, the hydrocarbon formation via hydrogenation of surface species resulted from CO_2 dissociative adsorption, contributing also to the observed decrease in CO_2 conversion. Site blocking by excess of surface CO_2 coverage could also retard CO_2 conversion [2].

As can be observed also in Fig. 15, CO_2 conversion vs. temperature curves obtained for positive (+2 V) and negative polarizations (-2V) are shifted to higher and lower conversion values, correspondingly, with respect to that obtained for open circuit conditions (0V).

The increase in conversion values obtained for positive polarization could be because upon application of positive potentials oxygen ions are transferred from the solid electrolyte to the Ni surface and could eliminate the deposited carbon on the Ni surface [66, 68, 69]. Moreover, positive polarization gives rise also to an increase of surface hydrogen coverage which could also contribute to gasification of surface carbon. However, CO_2 conversion decreases also with temperature as a result of the concomitant increase in the extent of carbon deposition and in the stability of the surface carbon species formed [66].

On the contrary, the decrease in CO_2 conversion levels observed under negative polarization could be due to the increased surface carbon formation as a result of the improved CO_2 dissociation, via O^{2-} abstraction, and enhanced hydrogen evolution.

The maximum CO_2 conversion was 28 % for a H_2/CO_2 ratio of 4 and under anodic polarization (2 V) and at temperature of 225 ºC. The maximum CO_2 rate enhancement ratio was about 1.6 for a H_2/CO_2 ratio of 4 and under anodic polarization (2 V) and at temperature of 350 ºC, which is in agreement with the fact that electrochemical promotion effect increases as temperature increases, as a result of the increased ionic conductivity at higher temperatures. Similar trends (not shown) in CO_2 conversion versus temperature dependence were obtained both under open circuit and polarization conditions using instead a H_2/CO_2 ratio of 1.

Fig. 17 compares CO_2 conversion vs. temperature curves obtained for different H_2/CO_2 ratios (4 and 1) under positive (Fig. 17a) and negative (Fig. 17b) polarizations, respectively.

As can be deduced from Fig. 17a, under positive polarization (V=2 V) where dissociative adsorption of H_2 is favoured, CO_2 conversion vs. temperature curve is shifted to lower conversion levels for the lower H_2/CO_2 ratio of 1. Therefore, decreasing hydrogen concentration in the reactive flow led to a decrease in CO_2 conversion as a result of the decrease in hydrogen surface coverage below that required by stoichiometry for CO_2 hydrogenation to the different hydrocarbons. On the contrary, as can be obtained from Fig. 17b, upon negative polarization (V=-2 V), where total CO_2 reduction via O^{2-} abstraction from the catalyst surface is favoured, CO_2 conversion vs. temperature curve is shifted to higher conversion levels for the lower H_2/CO_2 ratio of 1. This increase in conversion is thought to be due to the enhanced surface carbon formation. In fact, the lower hydrogen content in the gas feed mixture could also favour Ni poisoning by accumulation of adsorbed surface carbon as a result of the lesser hydrogen availability for surface carbon removal on using lower H_2/CO_2 ratios [2, 56–58], as seem to be resembled by the more pronounced slope (sharper CO_2 conversion decrease) of CO_2 conversion vs. temperature curve observed for the lower H_2/CO_2 ratio of 1 [2]. For a H_2/CO_2 ratio of 1, the maximum CO_2 conversion was about 20 % at 225 ºC and 2V, whereas the maximum CO_2 rate enhancement ratio slightly exceeded the unity.

As long as it was observed that the predominant products of the CO_2 hydrogenation reaction on Ni/YSZ were hydrocarbons (mainly C_2H_6 and C_3H_6), potentiostatic experiments were also carried out using the corresponding stoichiometric H_2/CO_2 ratio (around 3), at 400ºC and 90 l h^{-1}, for comparison with results obtained on Pt/YSZ under the same conditions.

The steady state response of CO_2 conversion and CO_2 rate enhancement ratio to different applied catalyst potentials (between -2 and 2 V), at 400 ºC and 90 l h^{-1} and using a H_2/CO_2 ratio of 3, is displayed in Fig. 18.

C_2H_6 and C_3H_6 are produced dominantly in the gas phase for all range of potentials.

CO_2 rate enhancement ratio values are also rather low (up to 2.4), but CO_2 conversion is fairly high (up to 22.8 %). The catalyst showed also a minimum at a certain potential (under open circuit conditions approx.), resembling an "inverted volcano type" electrochemical behaviour [8, 33], similar to that found for Pt/YSZ.

As commented above, also in the case of Ni/YSZ, application of negative potentials favours the dissociative adsorption of CO_2 on the Ni catalyst surface forming adsorbed CO which could be subsequently hydrogenated to hydrocarbons. On the contrary, application of positive potentials favours the dissociative adsorption of H_2 on the Ni catalyst surface, increasing the coverage of adsorbed hydrogen (electron donor) which induces hydrogen assisted CO_2 dissociative adsorption. Formed CO can be gradually hydrogenated to the different hydrocarbons. As commented above, carbon formation incoming from CO_2 reduction (18) and/or CO dissociation (14), via O^{2-} abstraction, could also contribute to CO_2 conversion, in special at highly negative potentials.

3.2.3 Electrochemically assisted CO_2 hydrogenation tests on Pd

The steady state effect of temperature on the behaviour of Pd/YSZ/Au was investigated through temperature programmed experiments (from 225 to 375 ºC) performed at different potentials and using a H_2/CO_2 ratio of 3 and 90 l h^{-1} of total gas flow rate.

Fig. 19a shows the effect of temperature on the conversion of CO_2 under open-circuit state (0 V, unpromoted conditions) and anodic (+2 V) polarization conditions, at temperatures from 225 to 350 ºC, using a H_2/CO_2 ratio of 3 and 90 l h^{-1} of total gas flow rate. As can be observed in Fig. 19b, the main products obtained were hydrocarbons (C_2H_6 and C_3H_6) and dimethyl ether (C_2H_6O), no CH_4 [10] and CO [70] formation was observed for the studied temperature range.

The mechanism of CO_2 hydrogenation over Pd/YSZ [10] has been proposed to be the same as commented above for Pt/YSZ. Under application of positive potentials, oxygen ions are pumped from the solid electrolyte to the catalyst surface, giving rise to an increase of the Pd catalyst work function [2–4, 10] which favours H_2 (electron donor) dissociative adsorption (10) on Pd increasing the surface coverage of adsorbed hydrogen (electron donor). CO_2 dissociative adsorption on Pd has been also reported to be enhanced by the presence of coadsorbed hydrogen (11) [10]. CO adsorbed species resulting from CO_2 dissociation can be gradually hydrogenated to hydrocarbons (C_2H_6 and C_3H_6 in this case) (13) and oxygenates, C_2H_6O (22) in this case.

$$2\,CO_2 + 6\,H_2 \rightarrow C_2H_6O + 3\,H_2O \qquad \Delta G^o = -36.8\ kJ\ mol^{-1} \quad (22)$$

In fact, it has been reported that, on large Pd particles, adsorbed CO is hydrogenated to dimethyl ether and higher hydrocarbons, instead to CH_4, because CO dissociative adsorption is also reported to be limited on big Pd particles [71-73], although large Pd particles are able to adsorb CO non dissociativelly [71]. Moreover, adsorbed CO is reported to inhibit hydrogen-assisted CO dissociation [71]. As commented above, CO was not detected in the reactor effluent. It seems that on large Pd particles CO_2 is reduced to form tightly adsorbed CO that is rapidly transformed to methanol and subsequently converted to dimethyl ether and higher hydrocarbons [70–76].

As can be observed in Fig. 19a, CO_2 conversion decreases on increasing temperature, in special under open circuit conditions, which according to the above findings for Ni/YSZ, it may suggest that carbon deposition is also produced in some extent over Pd/YSZ, especially at high temperature [72, 74, 77]. Carbon deposits are reported to supress formation of surface hydrogen adatoms by blocking of hydrogen adsorption sites [77], inhibiting the hydrogen-assisted CO_2 dissociation and, therefore, the CO_2 hydrogenation reaction [74, 77]. As commented above, under negative polarization (-2V), carbon deposition is expected to be increased by CO_2

reduction via O^{2-} removal from the catalyst surface. For this reason it was decided to do not perform any additional CO_2 hydrogenation tests under negative polarization.

As can be observed in Fig. 19b, for H_2/CO_2 ratios of 3, under open circuit conditions and 90 l h^{-1}, the formation of C_2H_6 (7), C_3H_6 (8) and C_2H_6O (22) on Pd is affected significantly by the temperature, with selectivities to C_2H_6, C_3H_6 and C_2H_6O up to about 5 %, 36 % and 96 %, respectively. Selectivity to C_2H_6 shows a slight dependence on temperature, whereas selectivity to C_2H_6O and C_3H_6 increases and decreases, respectively, on increasing temperature. Upon positive (2 V) polarization, the maximum value of C_2H_6, C_3H_6 and C_2H_6O selectivity is about 8.5 %, 31 % and 81 %, respectively. Selectivity to C_2H_6 is hardly affected by temperature, whereas selectivity to C_2H_6O and C_3H_6 decreases and increases, respectively, on increasing temperature.

CO_2 conversion levels were considerably high, up to about 17 %, under open circuit conditions (0V), and around 20 %, upon positive polarization (2V). A maximum value of CO_2 rate enhancement ratio of 1.3 was attained at 350 ºC, which also agrees with the fact that electrochemical promotion effect increases with temperature as a result of the increased ionic conductivity of the solid electrolyte.

In both cases, selectivity to C_2H_6O and C_3H_6 showed opposite trend towards temperature, which seems to indicate that they are formed through competitive reactions. The formation of both compounds is thermodynamically favoured under the utilised H_2/CO_2 ratio of three, which matched with that required by stoichiometry of the corresponding CO_2 hydrogenation reaction. As can be inferred also from Fig. 19b, application of positive potential (2 V) favours C_3H_6 formation at the expenses of C_2H_6O. This fact could be because, as reported previously in the literature [71], on relatively large Pd particles CH_3OH is primarily formed by hydrogenation of the adsorbed CO resulting from CO_2 dissociation and it is subsequently converted to C_2H_6O, and, as commented above, CH_3OH formation, and thus C_2H_6O

formation, is favoured around open circuit conditions were coverage of both reactants (CO_2 and H_2) is supposed to be very similar, whereas it is hindered for higher potential values.

The effect of polarization on catalyst performance over Pd/YSZ was also investigated through potentiostatic experiments performed under a H_2/CO_2 ratio of 3, at 300 ºC and 90 l h^{-1}.

The steady state response of CO_2 conversion and CO_2 rate enhancement ratio to different applied catalyst potentials (between -2 and 2 V) is displayed in Fig. 20a. Fig. 20b shows the effect of applied potential on the selectivity to C_2H_6, C_3H_6 and C_2H_6O.

As can be noticed in Fig. 20a, CO_2 rate enhancement ratios are around the unity, rendering very low promotion levels at this temperature, although CO_2 conversion and selectivity to the renewable fuel of most industrial interest (C_2H_6O) are rather high. The catalyst showed also an "inverted volcano type" electrochemical behaviour (Fig. 20a). The maximum value in CO_2 conversion was about 15.5 % at 2V. However, selectivity to C_2H_6 and C_2H_6O showed a "volcano type" electrochemical behaviour, i.e., they reach a maximum, of about 3.6 % and 72.4 %, respectively, at a certain potential (around 0 V), whereas C_3H_6 selectivity exhibits a concomitant minimum at the same potential, resembling an "inverted volcano type" electrochemical behaviour. The maximum value in C_3H_6 selectivity was about 35 %. As can be deduced from Fig. 20b, selectivity to C_2H_6O/C_2H_6 and C_3H_6 follows opposite trends against applied potential being a competition for the formation of the different hydrogenation products over the catalyst surface.

4. Conclusions

In this study, different tubular (Pt, Ni or Pd)/YSZ electrochemical catalysts has been successfully prepared by application and subsequent decomposition of a metallic precursor

paste (Pt/YSZ) or by electroless (Ni/YSZ and Pd/YSZ) and characterised by SEM, XRD and XPS techniques.

The hydrogenation of CO_2 over the different catalysts can be electrochemically assisted under atmospheric pressure, at relatively low temperatures and high gas flow rates and under realistic postcombustion CO_2 capture exiting gas compositions and discontinuous renewable H_2 flows. Selectivity to the different fuels of industrial interest can be modulated by modifying applied potential under given operating conditions.

CO_2 hydrogenation can be electrochemically enhanced for both positive and negative potentials, rendering an "inverted volcano type" electrochemical behaviour, by up to 3.2, 2.4 and 1.3 times for Pt, Ni and Pd, respectively, depending on the utilized operating conditions.

Both utilised preparation procedures resulted in relatively big metal particles which probably determined the comparatively high selectivity to methanol (up to 8 % at 400 ºC and H_2/CO_2=2), hydrocarbons (almost 100 % to C_2H_6 and C_3H_6) and dimethyl ether (up to 96 % at 300º C and H_2/CO_2=3) obtained for Pt, Ni and Pd, respectively, and the unusual small selectivity to CH_4 and CO observed for Ni and Pd.

The CO_2 hydrogenation on the Pt/YSZ catalyst at 400 ºC leads to the formation of CO, C_2H_6, C_3H_6 and methanol, but CH_4 was also formed for a H_2/CO_2 ratio of 2, although the maximum CH_4 selectivity attained was rather low (of about 3%). The conversion of CO_2 reaches a maximum of 24.5 % also for a H_2/CO_2 ratio of 2, but with very low promotion levels. Selectivities to C_2H_6, C_3H_6, CH_3OH and CH_4 were electrochemically enhanced by up to 6, 3, 800 and 30 times, respectively, depending on the utilised H_2/CO_2 ratio.

The same reaction on Ni/YSZ at temperatures between 225 and 400 ºC leads mainly to the formation of hydrocarbons (mostly C_2H_6 and C_3H_6). CO_2 conversion reaches a maximum of 28 % for a H_2/CO_2 ratio of 4 under anodic polarization (2V) and at 225 ºC, but with low promotion levels.

Hydrogenation of CO_2 on Pd/YSZ at temperatures in the range of 225-375 ºC results in the formation of C_2H_6, C_3H_6 and dimethyl ether (C_2H_6O) both under normal catalytic and polarization conditions. CO_2 conversion levels were considerably high, up to 20 % at 225 º C and increases upon positive polarization. Selectivity to C_2H_6, C_3H_6 and C_2H_6O reached values up to 8.5 %, 36 % and 96 %, respectively, but positive polarization favours C_3H_6 formation at the expenses of C_2H_6O.

Therefore, this study addresses some scale-up aspects, such as operation at high flow rates and atmospheric pressure, under realistic gas compositions and using catalyst-electrode configurations easily adaptable to the existing catalytic devices (conventional flow reactors), and, in the case of Ni, based on a cheap, widespread and non-precious catalyst, and prepared by a commercial ready procedure, which may have an impact on the potential practical application of the process for CO_2 recycling, contributing not only to controlling the global "Green-house Effect", but also to the availability of fuel sources for the future.

Acknowledgements

The authors acknowledge support from Ministerio de Ciencia e Innovación of Spain (Project ENE2010-15569). Pedro J. Martinez is grateful to Ministerio de Ciencia e Innovación of Spain for the research grant BES-2011-046902.

References

[1] G.A. Olah, A. Goeppert, G.K.S. Prakash, J. Org. Chem. 74 (2009) 487–498.

[2] F. Ocampo, B. Louis, A. Kiennemann, A. C. Roger, Mater. Sci. Eng. 19 (2011) 1–11.

[3] S.K. Hoekman, A. Broch, C. Robbins, R. Purcell, Int. J. Greenhouse Gas Control 4 (2010) 44–50.

[4] D.T. Whipple, P.J. Kenis, J. Phys. Chem. Lett. (2010) 3451–3458.

[5] E.I. Papaioannou, S. Souentie, A. Hammad, C.G. Vayenas, Catal. Today 146 (2009) 336–344.

[6] W. Wang, S. Wang, X. Ma, J. Gong, Chem. Soc. Rev. 40 (2011) 3703–3727.

[7] G. Karagiannakis, S. Zisekas, M. Stoukides, Solid State Ionics 162–163 (2003) 313–318.

[8] C.G. Vayenas, S. Bebelis, C. Pliangos, S. Brosda, D. Tsiplakides, Electrochemical Activation of Catalysis: Promotion, Electrochemical Promotion and Metal-Support Interactions, Kluwer Academic/Plenum Publishers, New York, 2001.

[9] G. Pekridis, K. Kalimeri, N. Kaklidis, E. Vakouftsi, E.F. Iliopoulou, C. Athanasiou, G.E. Marnellos, Catal. Today 127 (2007) 337–346.

[10] S. Bebelis, H. Karisali, C.G.Vayenas, Solid State Ionic 179 (2008) 1391–1395.

[11] S. Bebelis, H. Karasali, C.G. Vayenas, J. Appl. Electrochem. 38 (2008) 1127–1133.

[12] D. Theleritis, S. Souentie, A. Siokou, A. Katsaounis, C.G. Vayenas, ACS Catal. 2 (2012) 770–780.

[13] V. Jiménez, C. Jiménez-Borja, P. Sánchez, A. Romero, E.I. Papaioannou, D. Theleritis, S. Souentie, S. Brosda, J.L. Valverde, Appl. Catal., B 107 (2011) 210–220.

[14] D. Tsiplakides, S. Balomenou, Chem. Ind. Chem. Eng. Q. 14 (2008) 97–105.

[15] D. Tsiplakides, S. Balomenou, Catal. Today 146 (2009) 312–318.

[16] A. Anastasijevic, Catal. Today 146 (2009) 308–311.

[17] E. Ruiz, D. Cillero, P.J. Martínez, A. Morales, G. San Vicente, G. de Diego, J.M. Sánchez, Catal. Today 210 (2012) 55–66.

[18] A. Morales, EU EP 1 321 539 A2.

[19] W. Wang, J. Gong, Front. Chem. Sci. Eng. 5 (2011) 2–10.

[20] C. Guizard, A. Princivalle, Catal. Today 146 (2009) 367–377.

[21] E. Mutoro, C. Koutsodontis, B. Luerssen, S. Brosda, C.G. Vayenas, J. Janek, Appl. Catal., B 100 (2010) 328–337.

[22] Y.-x. Pan, C.-j. Liu, T.S. Wiltowski, Q. Ge, Catal. Today 147 (2009) 68–76.

[23] J.-S. Kim, S.-B. Lee, M.-J. Choi, K.-W. Lee, Catal. Today 115 (2006) 228–234.

[24] M. Kisida, K. Umakoshi, J.-i. Ishiyama, H. Nagata, K. Wakabayashi, Catal. Today 29 (1996) 355–359.

[25] A. de Lucas Consuegra, A. Caravaca, J. Gonzalez-Cobos, J. L. Valverde, F. Dorado, Catal. Commun. 15 (2011) 6–9.

[26] A. de Lucas-Consuegra, A. Caravaca, P.J. Martínez, J.L. Endrino, F. Dorado, J.L. Valverde, J. Catal. 274 (2010) 252–258.

[27] K.V.R. Chary, D. Naresh, V. Vichwanathan, M. Sadakane, W. Ueda, Catal. Commun. 8 (2007) 471–477.

[28] A. Mosquera, D. Horwat, L. Vazquez, A. Gutierrez, A. Erko, A. Anders, J. Andersson, J.L. Endrino, J. Mater. Res. 27 (2012) 829–836.

[29] K.S. Kim, N. Winograd, Surf. Sci. 43 (1974) 625–643.

[30] A.P. Grosvenor, M.C. Biesinger, R.S.C. Smart, N.S. McIntyre, Surf. Sci. 600 (2006) 1771–1779.

[31] S.W. Hong, C.H. Shin, J.W. Park, J. Electrochem. Soc. 149 (2002) G85–G88.

[32] C.H. Choi, S.H. Park, S.I. Woo, Phys. Chem. Chem. Phys. 14 (2012) 6842–6848.

[33] S. Brosda, C.G. Vayenas, J. Wei, Appl. Catal., B 68 (2006) 109–124.

[34] P.J. Lunde, F.L. Kester, Ind. Eng. Chem. Process Des. Dev. 13 (1) (1974) 27–33.

[35] N. Hoshi, T. Mizumura, Y. Hori, Electrochim. Acta 40 (1995) 883–887.

[36] P. Dube, G.M. Brisard, J. Electroanal. Chem. 582 (2005) 230–240.

[37] G.M. Brisard, A.P.M. Camargo, F.C. Nart, T. Iwasita, Electrochem. Commun. 3 (2001) 603–607.

[38] K.-P. Yu, W.-Y. Yu, M.-C. Kuo, Y.-C. Liou, S.-H. Chien, Y. Hori, Appl. Catal., B 84 (2008) 112–118.

[39] K. Shao, M. Chen, J. Mol. Catal. A: Chem. 170 (2001) 245–249.

[40] S.J. Choe, D.H. Park, D.S. Huh, Bull. Korean Chem. Soc. 21 (2000) 779–784.

[41] T.M. Gür, H. Wise, R.A. Huggins. J. Catal. 129 (1991) 216–224.

[42] P. Vernoux, F. Gaillard, C. Lopez, E. Siebert, Solid State Ionics 175 (2004) 609–613.

[43] I. Nova, L. Castoldi, L. Lietti, E. Tronconi, P. Forzatti, Catal. Today 75 (2002) 431–437.

[44] E.C. Corbos, X. Courtois, N. Bion, P. Marecot, D. Duprez, Appl. Catal., B 76 (2007) 357–367.

[45] A. de Lucas-Consuegra, F. Dorado, J.L. Valverde, R. Karoum, P. Vernoux, J. Catal. 251 (2007) 474–484.

[46] M. García-Diéguez, I.S. Prieta, M.C. Herrera, M.A. Larrubia, I. Malpartida, L.J. Alemany, Catal. Today 149 (2010) 380–387.

[47] R. Sahki, O. Benlounes, O. Chérifi, R. Thouvenot, M.M. Bettahar, S. Hocine, React. Kinet. Mech. Catal. 103 (2011) 391–403.

[48] F.J. Willians, M.S. Tikhov, A. Palermo, N. Macleod, R.M. Lambert, J. Phys. Chem. B 105 (2001) 2800–2808.

[49] M. Kuriyama, H. Tanaka, S. Ito, T. Kubota, T. Miyao, S. Naito, K. Tomishige, K. Kunimori, J. Catal. 252 (2007) 39–48.

[50] Y. Souma, H. Ando, M. Fujiwara, R. Kieffer, Energy Convers. Manage. 36 (1995) 593–596.

[51] C.K. Kuo, N.D. Patel, A. Tan, P. Sarkar, P.S. Nicholson, Solid State Ionics 53–56 (1992) 564–570.

[52] E. Vesselli, M. Rizzi, L. De Rogatis, X. Ding, A. Baraldi, G. Comelli, L. Savio, L. Vattuone, M. Rocca, P. Fornasiero, A. Baldereschi, M. Peressi, J. Phys. Chem. Lett. 1 (2010) 402–406.

[53] C. Schild, A. Wokaun, R.A. Koeppel, A. Baiker, J. Phys. Chem. 95 (1991) 6341–6346.

[54] M.A. Vannice, J. Catal. 44 (1976) 152–162.

[55] F. Mariño, M. Boveri, G. Baronetti, M. Laborde, Int. J. Hydrogen Energy 26 (2001) 665–668.

[56] S.J. Choe, H.J. Kang, S.J. Kim, S.B. Park, D.H. Park, D.S. Huh, Bull. Korean Chem. Soc. 26 (2005) 1682–1688.

[57] J.G. McCarty, H. Wise, J. Catal. 57 (1979) 404–416.

[58] P.K. Bajpai, N.N. Bakhshi, Can. J. Chem. Eng. 60 (1982) 4–10.

[59] J. Kuhn, O. Kesler, J. of Powder Sources 246 (2014) 430–437.

[60] M. Marinsek, Boletin de la Sociedad Española de Ceramica y Vidrio 50 (2011) 135–142. Doi:10.3989/cyv.182011.

[61] J.M. García-Vargas, J.L. Valverde, A. de Lucas-Consuegra, B. Gómez-Monedero, P. Sánchez, F. Dorado, Appl. Catal., A 431–432 (2012) 49–56.

[62] P. Djnovic, I.G.O. Crnivec, B. Erjavec, A. Pintar, Appl. Catal., B 125 (2012) 259–270.

[63] Y. Shu, M. Ichickawa, Catal. Today 71 (2001) 55–67.

[64] B.M. Weckhuysen, M.P. Rosynek, J.H. Lunsford, Catal. Lett. 52 (1998) 31–36.

[65] H. Estrade-Szwarckopf, B. Rousseau, J. Phys. Chem. Solids 53 (1992) 419–436.

[66] C.M. Finnerty, N.J. Coe, R.H. Cunningham, R.M. Ormerod, Catal. Today 46 (1998) 137–145.

[67] L.V. Mattos, E. Rodino, D.E. Resasco, F.B. Passos, F.B. Noronha, Fuel Process. Technol. 83 (2003) 147–161.

[68] T. Forita, K. Yamaji, T. Kato, H. Kisimoto, Y. Xiong, N. Sakai, M.E. Brito, H. Yokokawa, J. of Powder Sources 145 (2005) 133–138.

[69] J. Millichamp, T.J. Mason, N.P. Brandon, R.J.C. Brown, R.C. Maher, G. Manos, T.P. Neville, D.J.L. Brett, J. Powder Sources 235 (2013) 14–19.

[70] N. Furuya, T. Yamazaki, M. Shibata, J. Electroanal. Chem. 431 (1997) 39–41.

[71] F.A.P. Cavalcanti, C. Dossi, L.L. Sheu, W.M.H. Sachtler, Catal. Lett. 6 (1990) 289–300.

[72] A. Erdöhelyi, M. Pásztor, F. Solymosi, J. Catal. 98 (1986) 166–177.

[73] R. Thomson, C. Montes, M.E. Davis, E.E. Wolf, J. Catal. 124 (1990) 401–415.

[74] H. Yoshitake, T. Kikkawa, G. Muto, K. Ota, J. Electroanal. Chem. 396 (1995) 491–498.

[75] C. Schild, A. Wokaun, J. Mol. Catal. 63 (1990) 223–242.

[76] L. Fan, K. Fujimoto, Appl. Catal., A 106 (1993) L1–L7.

[77] S.K. Shaikhutdinov, M. Frank, M. Bäumer, S.D. Jackson, R.J. Oldman, J.C. Hemminger, H.J. Freund, Catal. Lett. 80 (2002) 115–121.

(a) (b)

Fig. 1. SEM micrograph of the Pt catalyst-working electrode film: (a) as prepared, (b) after reduction and testing.

(a) (b)

Fig. 2. SEM micrograph of the Ni catalyst-working electrode film: (a) as prepared, (b) after reduction and testing.

(a) (b)

Fig. 3. SEM micrograph of the Pd catalyst-working electrode film: (a) as prepared, (b) after reduction and testing.

Fig. 4. XRD analysis of the Pt catalyst-working electrode film: (a) as prepared, (b) after reduction and testing.

Fig. 5. XRD analysis of the Ni catalyst-working electrode film: (a) as prepared, (b) after reduction and testing.

Fig. 6. XRD analysis of the Pd catalyst-working electrode film: (a) as prepared, (b) after reduction and testing.

(a) (b)

Fig. 7. XPS spectra of the Pt catalyst-working electrode film: (a) as prepared, (b) after reduction and testing.

(a) (b)

Fig. 8. XPS spectra of the Ni catalyst-working electrode film: (a) as prepared, (b) after reduction and testing.

(a) (b)

Fig. 9. XPS spectra of the Pd catalyst-working electrode film: (a) as prepared, (b) after reduction and testing.

Fig. 10. Influence of the applied potential on (a) CO_2 conversion (■) and CO_2 rate enhancement ratio (●) and on (b) selectivities to C_2H_6 (▲), C_3H_6 (▼) and CO (◆) over Pt/YSZ/Au. (400 ºC, 90 l h^{-1}, H_2/CO_2 = 1).

Fig. 11. Influence of the applied potential on (a) CO_2 conversion (■) and CO_2 rate enhancement ratio (●) and on (b) selectivities to C_2H_6 (▲), C_3H_6 (▼), CO (◆), CH_3OH (⬟) and CH_4 (★) over Pt/YSZ/Au. (400 ºC, 90 l h^{-1}, H_2/CO_2 = 2).

Fig. 12. Influence of the applied potential on (a) CO_2 conversion (■) and CO_2 rate enhancement ratio (●) and on (b) selectivities to C_2H_6 (▲), C_3H_6 (▼), CO (◆) and CH_3OH (⬟) over Pt/YSZ/Au. (400 ºC, 90 l h^{-1}, H_2/CO_2 = 3).

Fig. 13. Influence of the applied potential on (a) CO_2 conversion (■) and CO_2 rate enhancement ratio (●) and on (b) selectivities to C_2H_6 (▲), C_3H_6 (▼), CO (◆) and CH_3OH (⬟) over Pt/YSZ/Au. (400 ºC, 90 l h^{-1}, H_2/CO_2 = 4).

Fig. 14. Effect of H_2/CO_2 ratio on the potentiostatic variation of CO_2 conversion (a), CO_2 rate

enhancement ratio (b) and selectivities to CO (c), C_3H_6 (d), C_2H_6 (e) and CH_3OH (f) on Pt/YSZ/Au. (400 ºC, H_2/CO_2 = 4 (■), H_2/CO_2=3 (●), H_2/CO_2=2 (▲) and H_2/CO_2 = 1 (▼), 90 l h^{-1}).

Fig. 15. Influence of temperature on CO_2 conversion under open circuit conditions (0V, unpromoted conditions) (■), upon negative polarization (-2V) (●) and upon positive polarization (2V) (▲) over Ni/YSZ/Au. (225-400 ºC, 90 l h^{-1}, H_2/CO_2 = 4).

(a) (b)

Fig. 16. C 1s XPS spectra of the Ni catalyst-working electrode film: (a) as prepared, (b) after reduction and testing.

Fig. 17. Influence of temperature on CO_2 conversion upon (a) positive (2V) and (b) negative (-2V) polarization for different H_2/CO_2 ratios over Ni/YSZ/Au. (225-375 ºC, 90 l h^{-1}, H_2/CO_2 = 4 (■) and H_2/CO_2 = 1 (▲)).

Fig. 18. Influence of the applied potential on CO_2 conversion (■) and CO_2 rate enhancement ratio (●) over Ni/YSZ/Au. (400 ºC, 90 l h^{-1}, H_2/CO_2 = 3).

Fig. 19. Influence of temperature on (a) CO_2 conversion (■, □) and on (b) selectivities to C_2H_6 (▲, △), C_3H_6 (▼, ▽) and C_2H_6O (⬟,⬠) over Pd/YSZ/Au under open circuit conditions (0V, unpromoted conditions) (filled symbols) and upon positive polarization (2V) (open symbols). (225-350 ºC, 90 l h^{-1}, H_2/CO_2 = 3).

Fig. 20. Influence of the applied potential on (a) CO_2 conversion (■) and CO_2 rate

enhancement ratio (●) and on (b) selectivities to C_2H_6 (▲), C_3H_6 (▼) and C_2H_6O (⬟) over Pd/YSZ/Au. (300 ºC, 90 l h^{-1}, H_2/CO_2 = 3).

Graphical Abstract (for review)

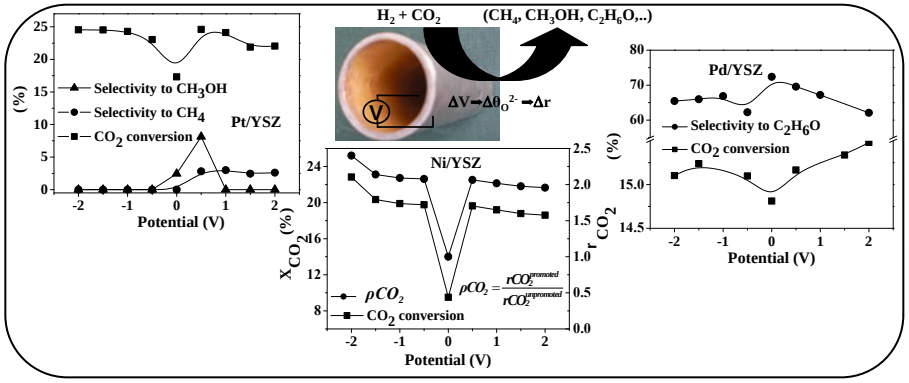

Highlights

- Electroassisted CO_2 hydrogenation on (Pt, Ni or Pd)/YSZ under realistic conditions.
- Boost on CO_2 conversion and fuel selectivity by transfer of O^{2-} to or from metal.
- CH_4 and CH_3OH formation on Pt favoured at high and low O^{2-} coverage for H_2/CO_2 =2.
- CO_2 hydrogenation on Ni leads mainly to hydrocarbons (mostly C_2H_6 and C_3H_6).
- C_2H_6O formation on Pd favoured at high temperature and low O^{2-} level for H_2/CO_2 =3.

Figure

Click here to download high resolution image

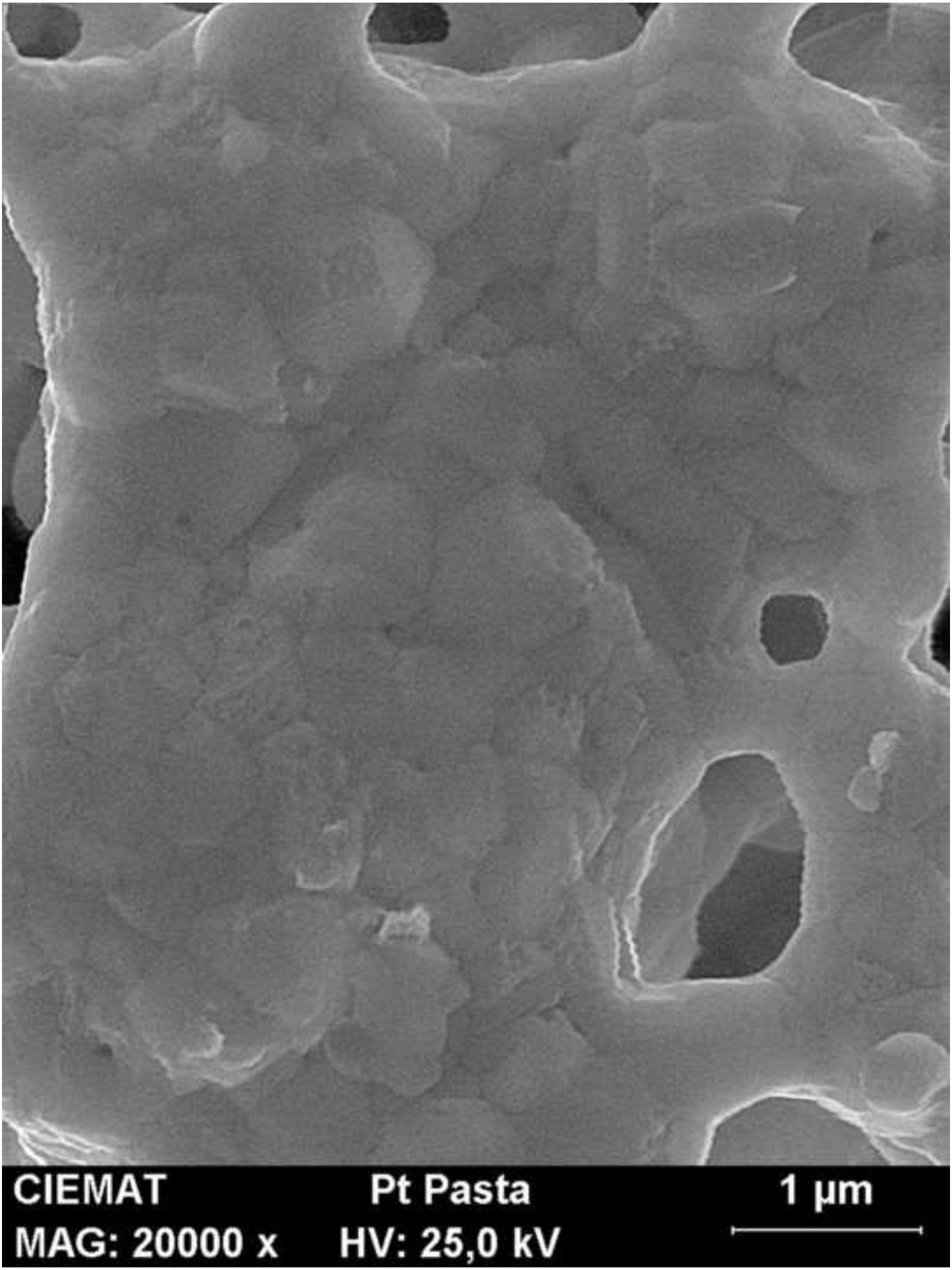

Figure

Click here to download high resolution image

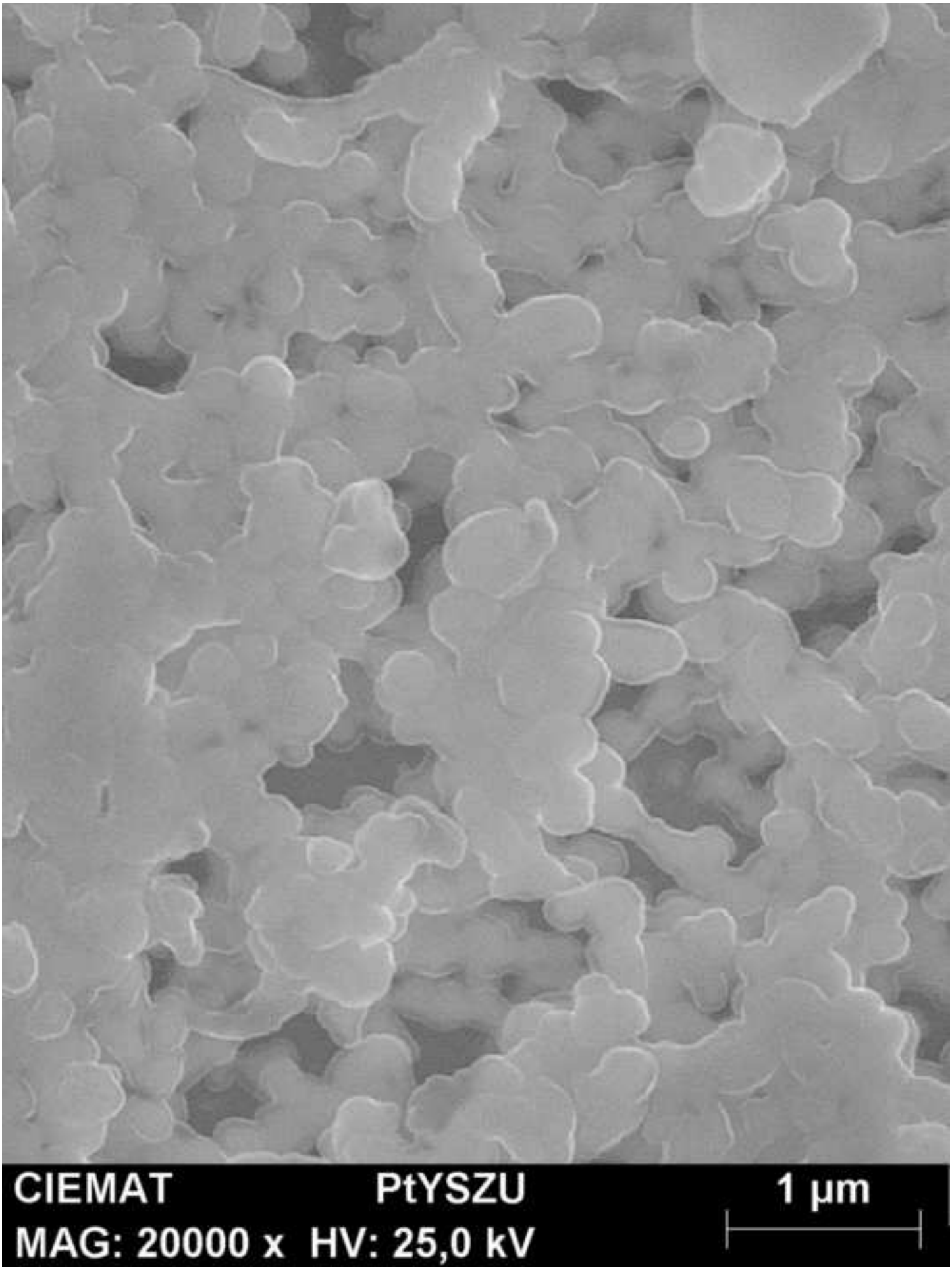

Figure

Click here to download high resolution image

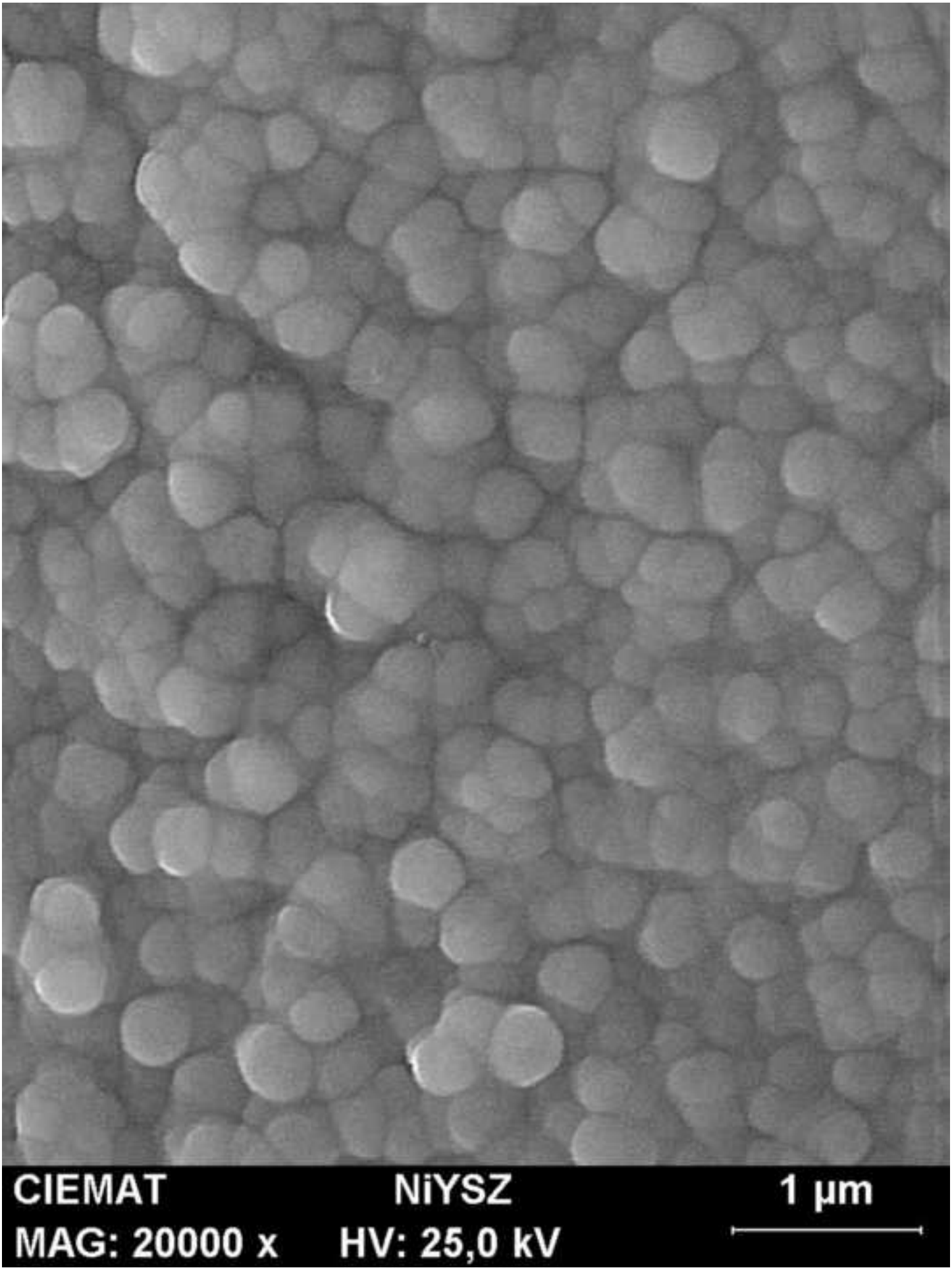

Figure

Click here to download high resolution image

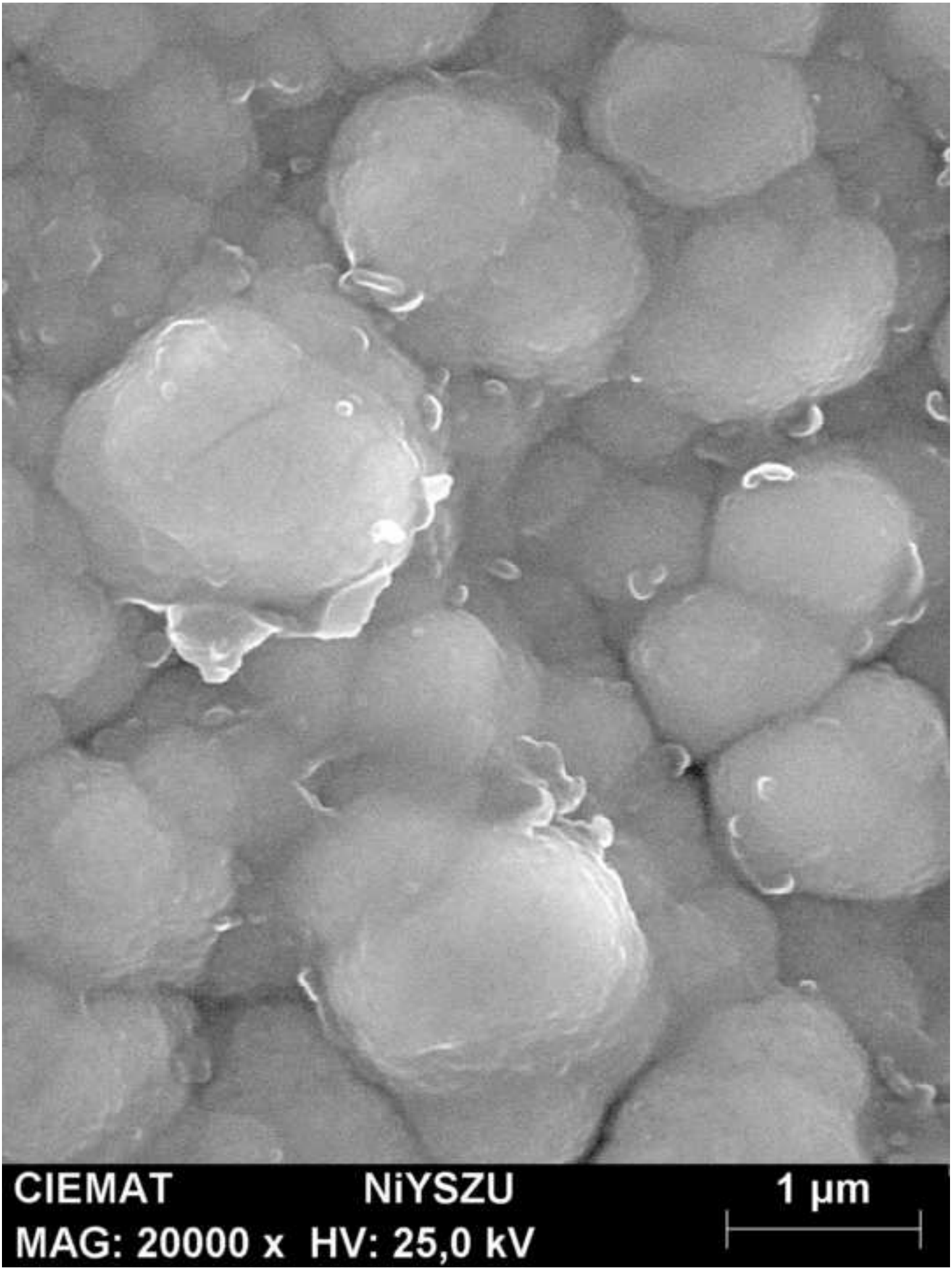

Figure

Click here to download high resolution image

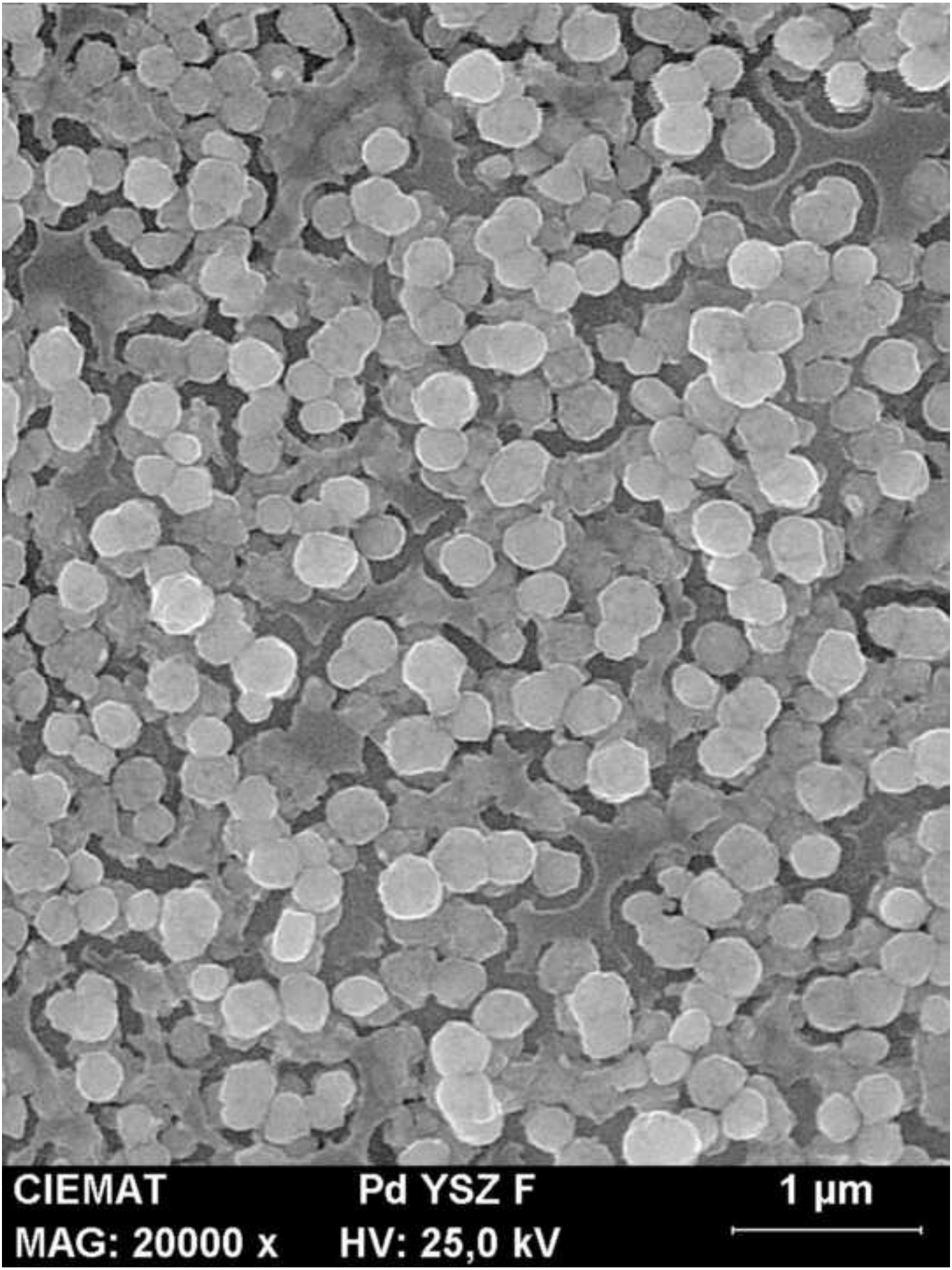

Figure

Click here to download high resolution image

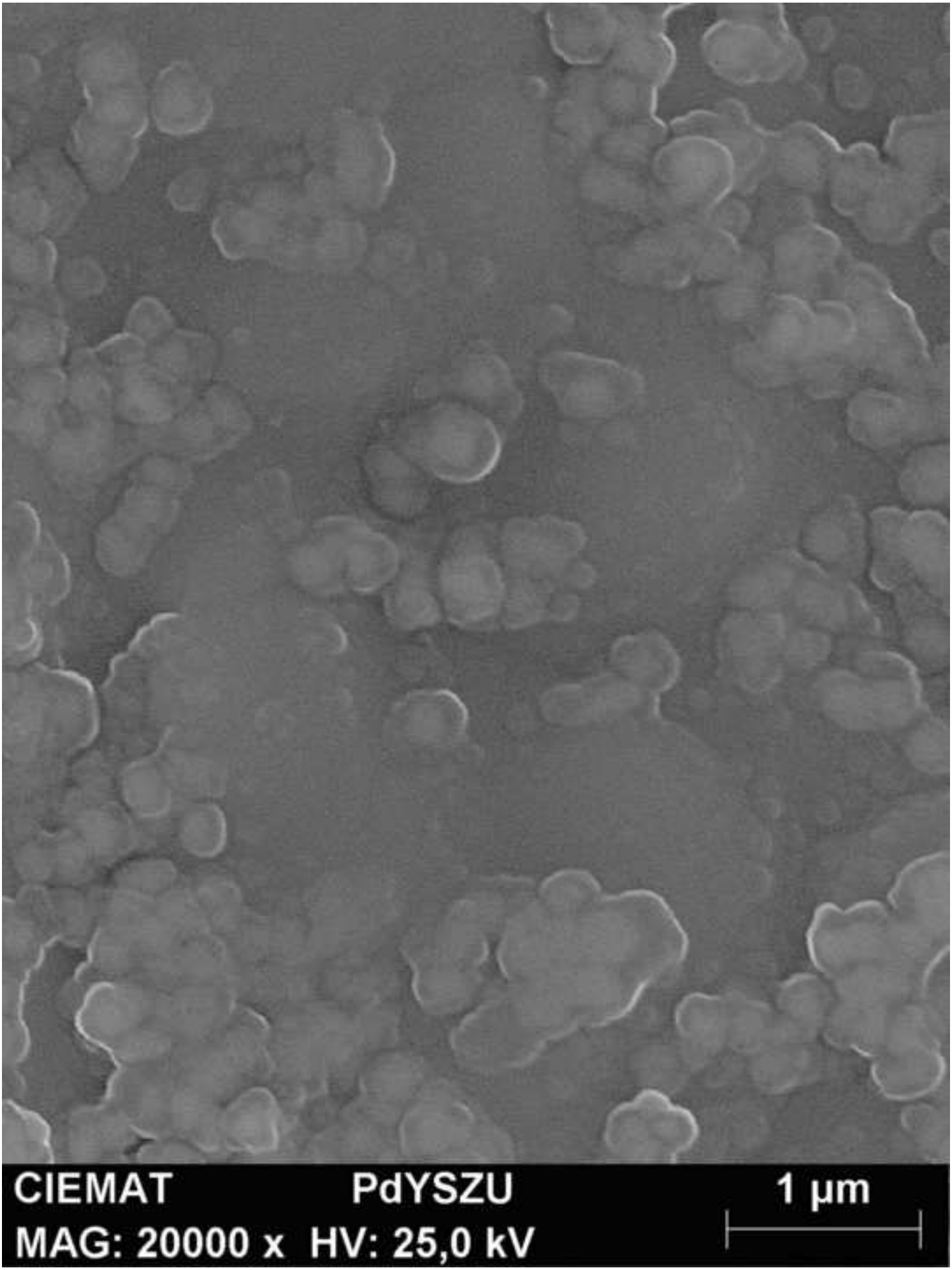

Figure
Click here to download high resolution image

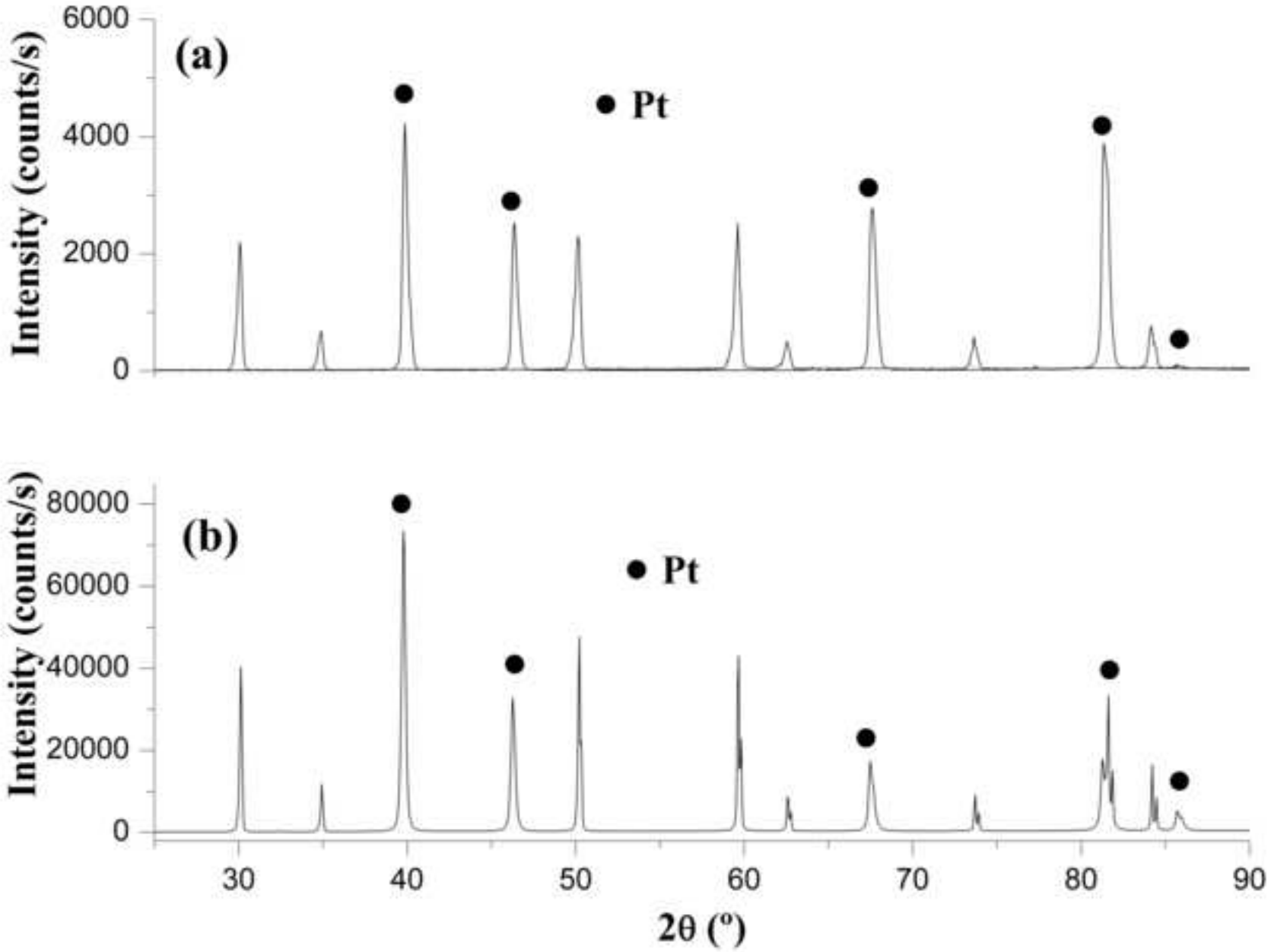

Figure

Click here to download high resolution image

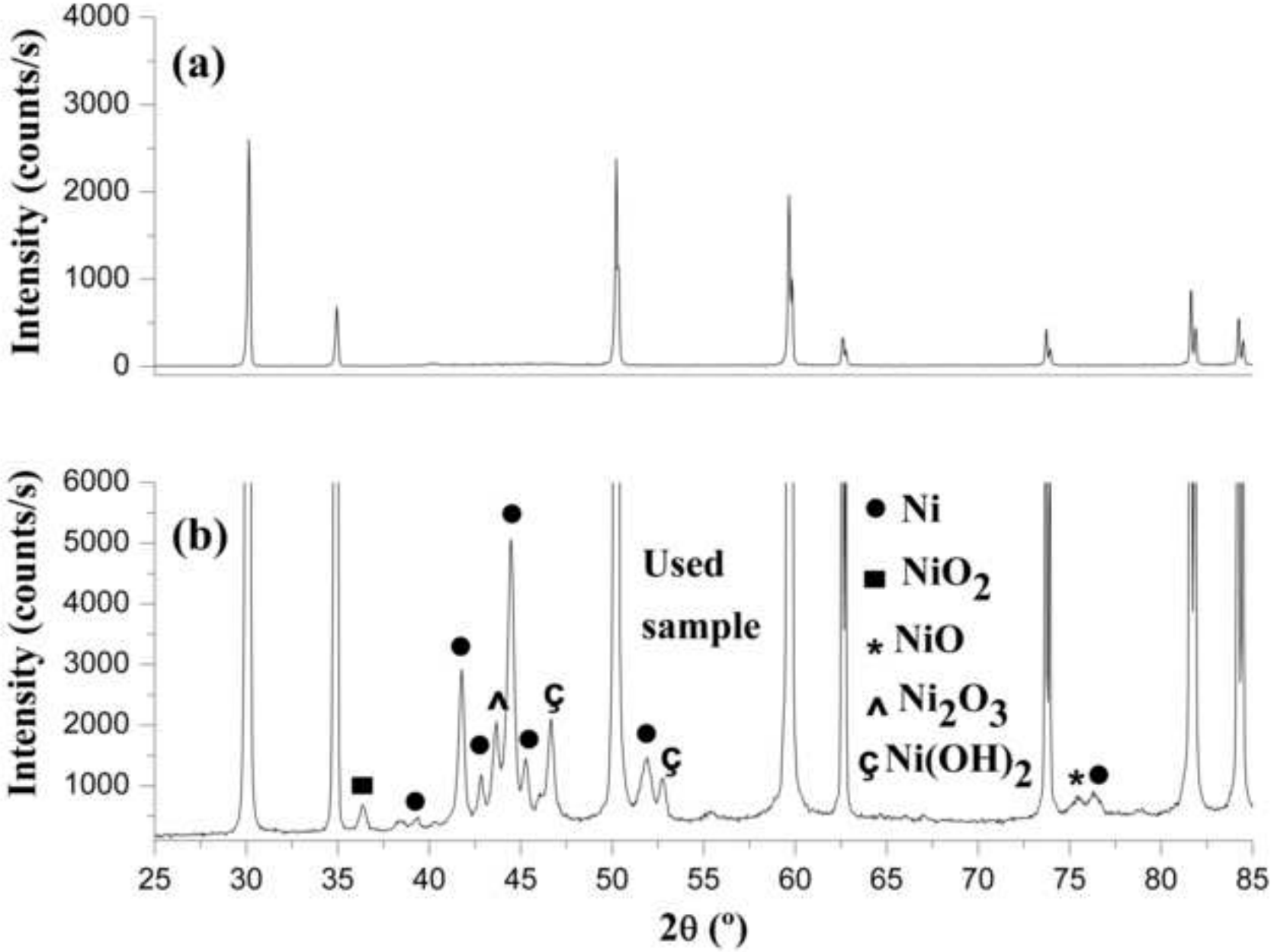

Figure
Click here to download high resolution image

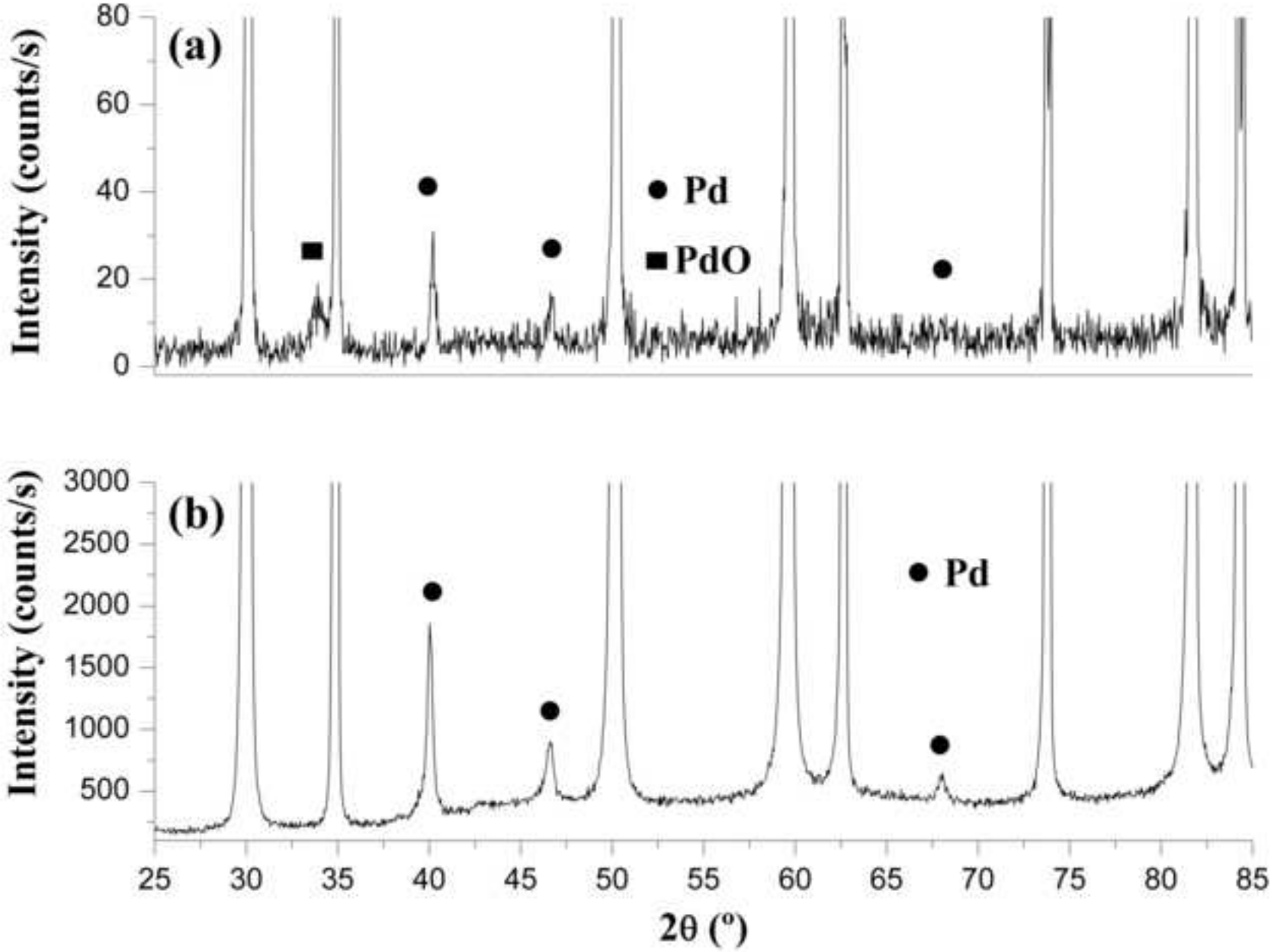

Figure

Click here to download high resolution image

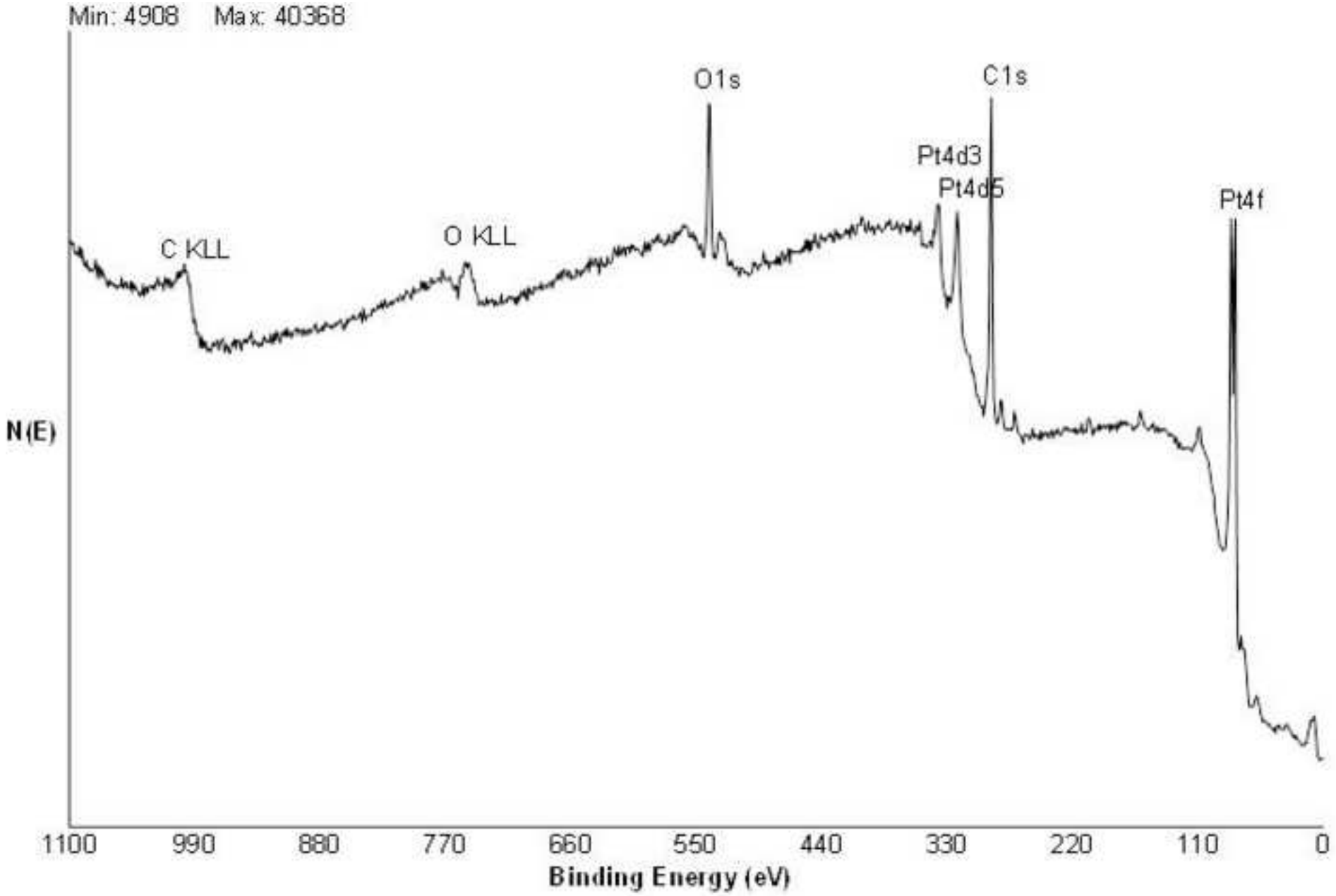

Figure

Click here to download high resolution image

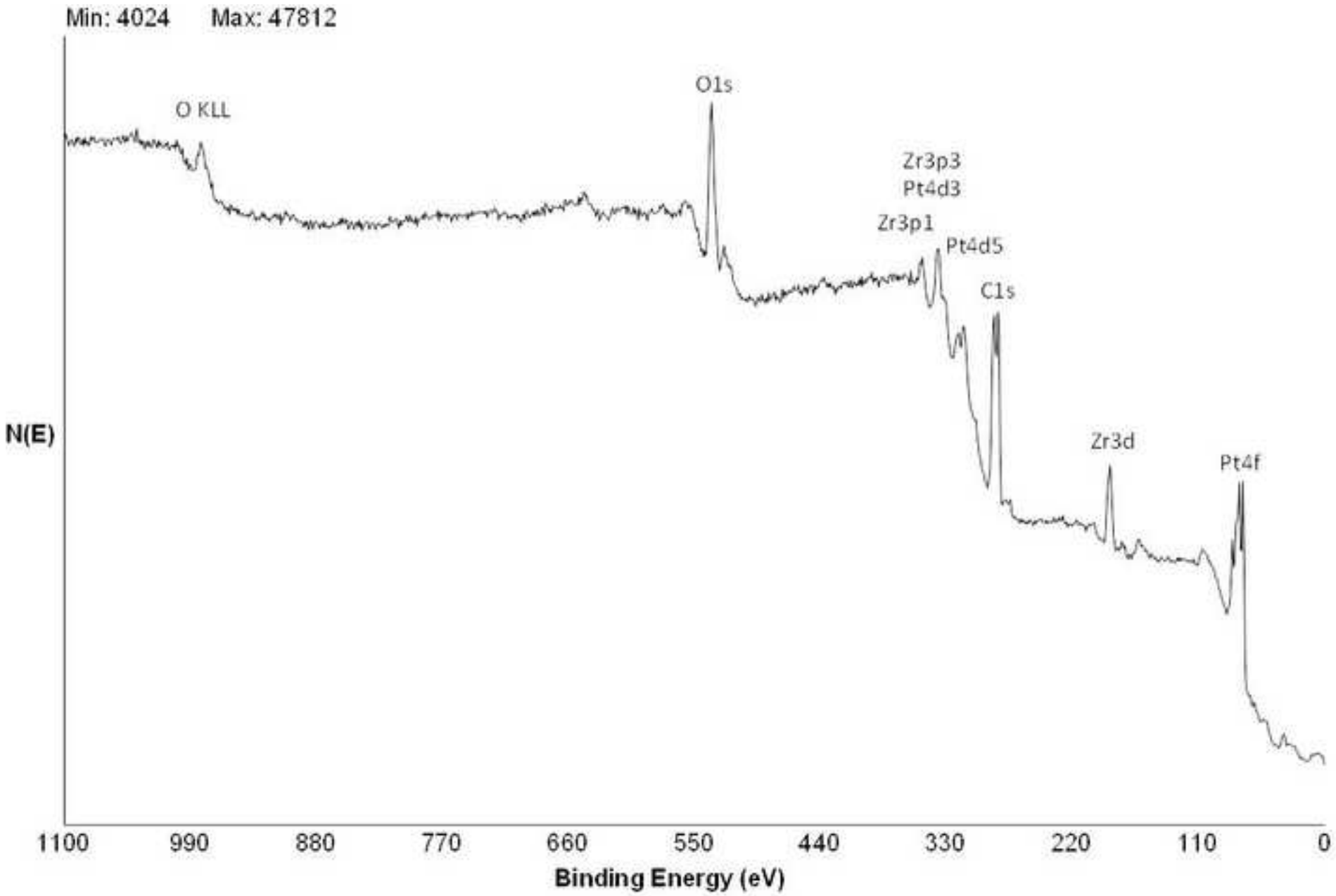

Figure

Click here to download high resolution image

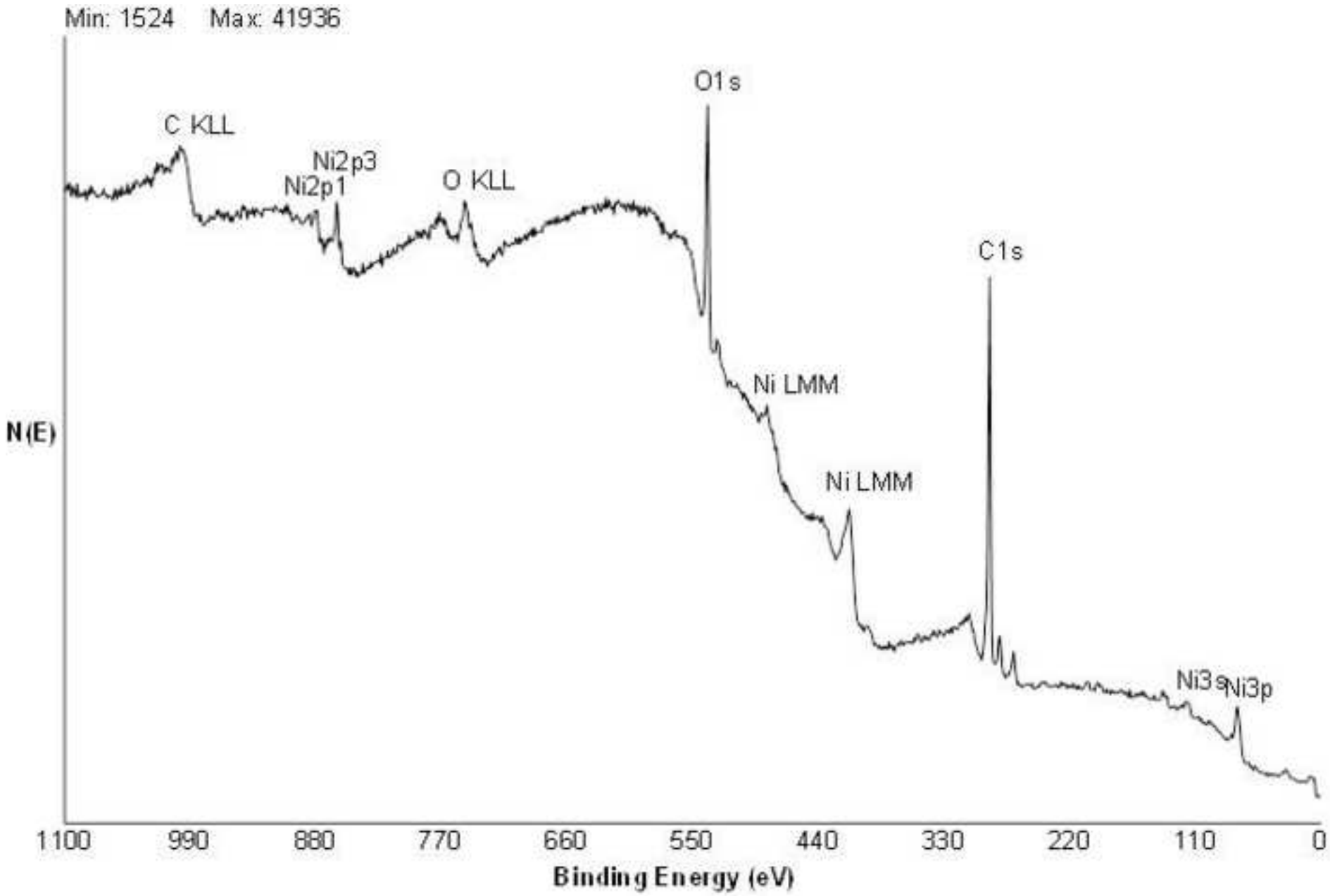

Figure

Click here to download high resolution image

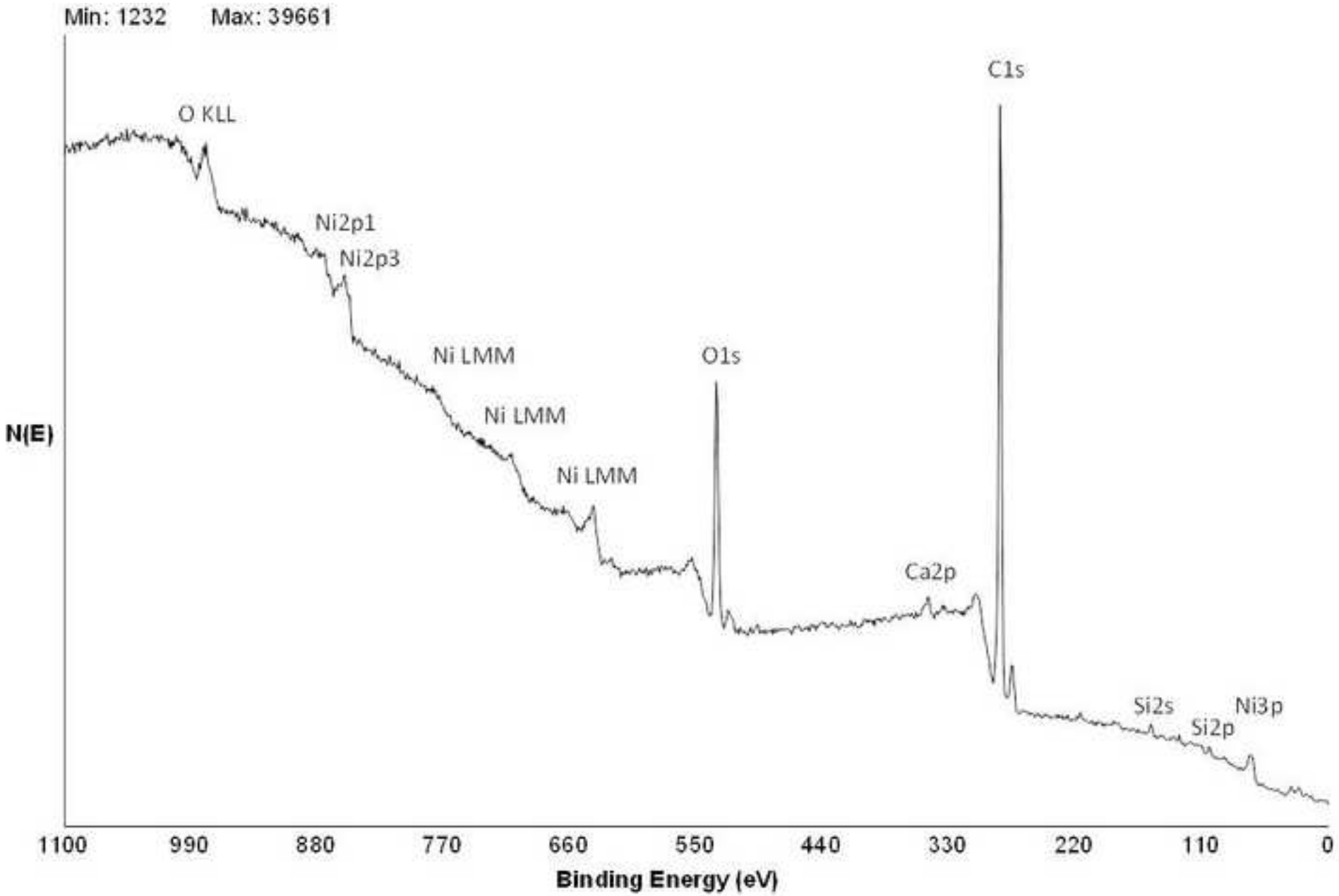

Figure

Click here to download high resolution image

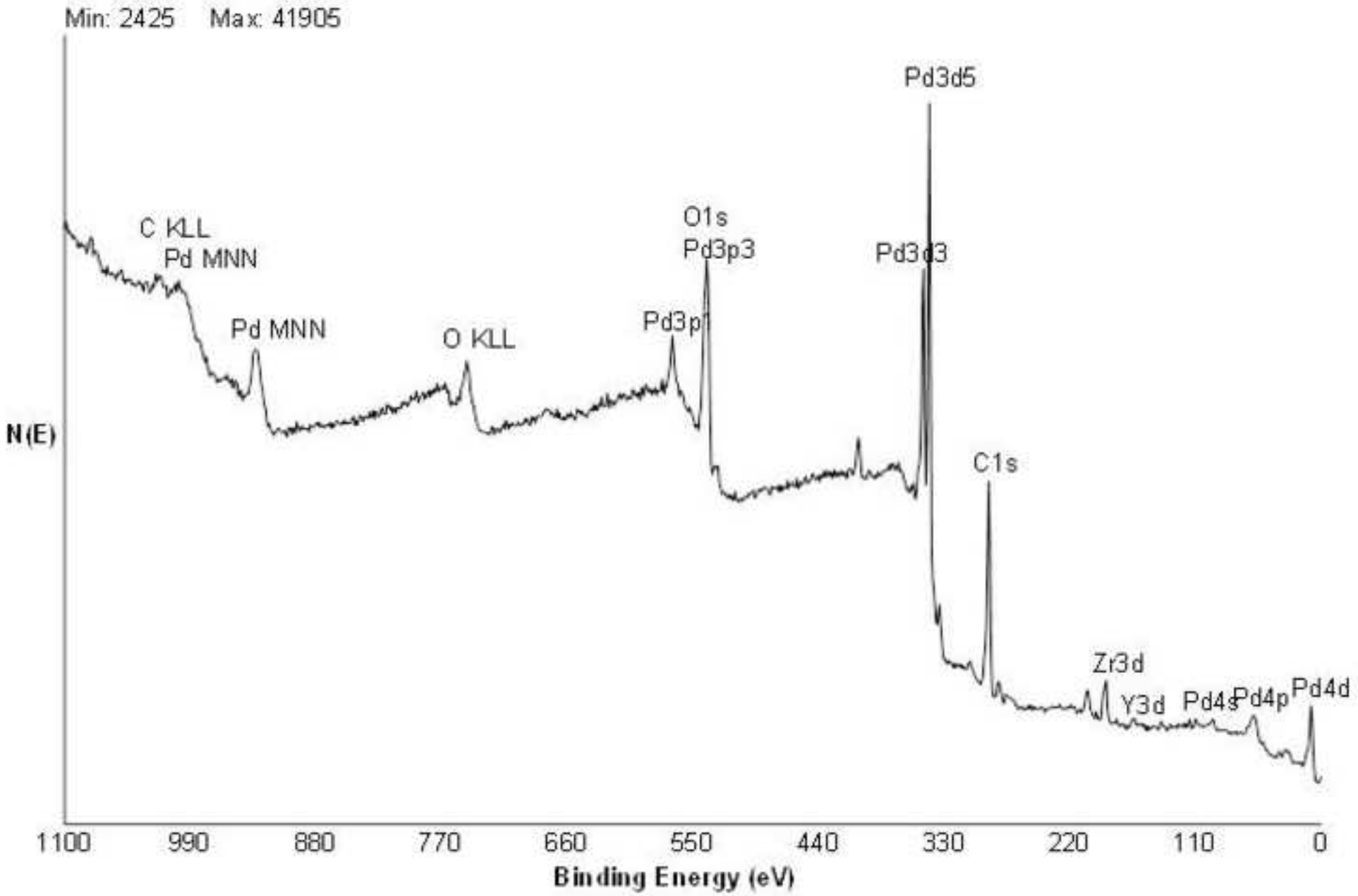

Figure

Click here to download high resolution image

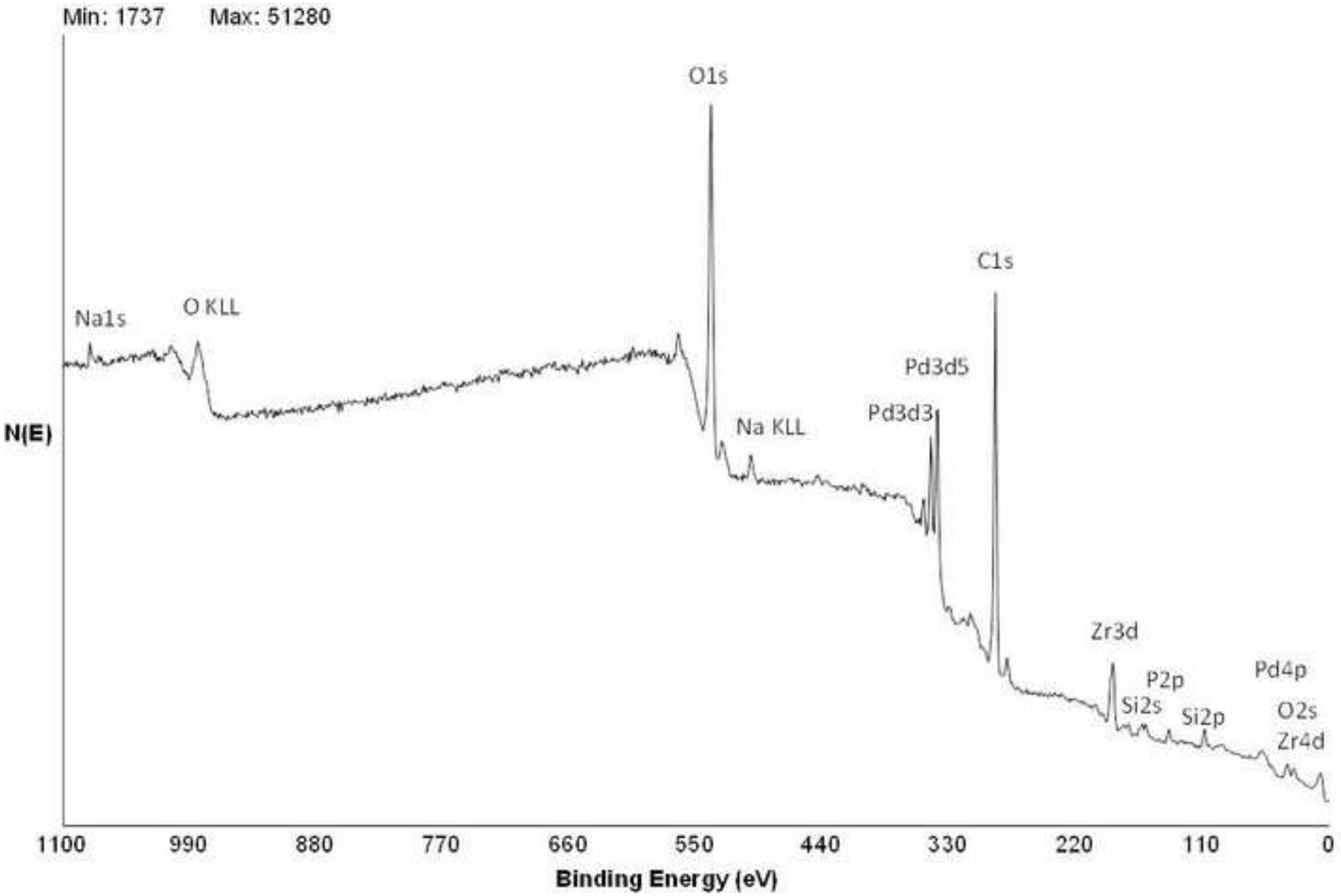

Figure
Click here to download high resolution image

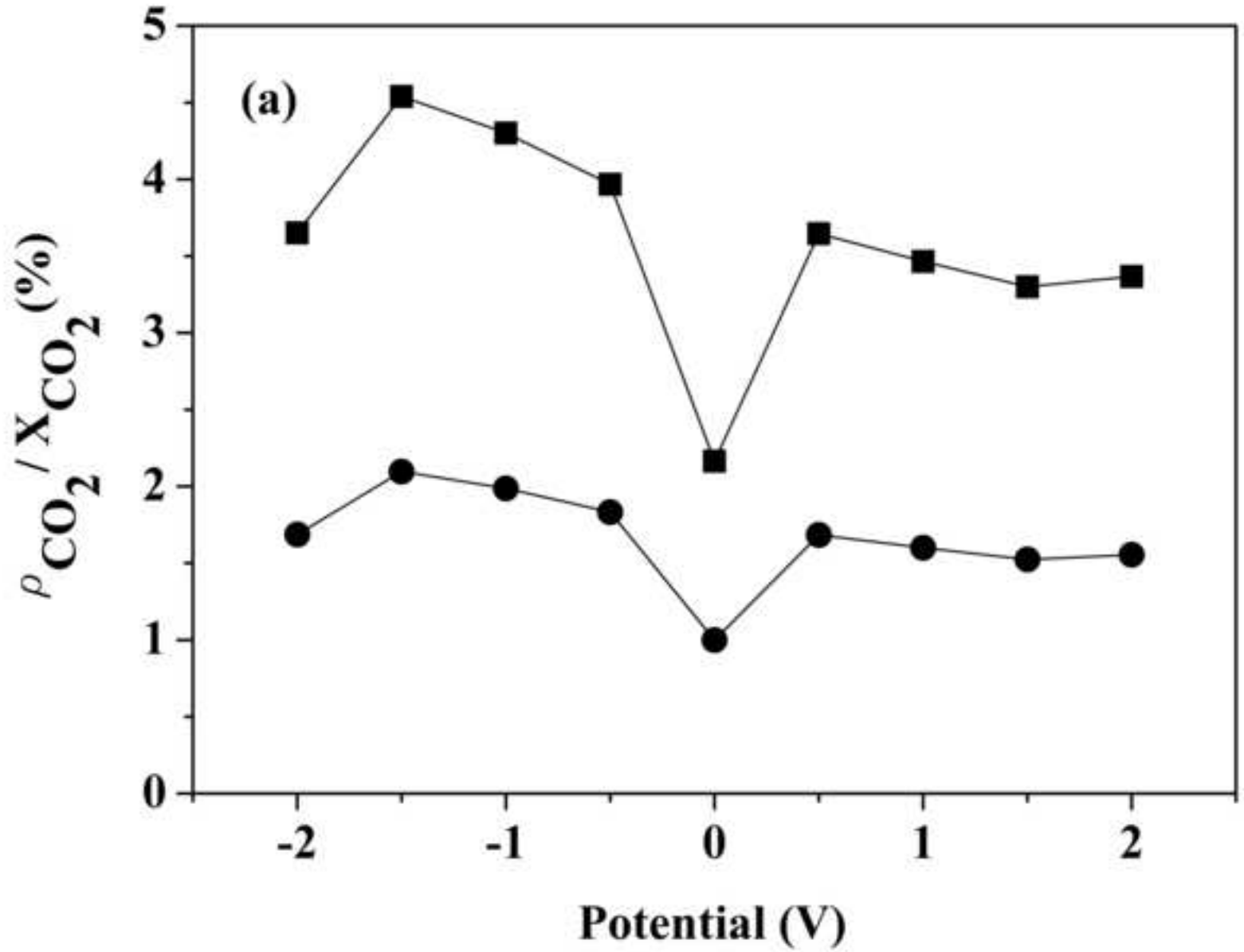

Figure
Click here to download high resolution image

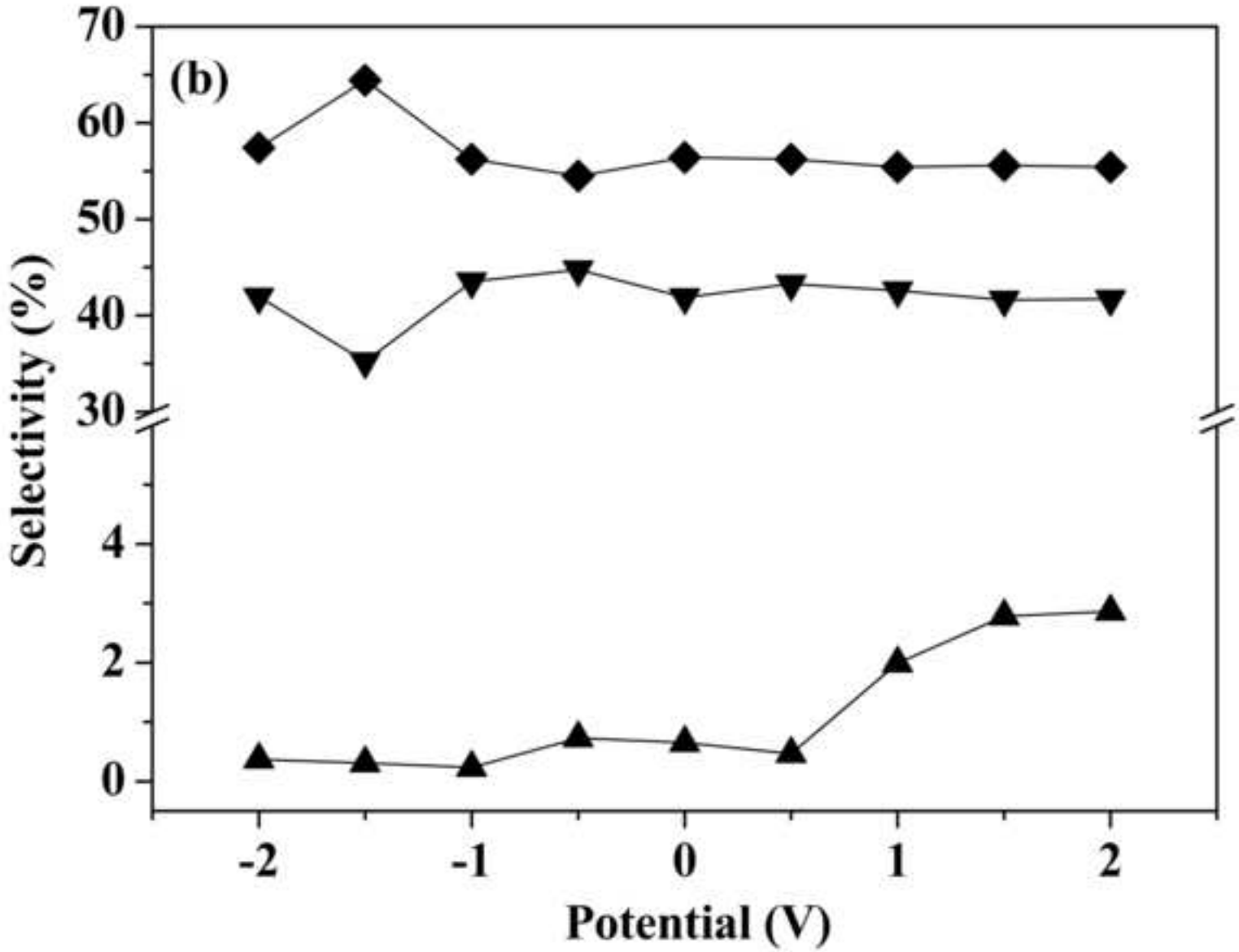

Figure
Click here to download high resolution image

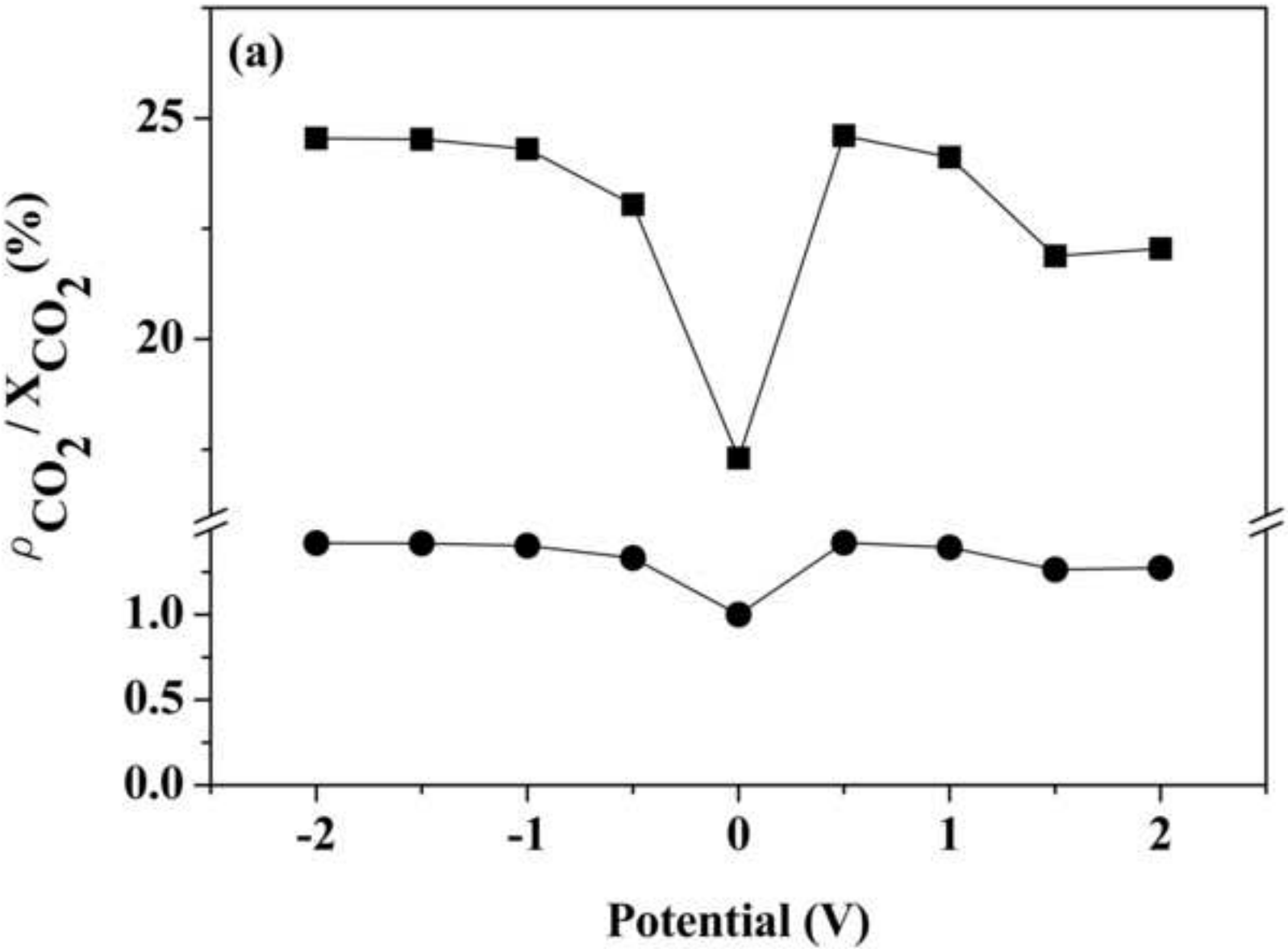

Figure
Click here to download high resolution image

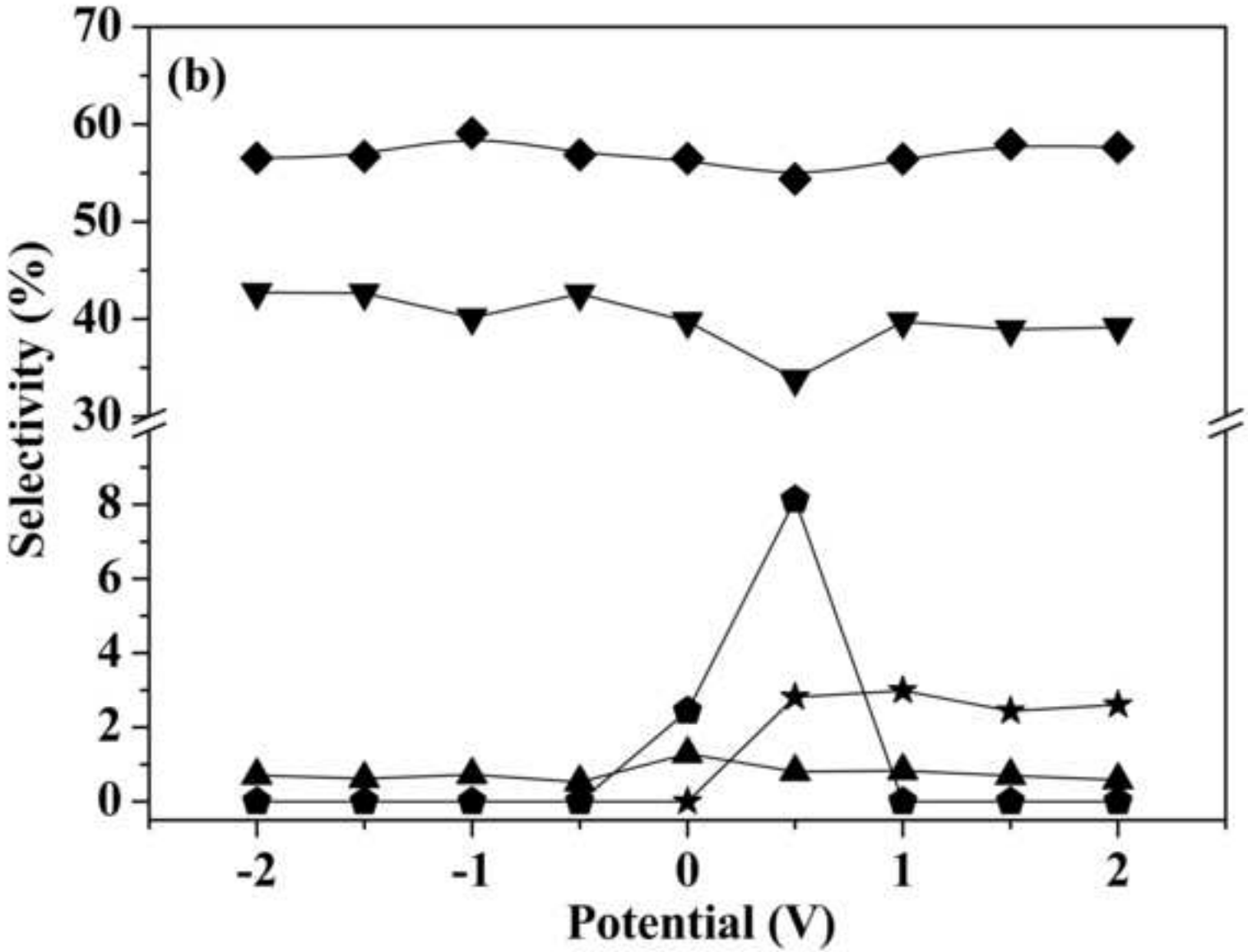

Figure
Click here to download high resolution image

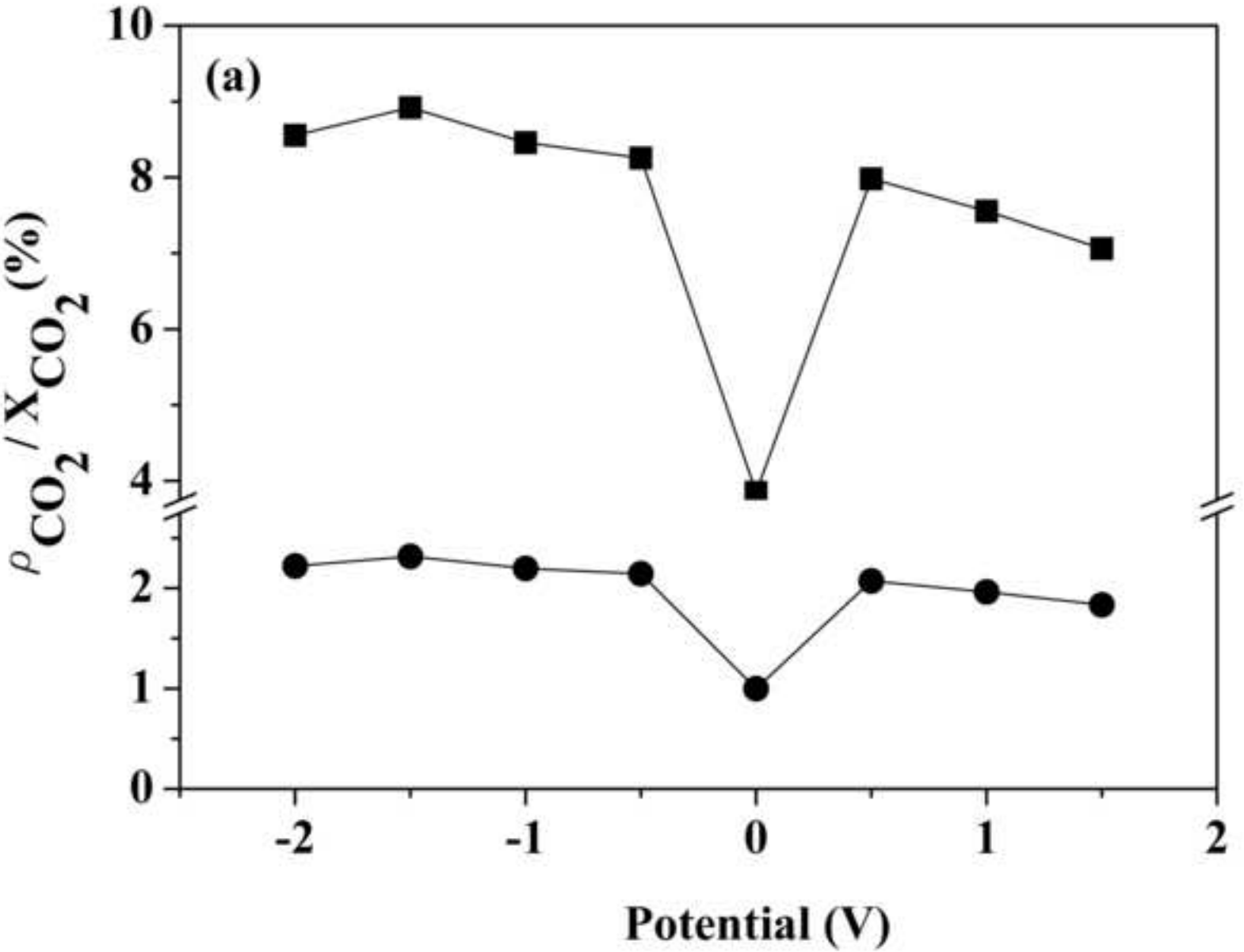

Figure
Click here to download high resolution image

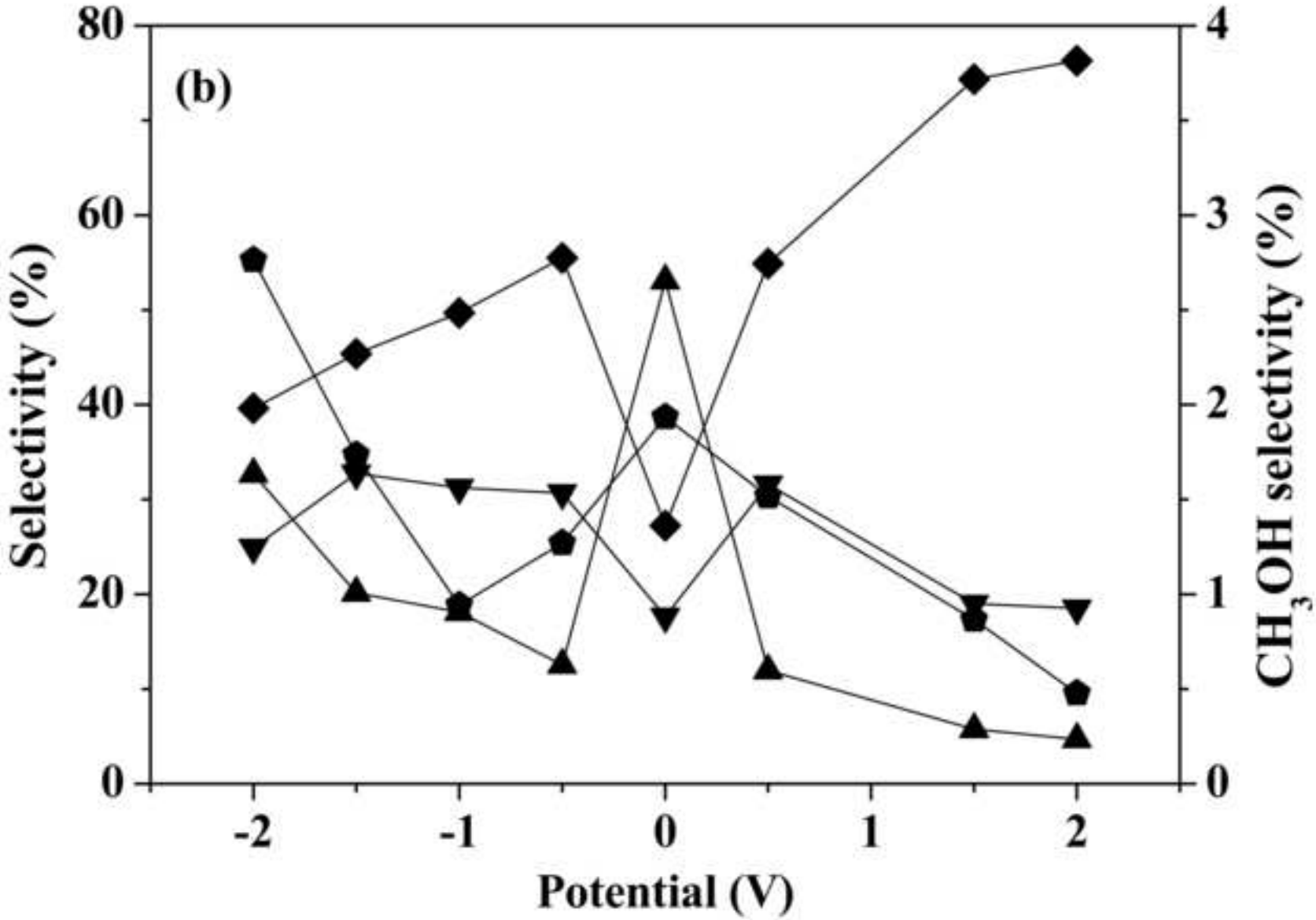

Figure
Click here to download high resolution image

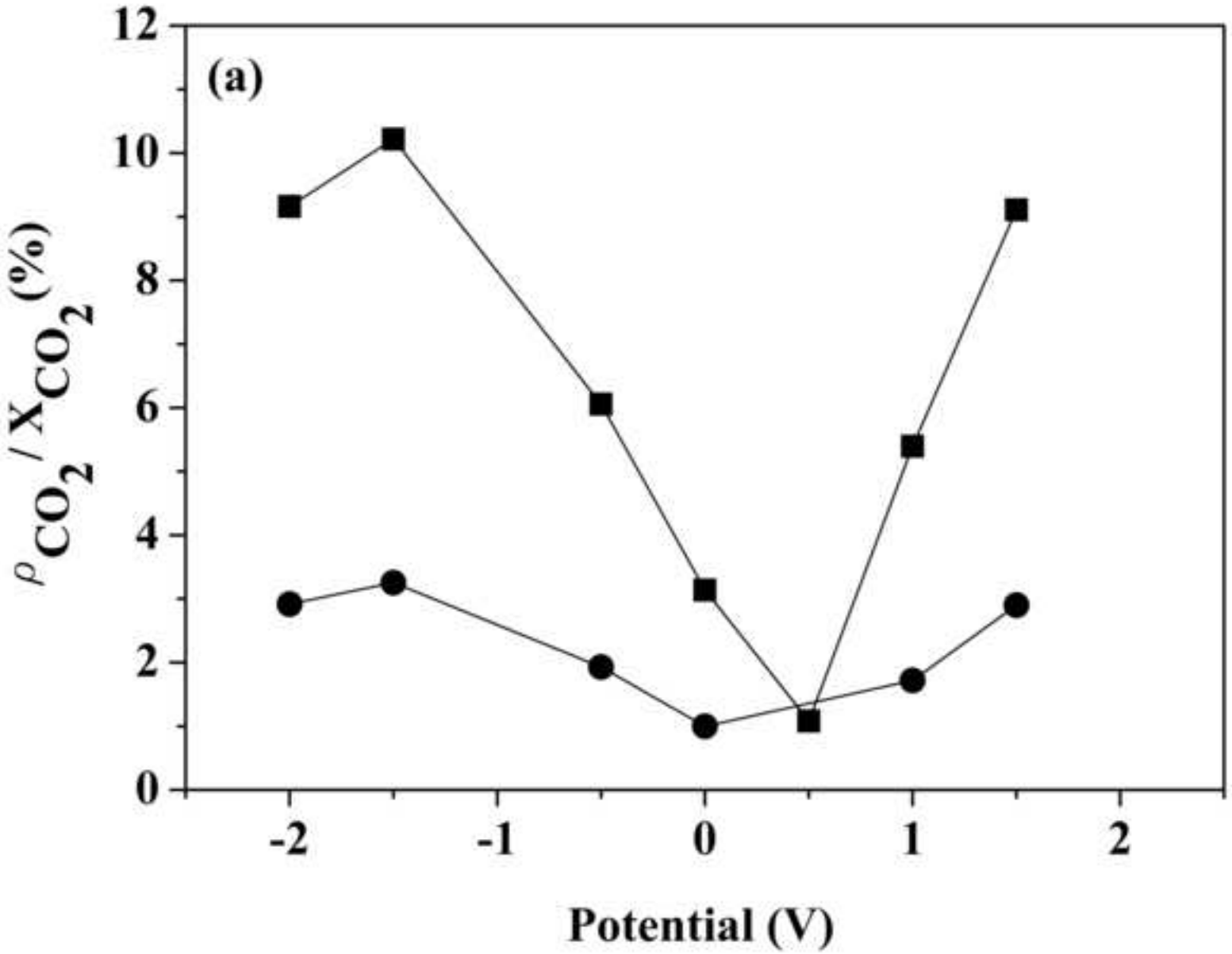

Figure
Click here to download high resolution image

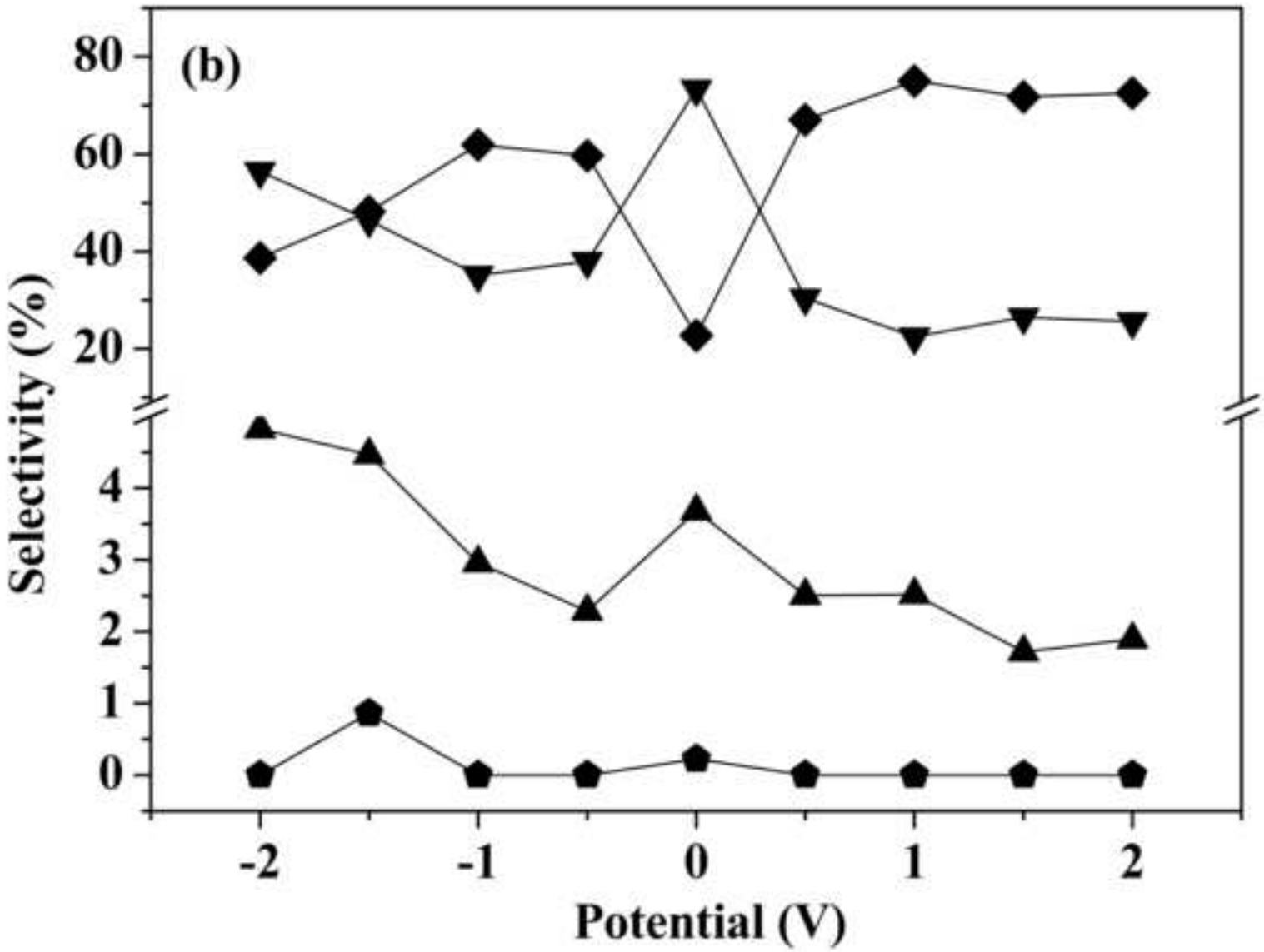

Figure
Click here to download high resolution image

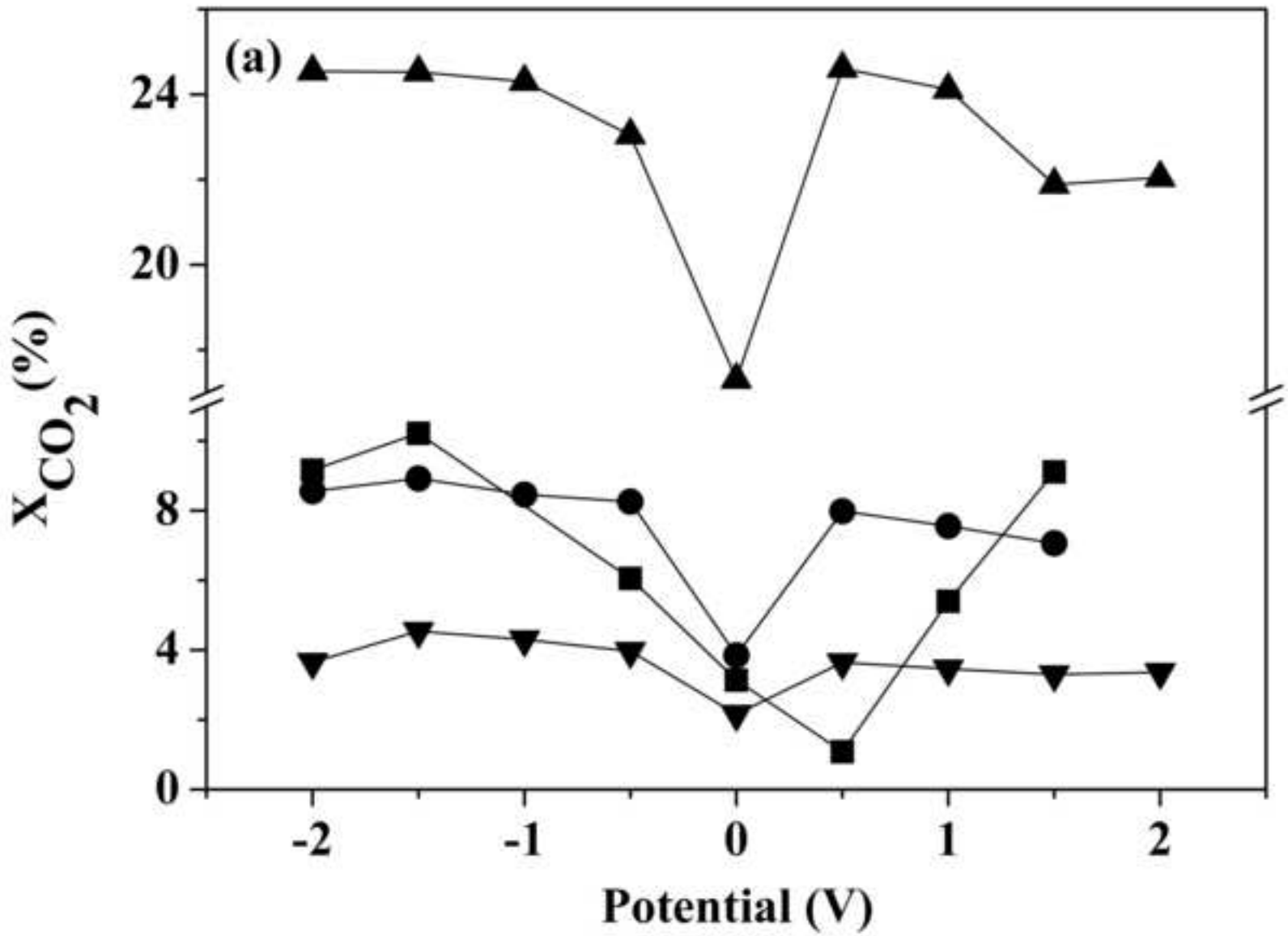

Figure
Click here to download high resolution image

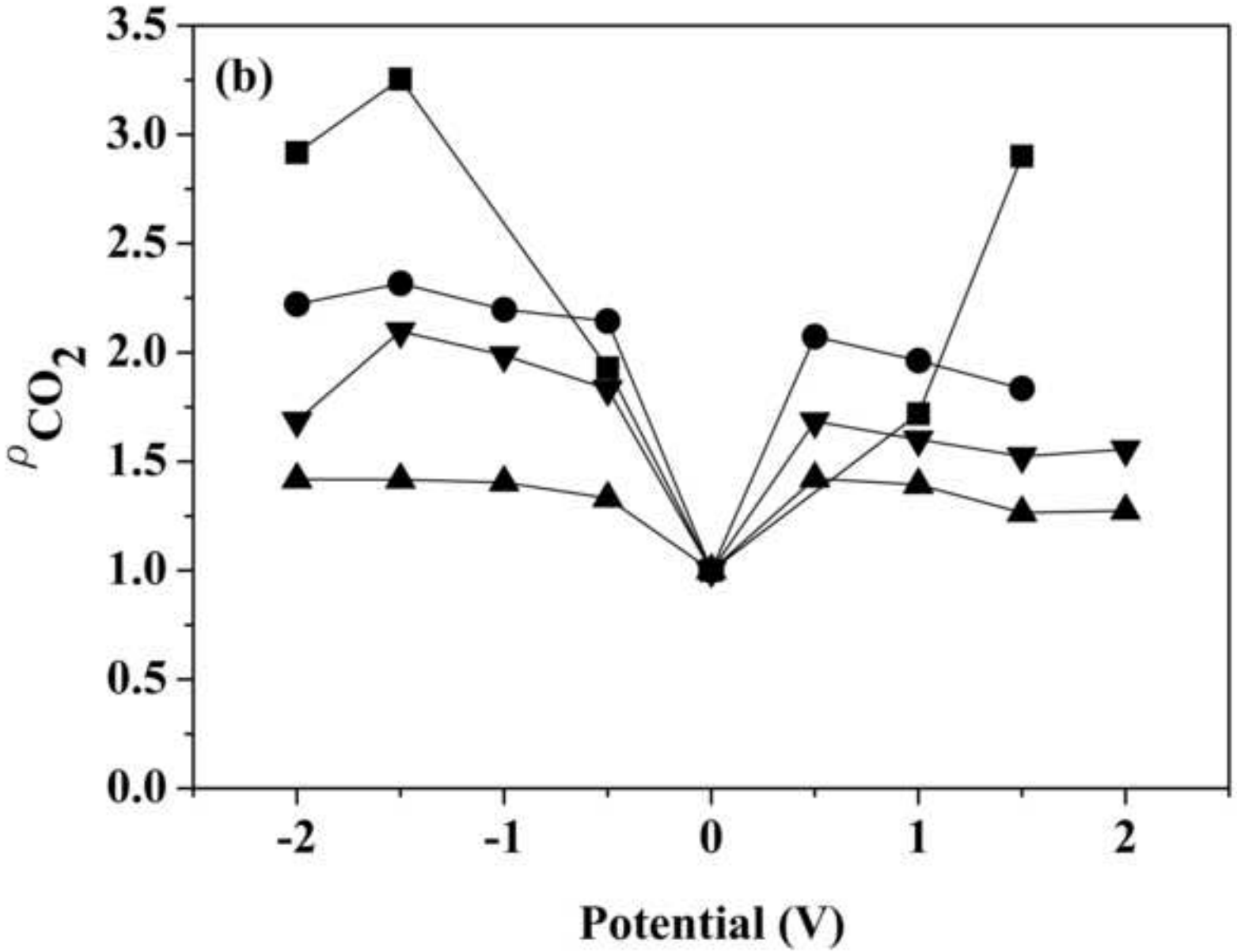

Figure
Click here to download high resolution image

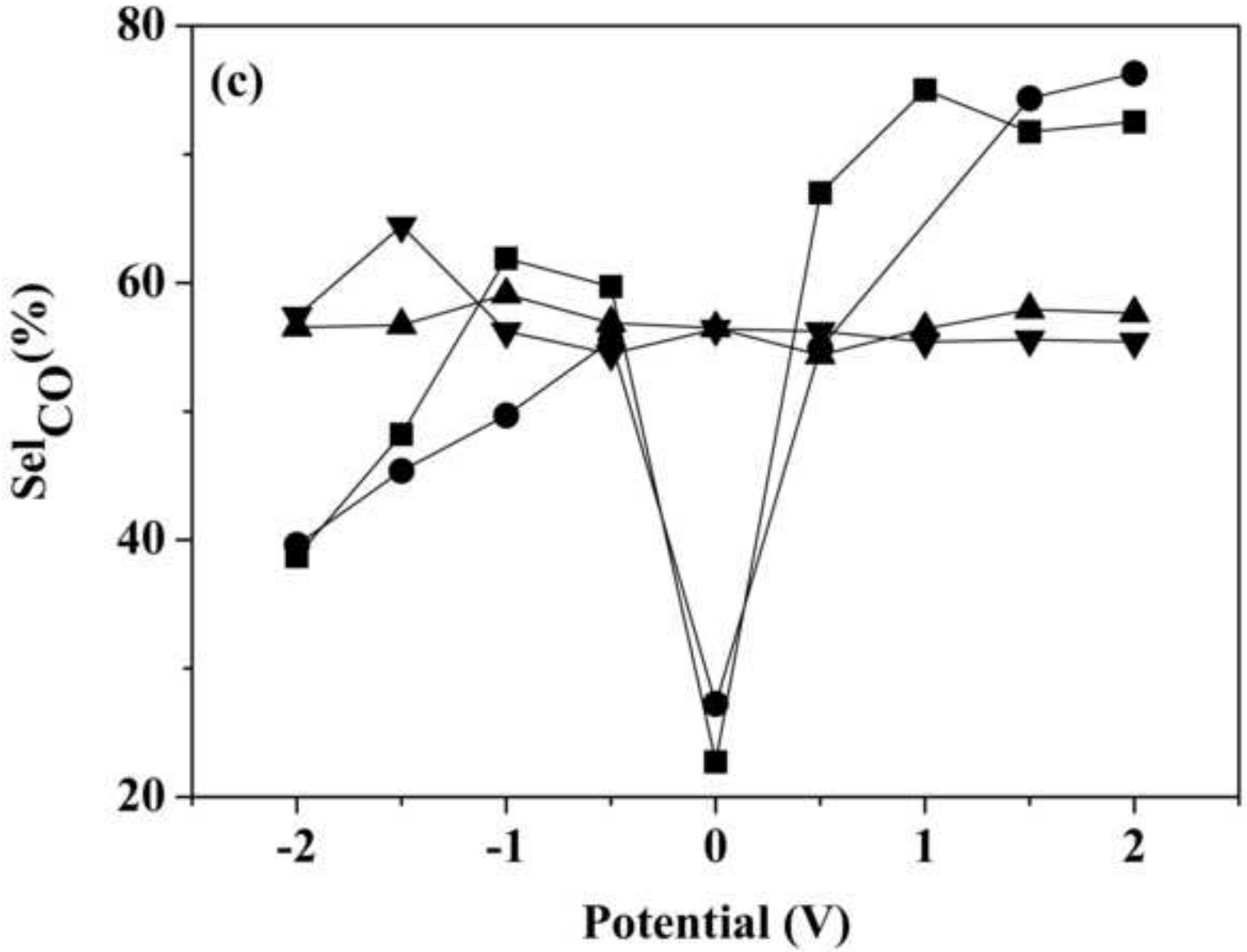

Figure
Click here to download high resolution image

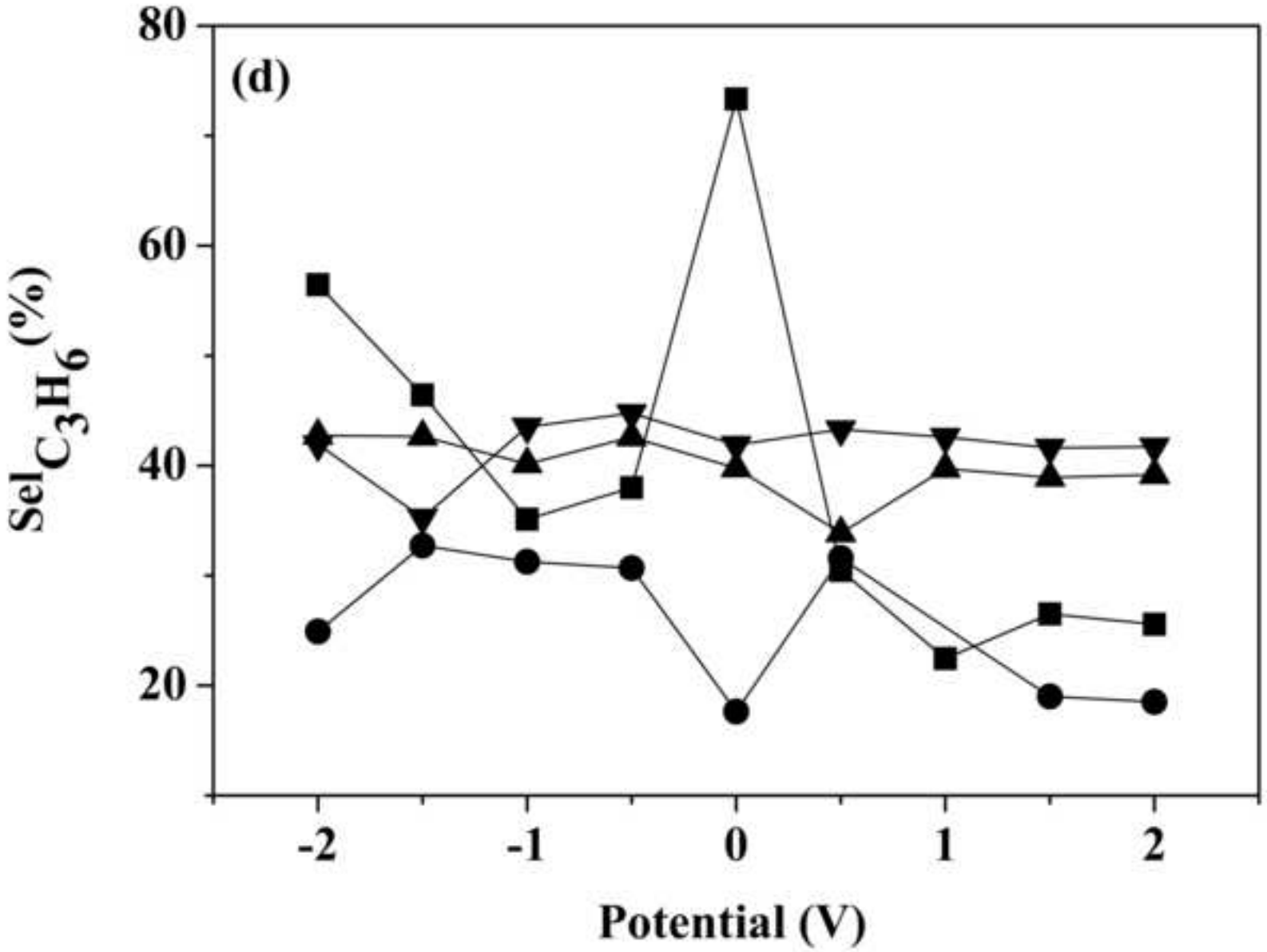

Figure
Click here to download high resolution image

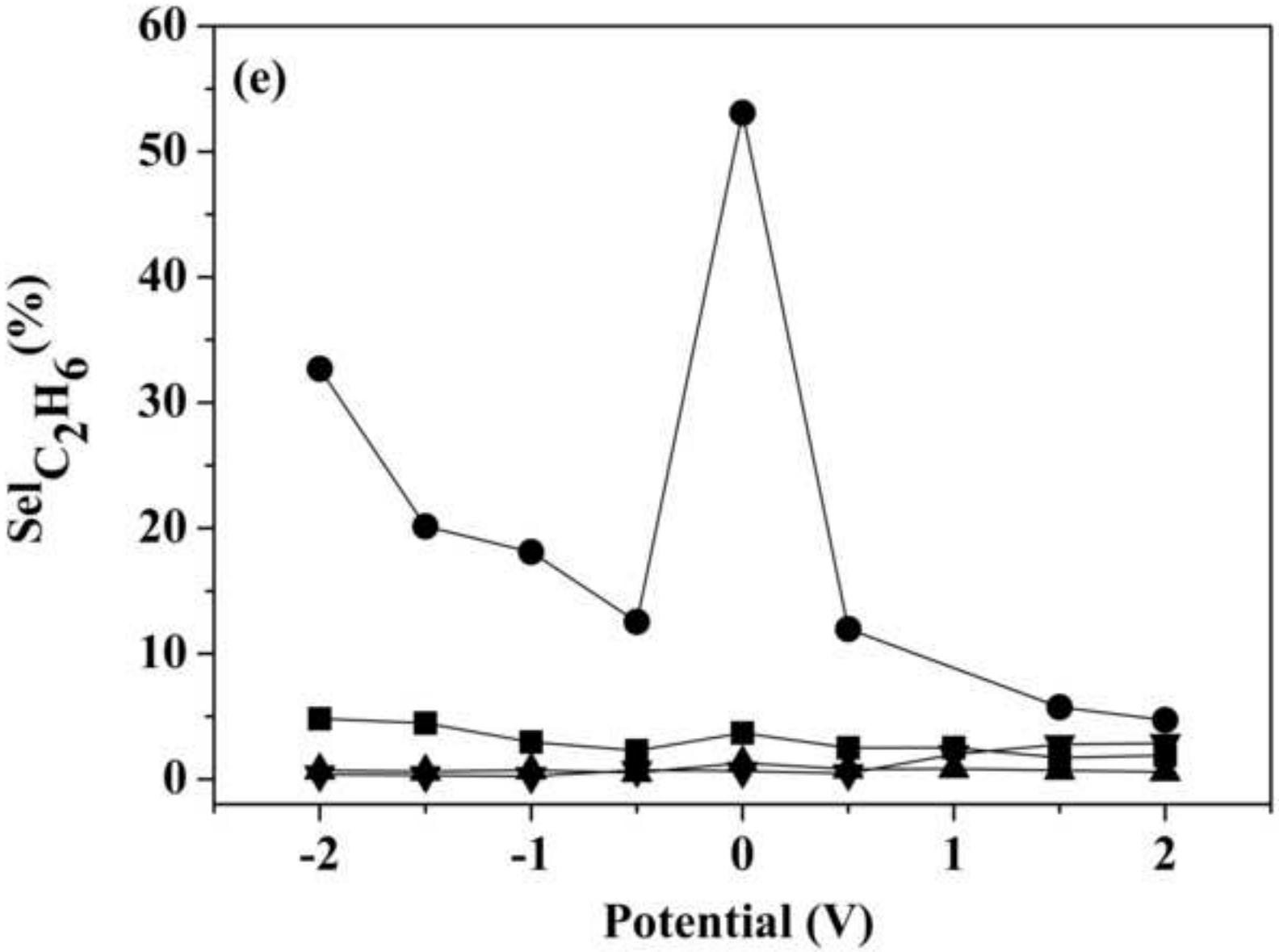

Figure
Click here to download high resolution image

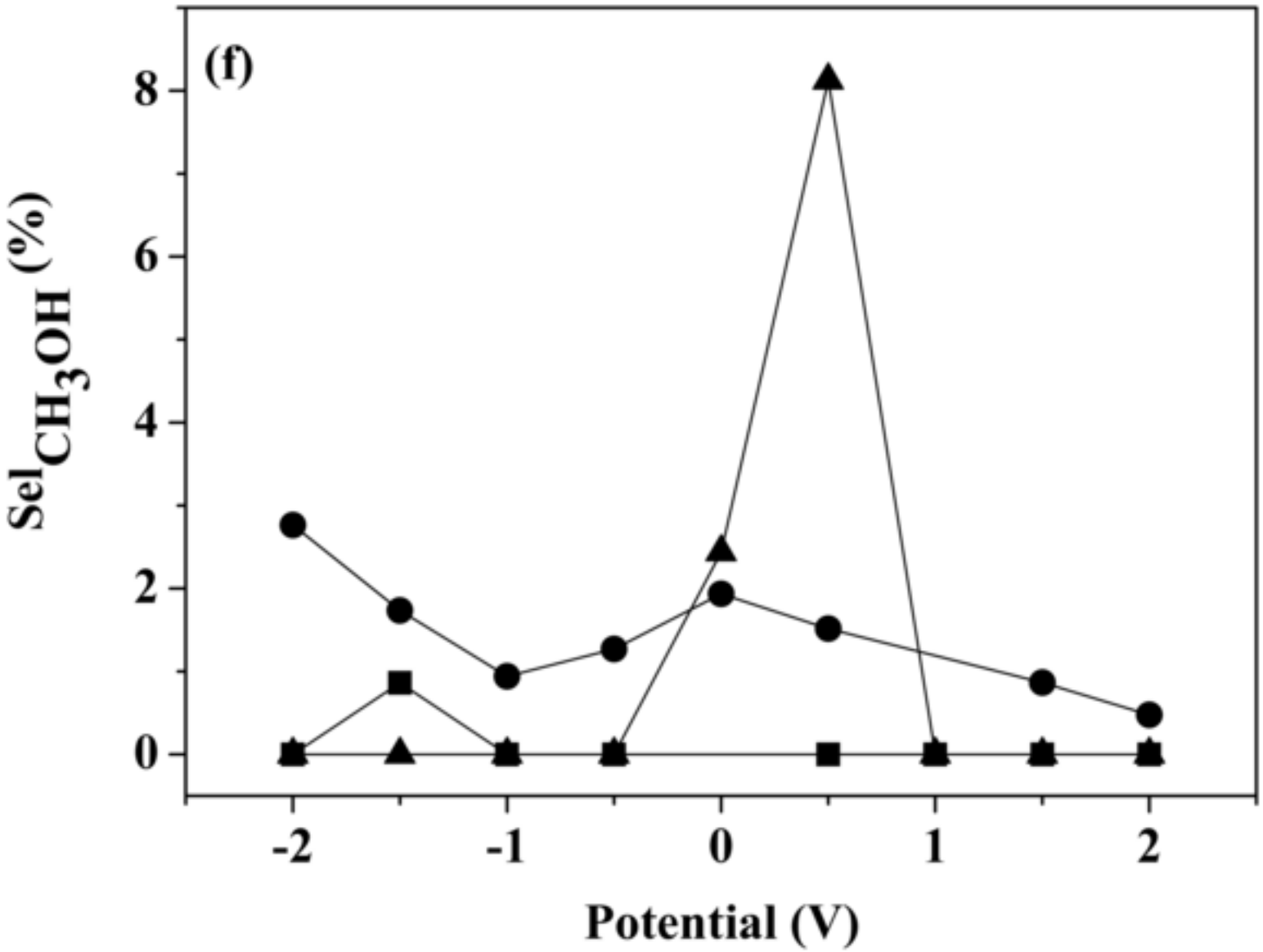

Figure
Click here to download high resolution image

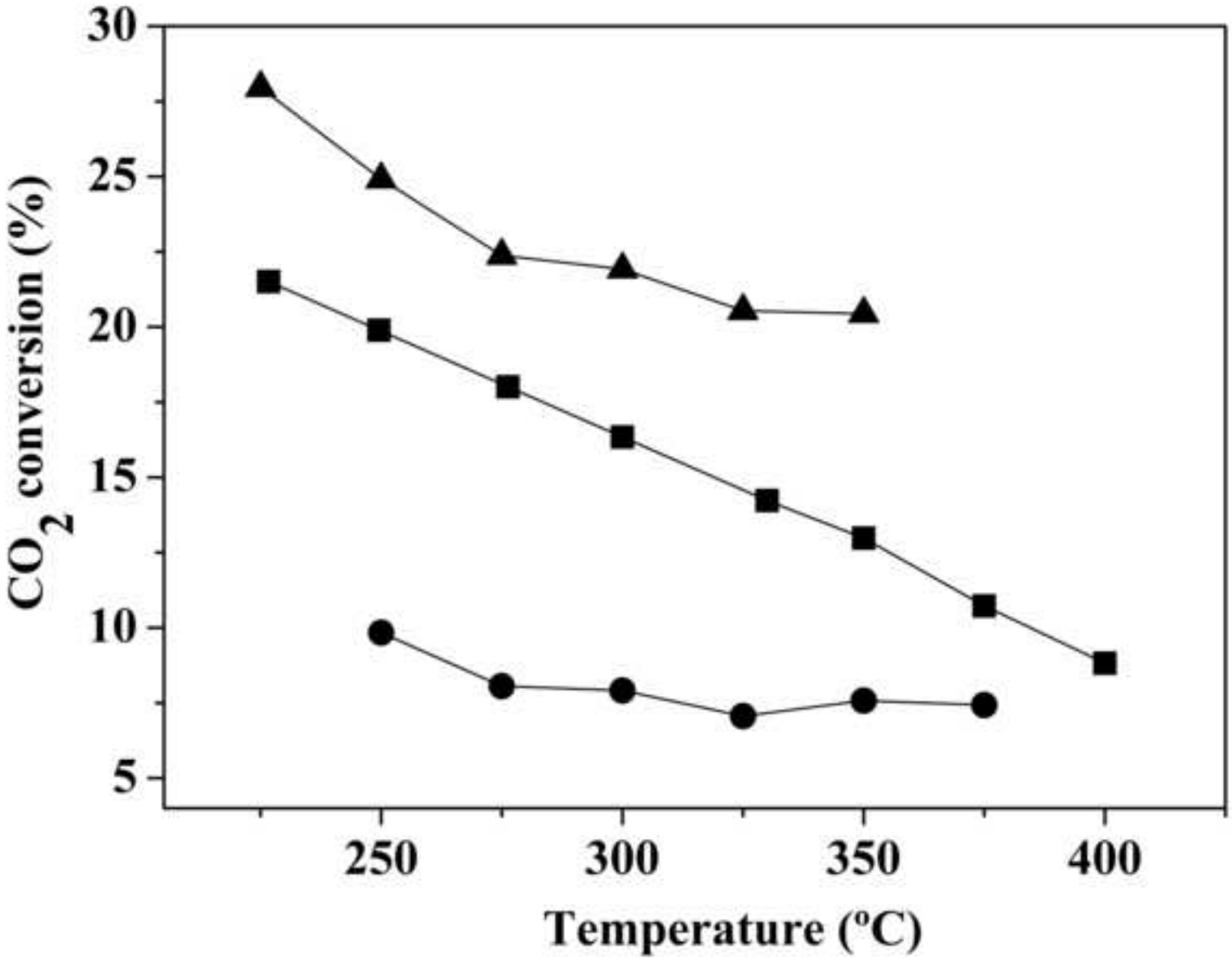

Figure

Click here to download high resolution image

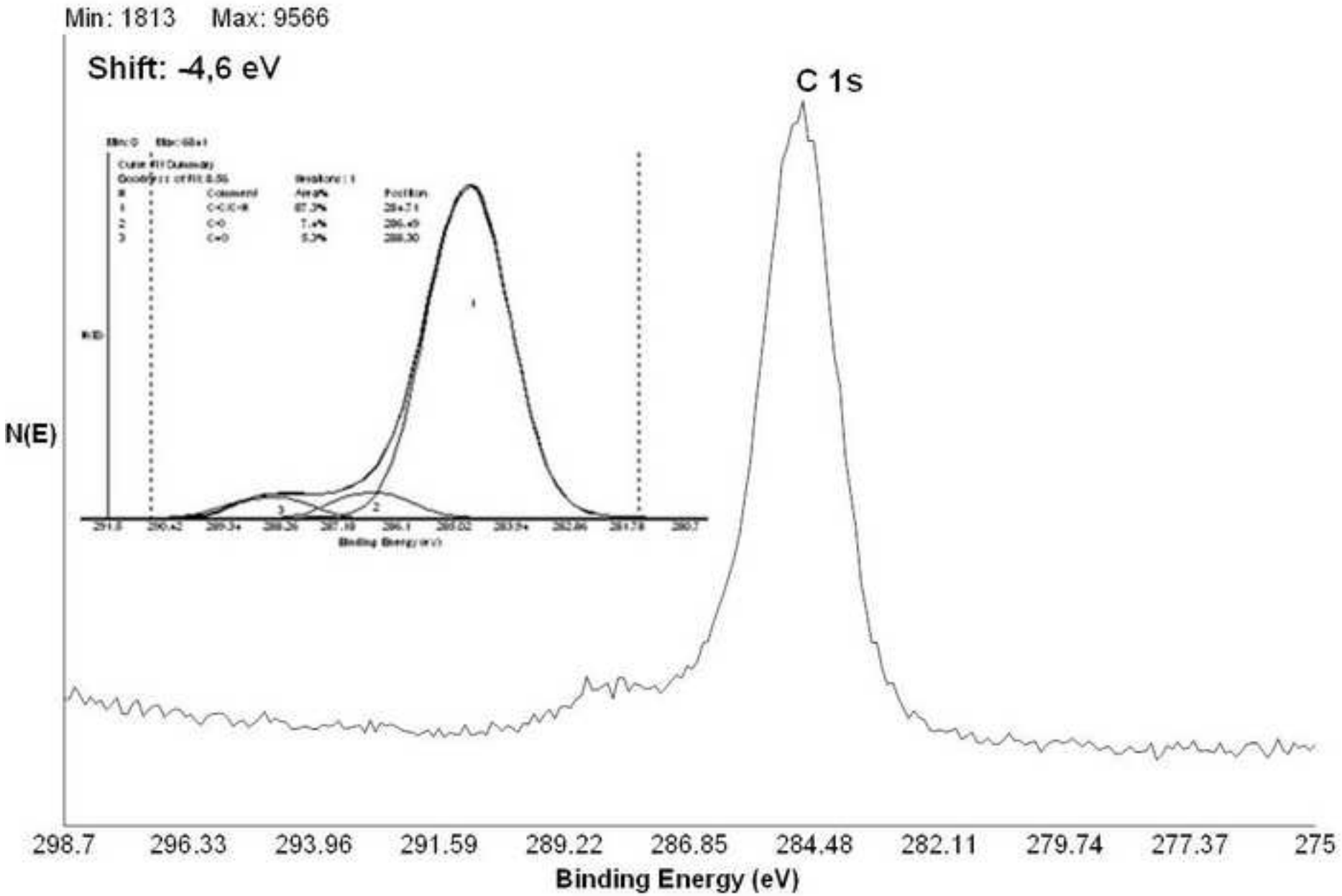

Figure

Click here to download high resolution image

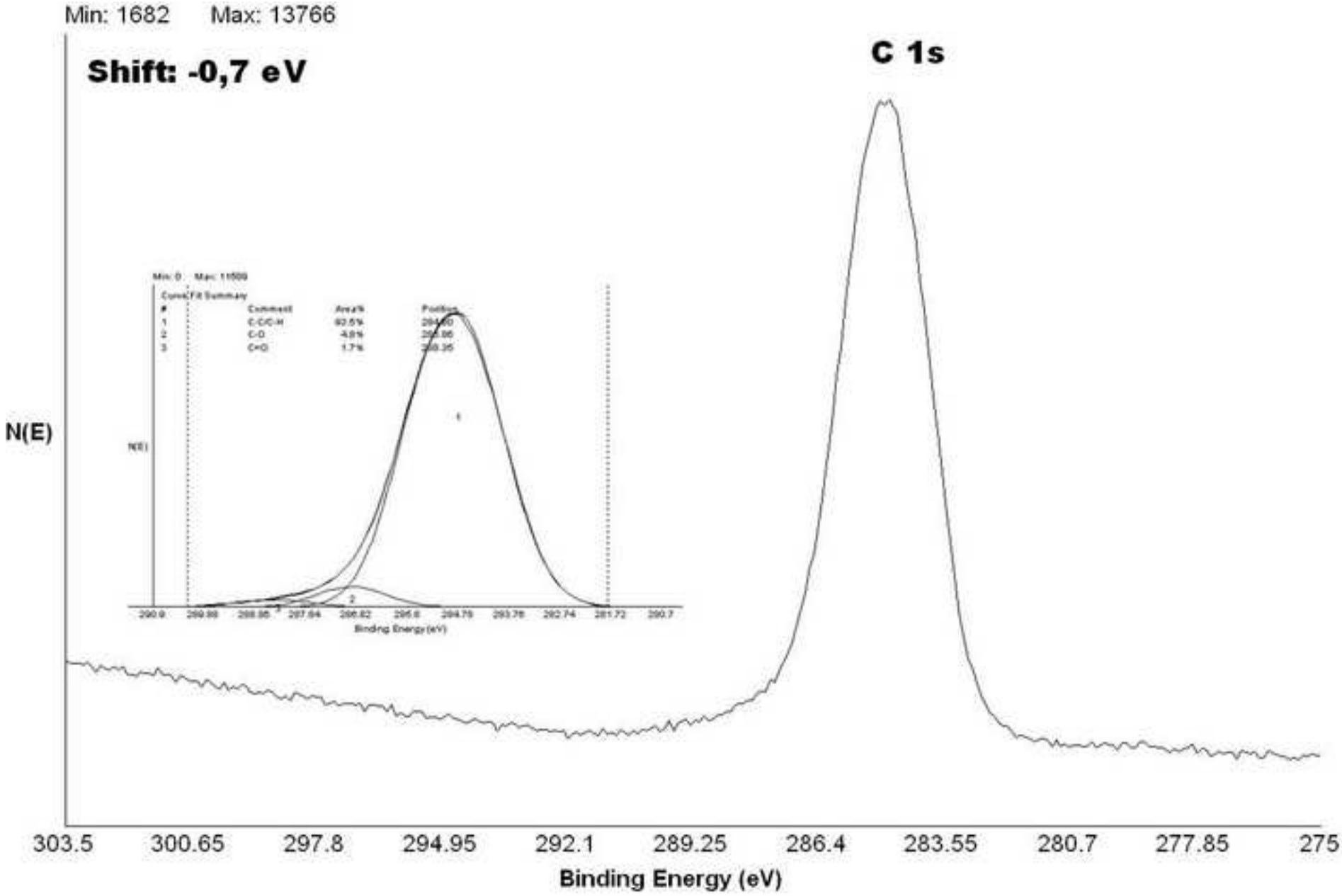

Figure
Click here to download high resolution image

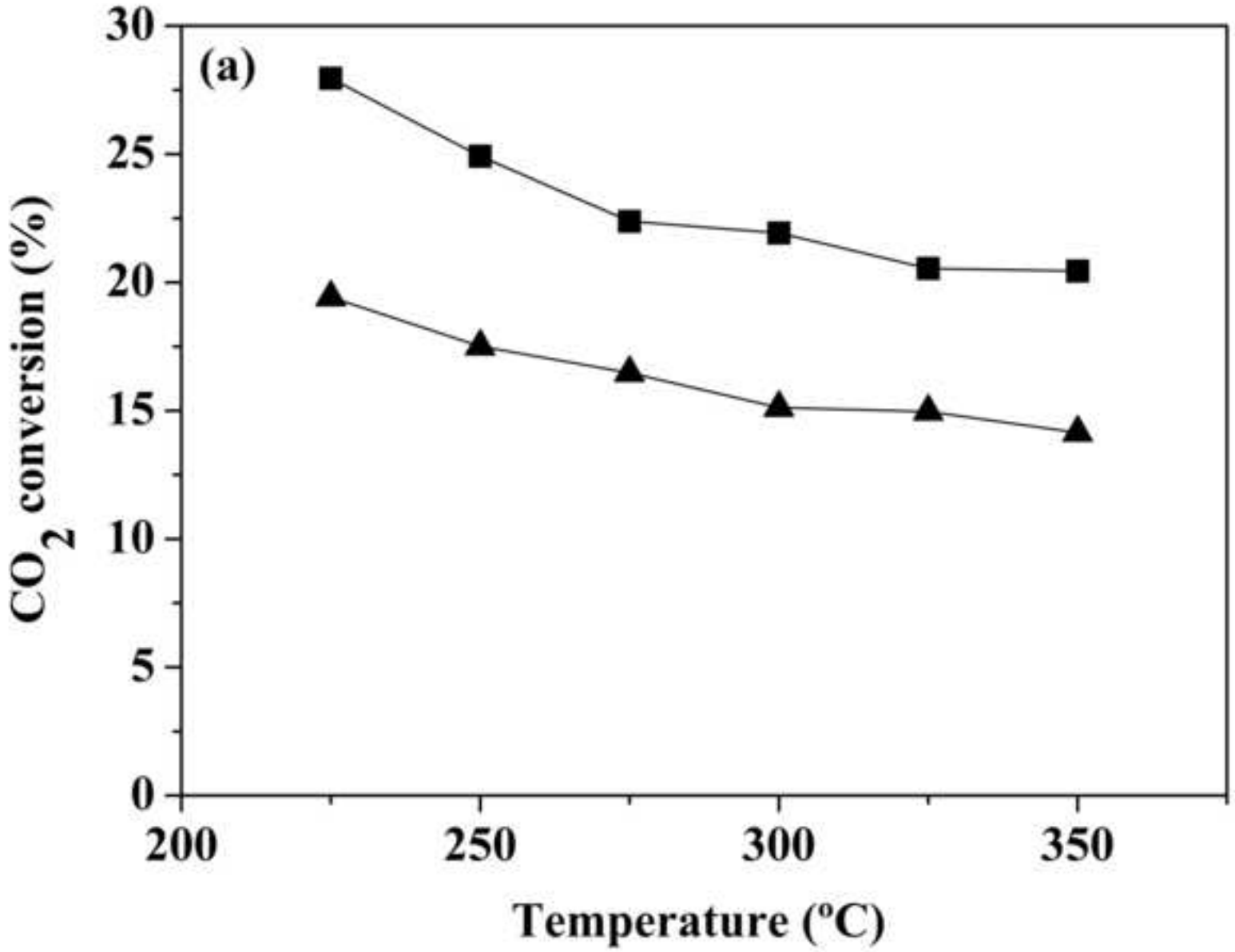

Figure
Click here to download high resolution image

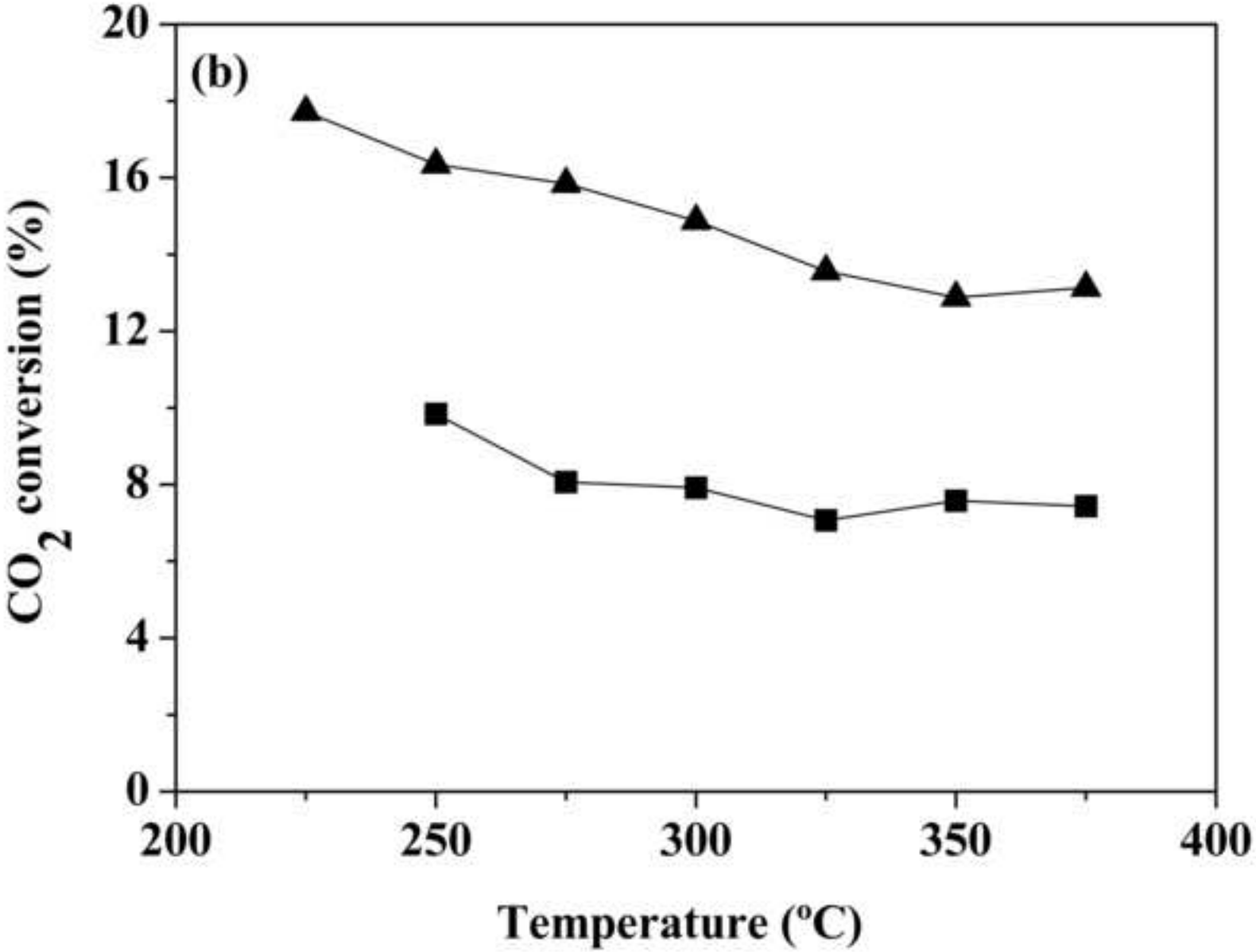

Figure
Click here to download high resolution image

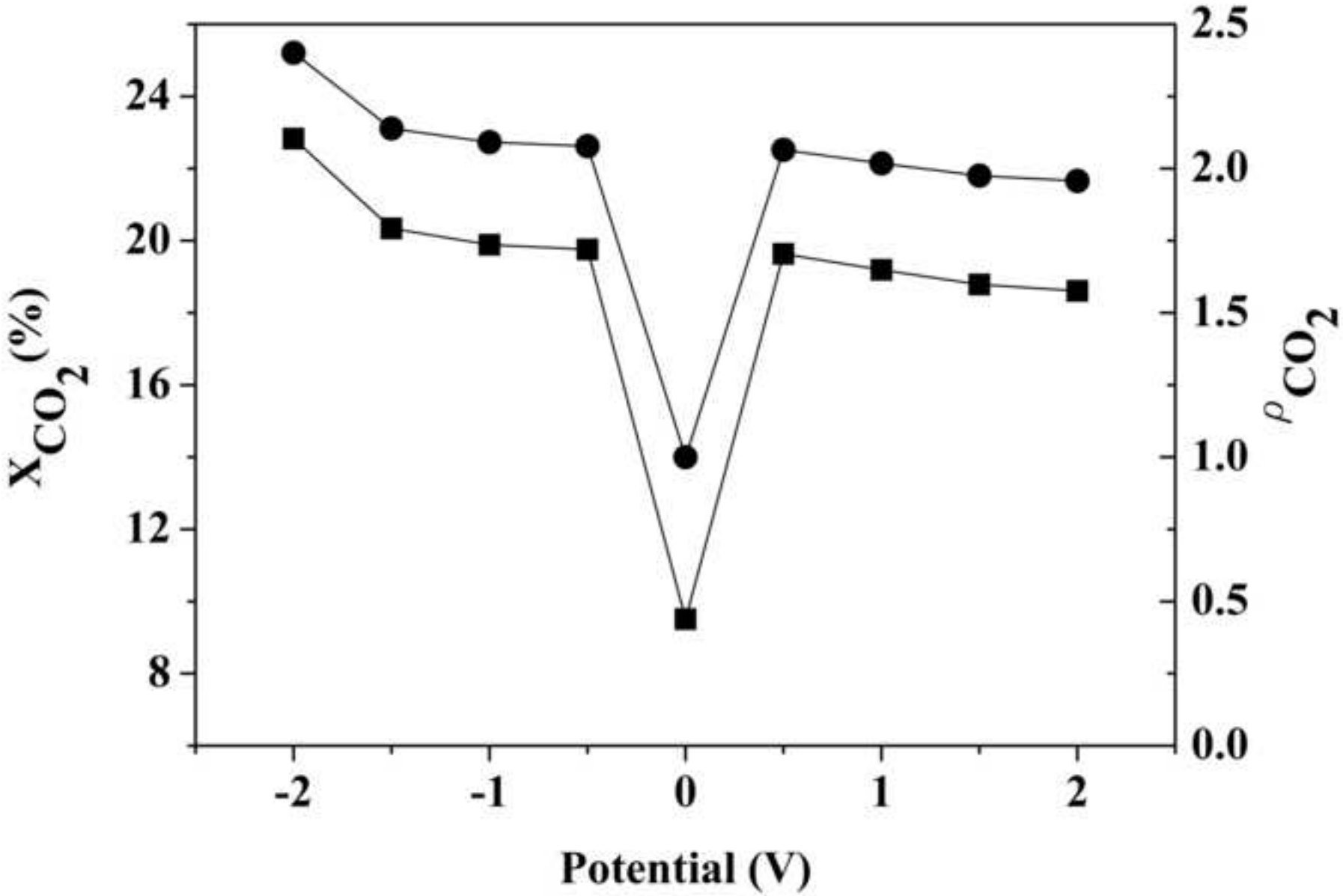

Figure
Click here to download high resolution image

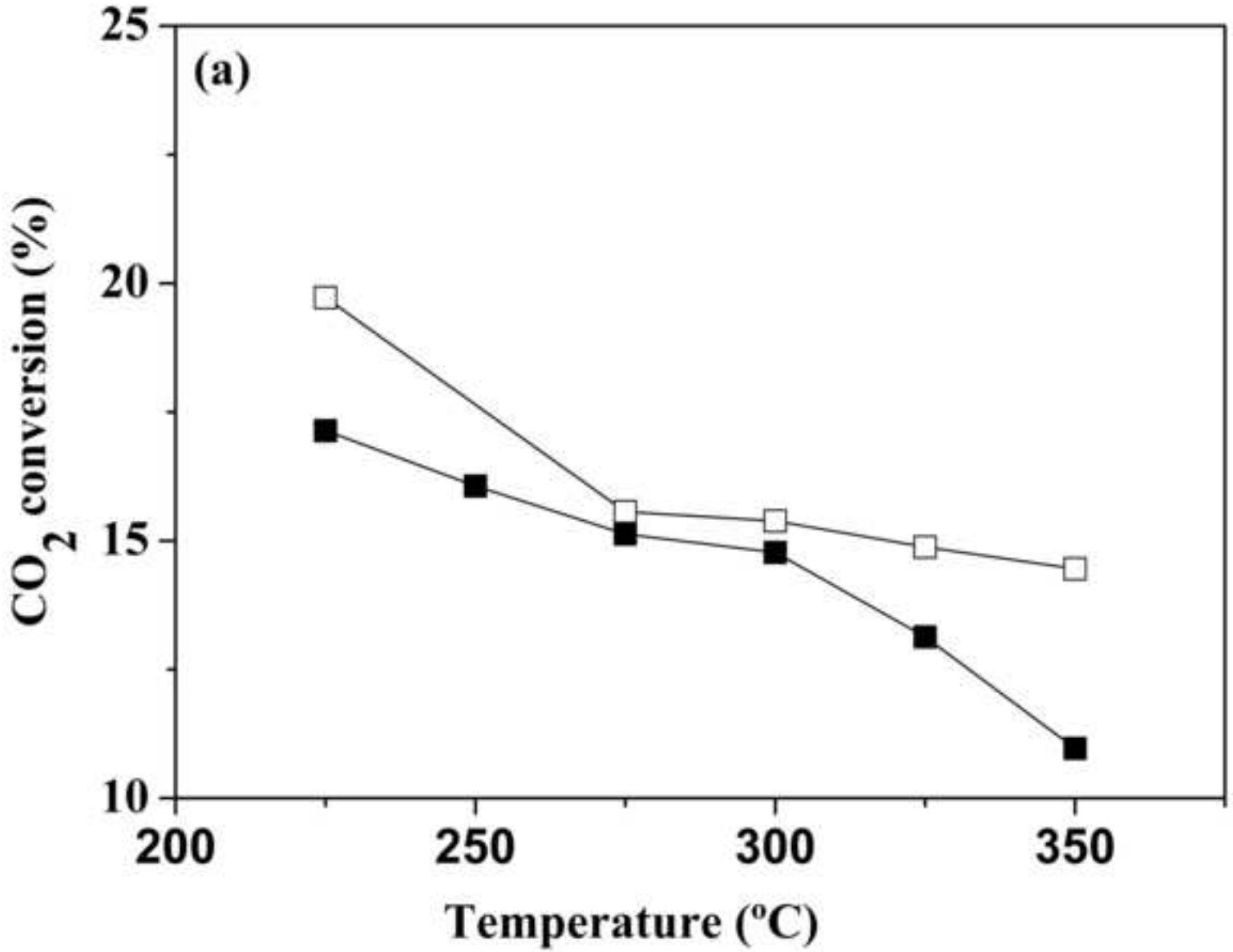

Figure
Click here to download high resolution image

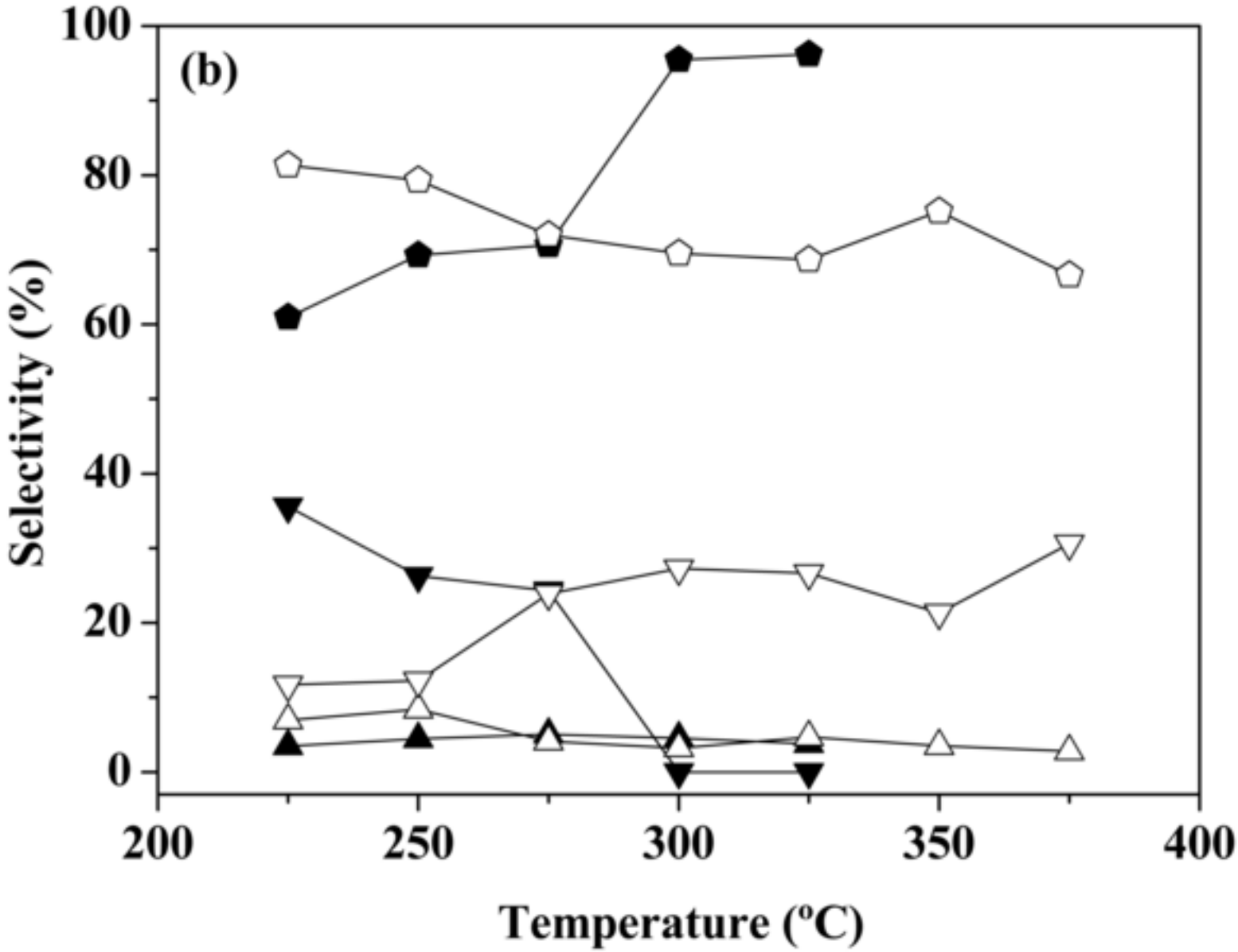

Figure
Click here to download high resolution image

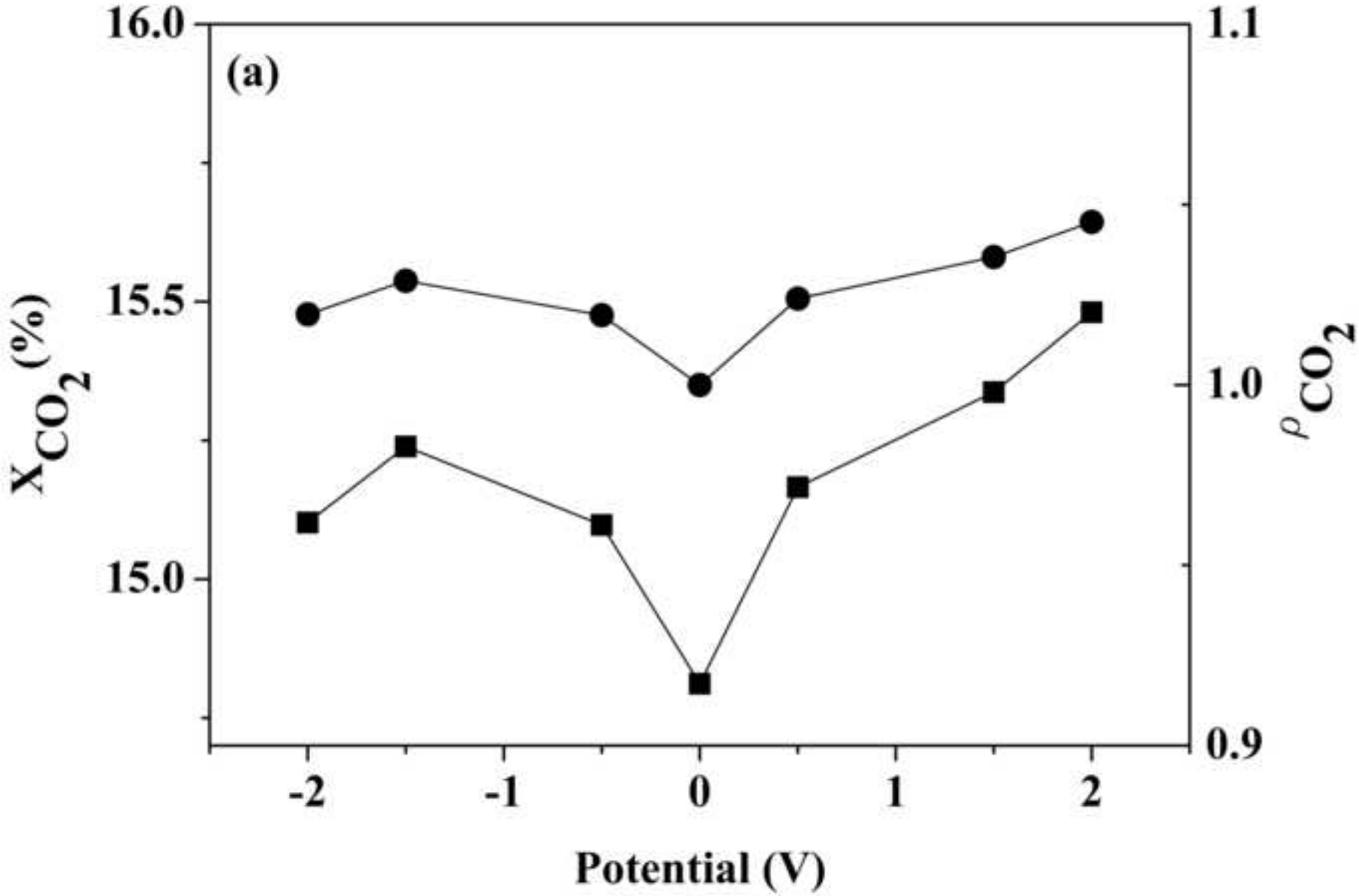

Figure
Click here to download high resolution image